5.0 STUD SUMMARY

VARIABLE DATA	PER PAR'S. 4.3.1-4.3.3 SHIELDING NO. 1 TOP	PER PAR'S. 4.3.1-4.3.3 SHIELDING NO. 1 BOTTOM	PER PAR'S. 4.3.1-4.3.3 SHIELDING NO. 2 TOP	PER PAR'S. 4.3.1-4.3.3 SHIELDING NO. 2 BOTTOM	PER PAR'S. 4.4.1-4.4.3 SHIELDING NO. 3 TOP *	PER PAR'S. 4.4.1-4.4.3 SHIELDING NO. 3 BOTTOM	PER PAR. 4.5.1-4.5.3 SHIELDING NO. 4 TOP *	PER PAR. 4.5.1-4.5.3 SHIELDING NO. 4 BOTTOM
SIZE	3/8-UNC	3/8-16 UNC	3/8-16 UNC	7/16-14 UNC	3/8-16 UNC	3/8-16 UNC	3/8-16 UNC	3/8-16 UNC
A_t [IN^2]	.0775	.0775	.0775	.106	.0775	.0775	.0775	.0775
MAT. AT 450°F	17-4 PH. S.S.-A	17-4 PH. S.S.-A	NITRONIC -60	304 S.S.	NITRONIC -60	NITRONIC -60	NITRONIC -60	17-PH. S.S.-A
S_y	123.0	123.0	33.5	20.1	33.5	33.5	33.5	123.0
S_u	128.6	128.6	79.0	64.0	79.0	79.0	79.0	128.6

IMPACT ORIENTATIONS (i) DEGREES.

	0	90	45	0	90	45	0	90	45	0	90	45	0	90	45	0	90	45	0	90	45	0	90	45
σ_e	46.7	53.1	109.	54.6	99.4	78.8	USE "BOTTOM" DATA			31.9	15.9	19.5	-	-	-	25.2	38.1	50.1	-	-	-	74.3	67.9	9
σ_A	27.1	52.2	105.6	40.	84.	68.6	21.8	21.4		29.3	11.6	12.3	0.	0.	0.	22.1	37.3	49.	0.	0.	0.	72.2	67.0	9.
$P_A = \sigma_A \times A_t$ [K]	2.1	4.0	8.2	3.1	6.5	5.3	1.7	1.6		3.1	1.2	1.3	0.	0.	0.	1.7	2.9	3.8	0.	0.	0.	5.6	5.2	7

* NO WELDS AT STUDS TO TOPPLATE.

Pg. 111a

5.1 STUD WELD STRESSES

SHIELDING PIECES #1 AND #2 TOP STUDS PENETRATE AND ARE WELDED TO THE BASKET TOP PLATE. SEE SHEETS 10 AND 11 OF 159C5238 IN APPENDIX A. THE DESIGN LOADS FOR EACH PIECE COME FROM THE TABLE IN 5.0 ON PAGE 111 OF THIS SHIELDING REPORT. THE WELD CONFIGURATIONS ARE AS FOLLOWS.

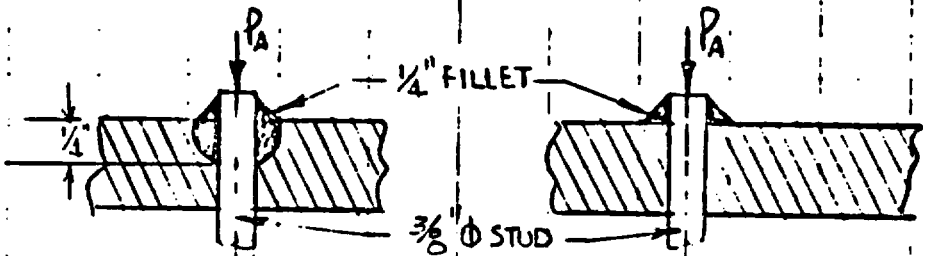

STRESSED AREAS

$$A_1 = \pi\left(\tfrac{3}{8}\right)\left(\tfrac{1}{4}\right)(2) = 0.6\ in^2$$

$$A_2 = \pi\left(\tfrac{3}{8}\right)\left(\tfrac{1}{4}\right) = 0.3\ in^2$$

WELD STRESSES

$$S = \frac{P_{AXIAL}}{A}\ ;\ P_{AXIAL} \text{ IS FROM 5.0}$$

$$S_1 = \frac{8.2}{0.6} = 13.7\ ksi$$

$$S_2 = \frac{3.1}{0.3} = 10.3\ ksi$$

FOR 308 FILLER S = 45 ksi × .577
= 26 ksi @ 450°F

JOB NO. _____ DATE _____ BY B.K.T. CH'K _____

CUSTOMER _____ PROJECT _____

SUBJECT _____

6.0 URANIUM PLATE - COMBINED STRESS VS. IMPACT ORIENTATION

DEG. ORIENTATION	SHIELDING NO.1 PER REF. 3 (B_A+B_B) [KSI] CASE # 4	450°F S_y	SHIELDING NO.2 PER REF. 3 (B_A+B_B) [KSI] CASE # 4	450°F S_y	SHIELDING NO.3 PAR.4.4.1-4.4.3 B_{ij} [KSI]	450°F S_y	SHIELDING NO.4 PAR.4.5.1-4.5.3 B_{ij} [KSI]	450°F S_y
0.	9.64		.94		4.21		12.3	
90.	4.29 CASE # 3	46.0	6.69 CASE # 3	46.0	6.71	46.0	11.5	46.0
45.	9.83 CASE # 5		6.87 CASE # 5		8.94		15.55	

7.0 THERMAL EVALUATION

Due to the difference in thermal expansion between the uranium shielding - support assembly and the basket, thermal strains are introduced. The combined thermal expansion coefficient of the shielding - support assembly is less than the basket coefficient resulting in positive strains in the members of the shielding assembly. The basis for the preceding analysis described in Par. 1 is to assure the structural integrity is maintained during load application by comparing the load carrying capacity of the structural members with the external loads.

Contrary to the stresses produced by mechanical loads,yielding due to thermal loads causes relaxation of the thermal stresses and it can be shown that the static thermal strains in a structure do not effect the load carrying capacity of its members. Failure due to thermal loads is the result of repetitive cycling rather than a single application of thermal stress. The method used for evaluating the limit load of the assembly should not be applied to the computed thermal stresses. The criteria for failure is based on the mechanical loads. The thermal loads are excluded when evaluating the load carrying capacity of a member in the accident mode against the total combined external load.

REFERENCES

1. Design of Welded Structures - By Blodgett
2. Machinery's Handbook - 18th Edition
3. Stardyne 3 - Static Member Loads and Stress Output, Retained in Stearns-Roger File under Job Number C-18813-2.
4. Engineering Vibrations - By Jacobsen and Ayre (McGraw-Hill 1958)
5. MRI/Stardyne 3 - Static and Dynamic Structural Analysis Program.
6. Roark - Formulas for Stress and Strain - 4th Edition
7. Criteria of the ASME Boiler & Pressure Vessel Code for Design by Analysis in Sections III and VIII, Division 2 - Library of Congress Catalog No. 56-3934
8. Subsection - NA of the Nuclear Code - Summer Addenda 1976
9. Plasticity - Theory and Application - By A. Mendelson
10. Plastic Design in Steel - By Asce
11. S.R. - Dyrec - Dynamic Analysis Program
12. Report Concerning Fin Impact Analysis - by R. E. Nickell Pacifica Technology

NEDO-21796
STEARNS-ROGER
APPENDIX A

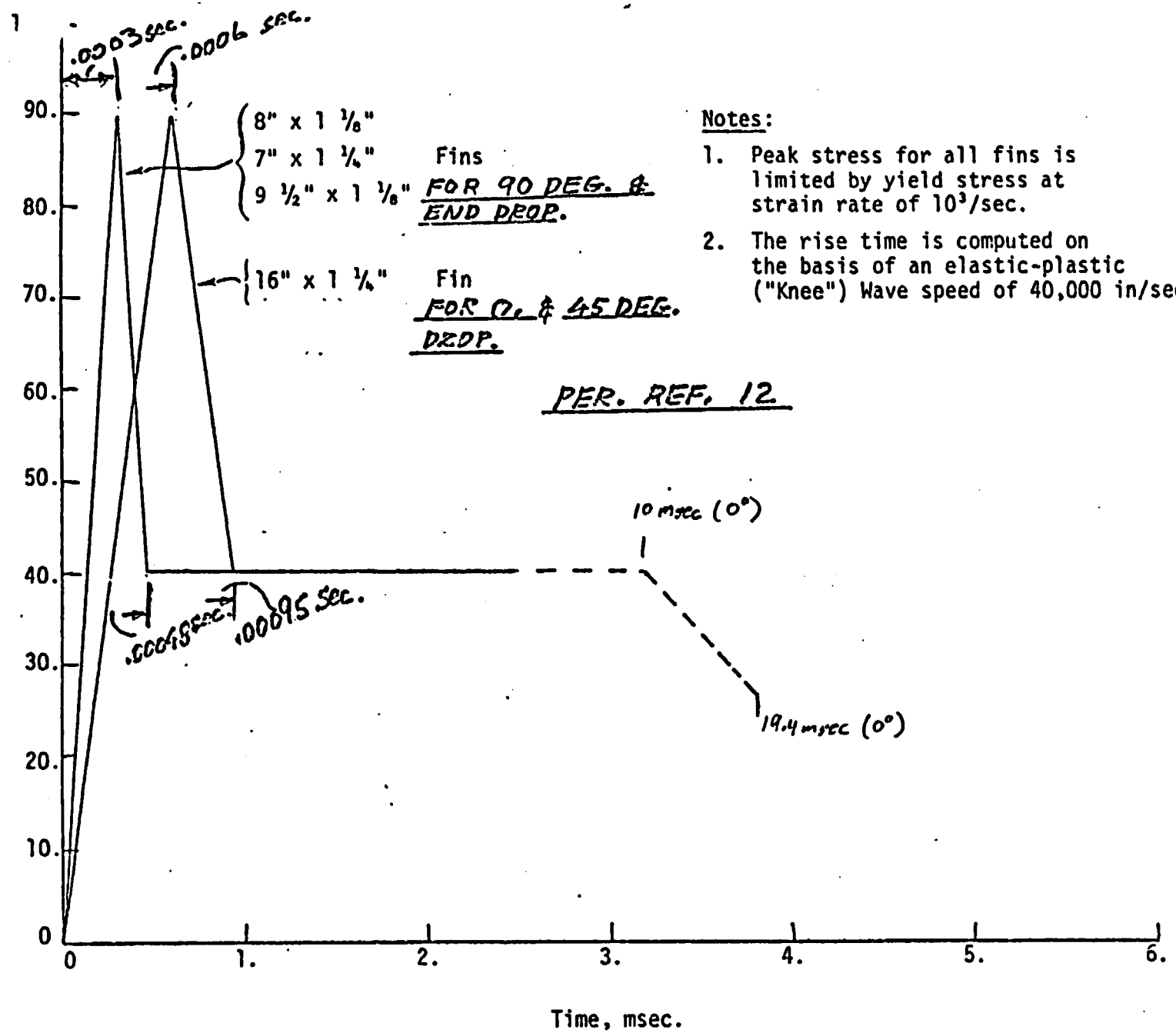

Notes:

1. Peak stress for all fins is limited by yield stress at strain rate of 10^3/sec.
2. The rise time is computed on the basis of an elastic-plastic ("Knee") Wave speed of 40,000 in/sec.

Figure 5.

NEDO-21796
STEARNS-ROGER
APPENDIX B

B. Physical Properties (Cont'd)

- o low temperature - 40°F
- o normal temperature - 450°F
- o high temperature - 1000°F

1. 304/216 Stainless Steel

The following table, Table 2, shows the properties and references used for 304 and 216 stainless steel in these evaluations.

TABLE 2

304/216 SST Properties

Item	Temperature -40°F	450°F	1000°F	References
304, yield stn, ksi (.2% off-set)	140.0	20.1	15.6	(1), (2), (2)
304, Mod. of Elasticity E x 10^6 ksi	29.0	26.2	22.5	(3), (1), (4)
304, coeff. of thermal expansion α x 10^{-6} in/in/°F	8.4	9.65	10.1	(1), (2), (4)
216, yield stn, ksi (.2% off-set)	>62.4	44.9	36.3	(15), (15), (15)

2. Depleted Uranium

The following table, Table 3, shows the properties and references used for depleted uranium metal in these evaluations.

TABLE 3

Depleted Uranium Properties

Item	-40°F	Rt	450°F	1000°F	References
Yield, stn, ksi (.2% off-set)	>51.0	51.0	46.0	10.0	(5), (6), (7), (5), & (7)
Mod. of elasticity E x 10^6 psi	30.2	29.5	26.6	20.1	(8), (5), (8), (8)
Coeff. of thermal exp. α x 10^{-6} in/in/°F	7.6	-	8.56	10.8	(8), -, (8), (8)

C. Dynamic Properties

A great many materials used in shipping cask construction exhibit increased strength (yield and ultimate) with increased strain-rate. BMI-1954 (Reference 9) documents this phenomenon for a number of materials including stainless steel and depleted uranium metal. Also see References 12 and 13.

In this analysis no credit will be taken for this increased strength. However, it should be remembered that the margins of safety based on static properties will be greater under actual conditions.

IV. Force-Time Justification/Design Basis Loading

A. Introduction:

The force-time behavior of the IF-300 cask was initially defined in 1973 as part of the original design and analysis report, NEDO-10084-1. This definition, based on the correlation of fin bending tests conducted at ORNL, was obtained by dividing the cask drop height (H) by the cask stopping distance (S) thus:

$$g = \frac{H}{S}$$

This relationship was derived as follows

W.H = cask potential energy
W = cask weight
H = cask drop height

F.S = cask energy dissipation
F = fin bending force (assumed constant)
S = cask stopping distance

Since:

W.H = F.S (to dissipate all energy)

then by rearranging: $\frac{F}{W} = \frac{H}{S} = g$

NEDO-21796

STEARNS-ROGER

APPENDIX C

NEDO-10084-3
September 1984

FIGURE WITHHELD UNDER 10 CFR 2.390

FIGURE WITHHELD UNDER 10 CFR 2.390

JOB NO. DATE BY CH'K

CUSTOMER PROJECT

SUBJECT

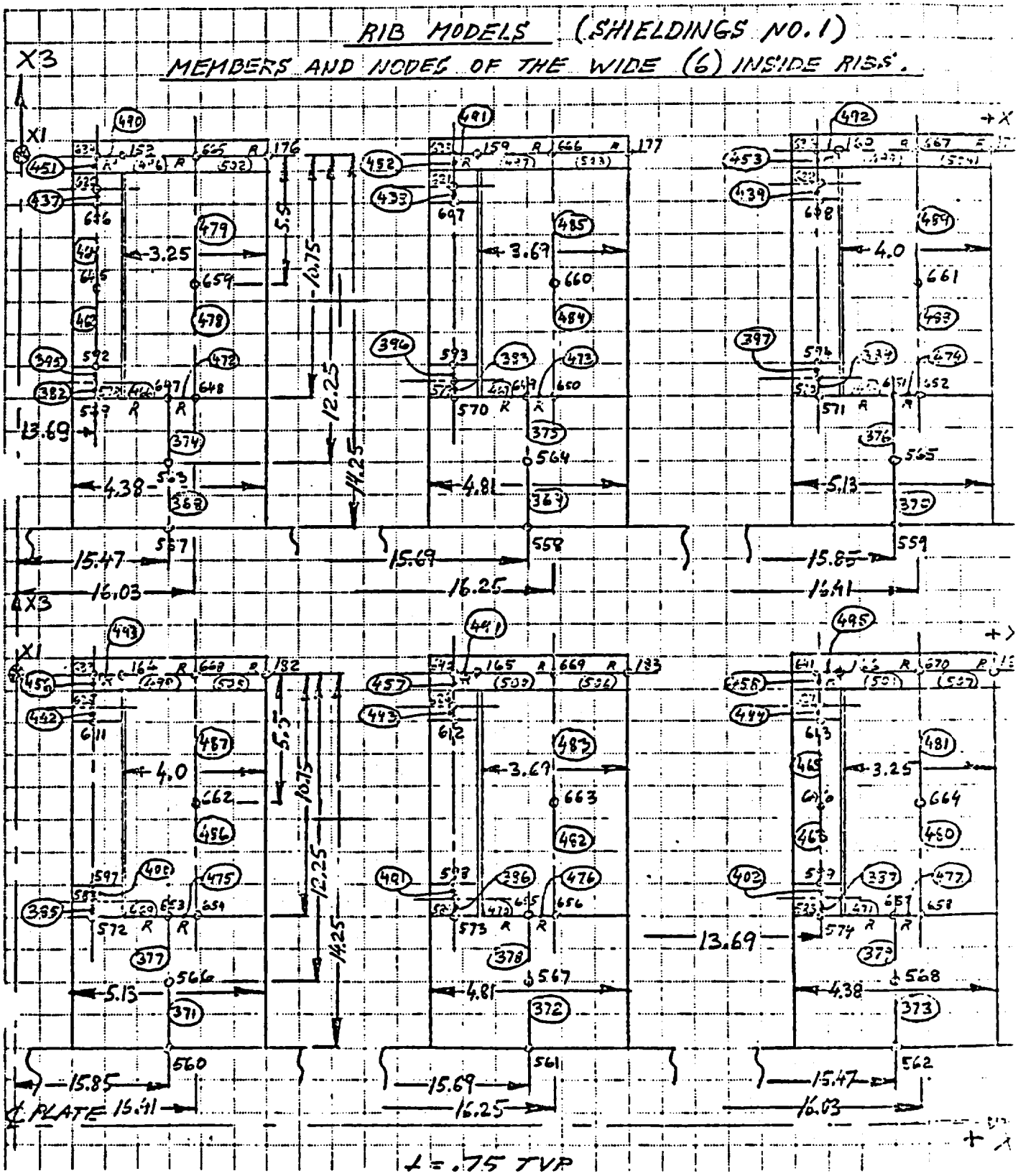

FORM 62.114
REV. 4-75

Stearns-Roger

NEDO-10084-3
September 1984

PAGE

JOB NO. DATE BY CH'K

CUSTOMER PROJECT

SUBJECT

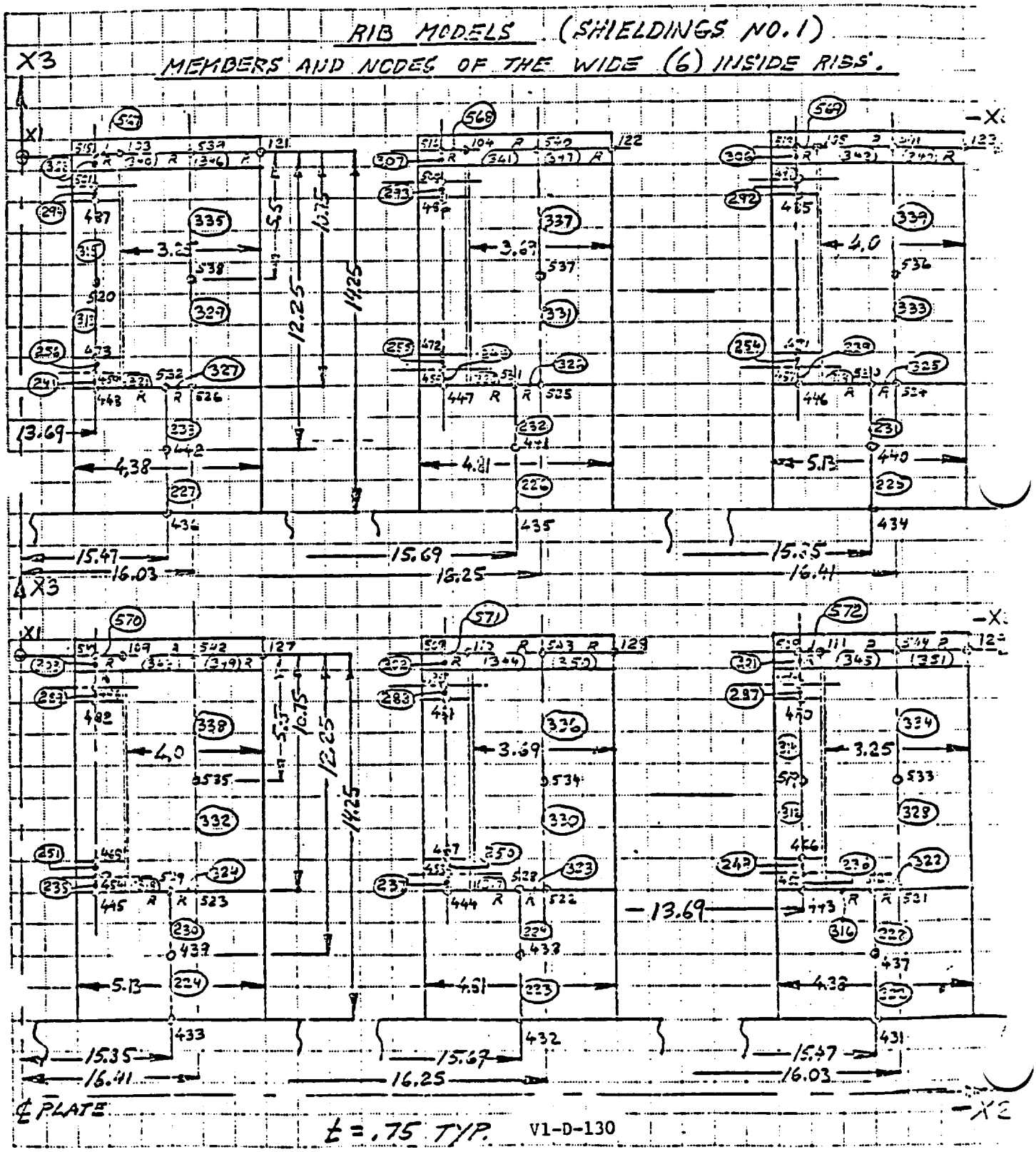

JOB C-18813-TOPPLATE SHIELDING NO. 1-2 ASSEMBLY MODEL.

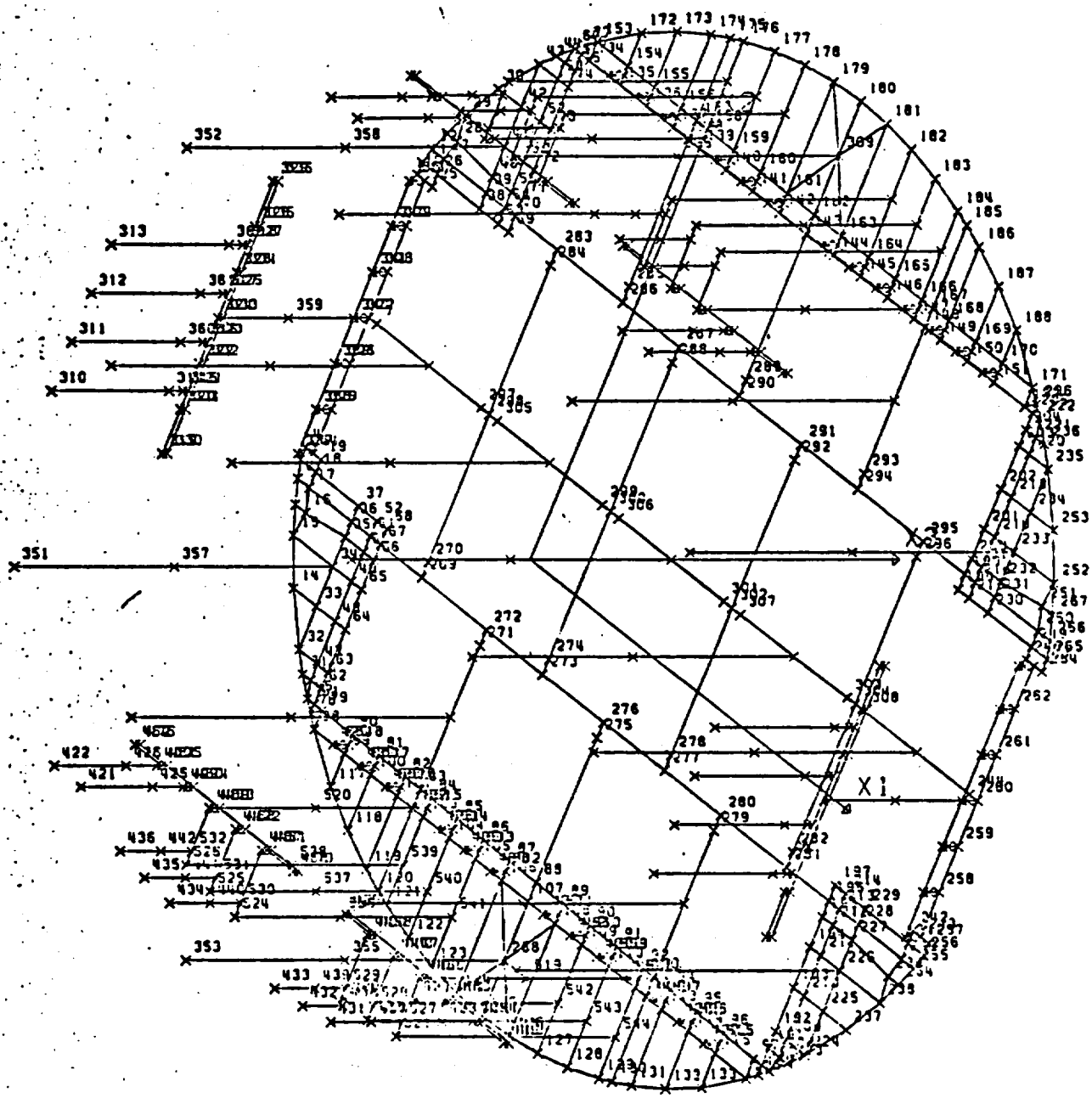

MRI/STARDYNE FINITE ELEMENT MODEL PROJECTION ON X1-X2 PLANE CASE NO. 1

V1-D-131

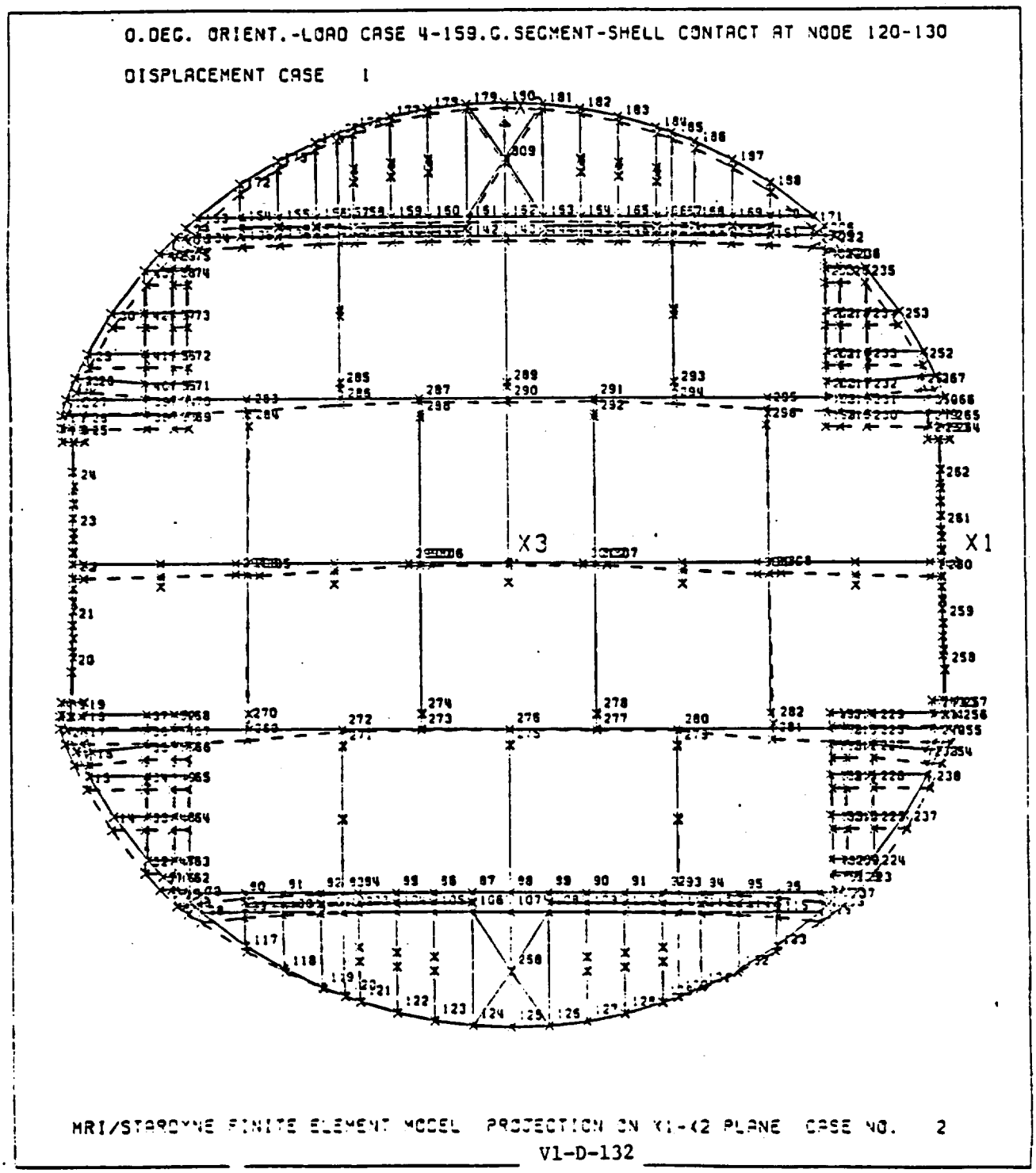
0.DEG. ORIENT.-LOAD CASE 4-159.G.SEGMENT-SHELL CONTACT AT NODE 120-130
DISPLACEMENT CASE 1
X3
X1
MRI/STARDYNE FINITE ELEMENT MODEL PROJECTION ON X1-X2 PLANE CASE NO. 2

NEDO-21796
APPENDIX E

THERMAL STRESS ANALYSIS

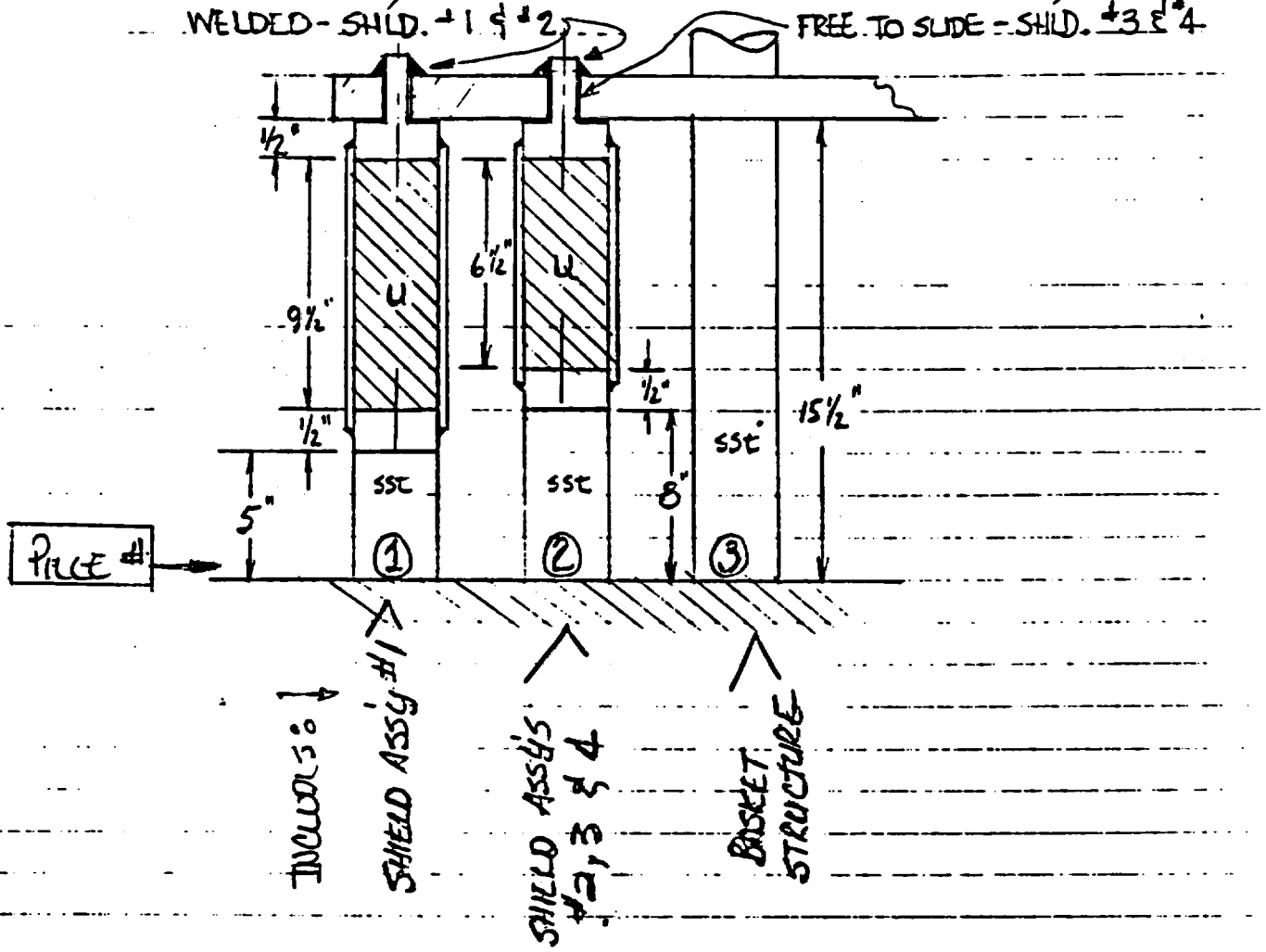

FIGURE 1

THE ABOVE FIGURE 1 REPRESENTS THE THREE TYPES OF STRUCTURES WHICH CONSTITUTE THE INTERNAL SHIELDING AND BASKET INTERFACE. THE FOLLOWING TABLES GIVE THE GEOMETRICAL PROPERTIES OF THE COMPONENTS.

TABLE 1
SHIELDING ASSY AREAS

SHIELD ASSY #	# ASSYS/BSKT	AREAS/ASSY, IN²		
		URANIUM	CLAD	SUPPORTS
1	4	11.8	1.57	18.2
2	2	11.8	1.71	5.6
3	4	3.25	0.92	1.5
4	4	2.2	0.58	1.1
Σ AREAS	14	92.6	16.9	26.4

TABLE 2
FUEL STRUCTURE AREAS

STRUCTURE	# /BASKET	AREA/ITEM, IN²	AREA/BSKT, IN²
SUPPORT POST	4	3.98	15.9
CELL DIVIDERS	9	1.50	13.5
I-BEAM SUPPORTS	2	5.75	11.5
Σ AREAS			40.9

CASE 1 - 450°F (NORMAL)

$E_U = 26.6 \times 10^6$ psi
$\alpha_U = 8.56 \times 10^{-6}$ IN/IN/°F

$E_{ST} = 26.2 \times 10^6$ psi
$\alpha_{ST} = 9.65 / 10^{-6}$ IN/IN/°F

$\Delta T = (450°F - 70°F) = 380°F$

SEE FIGURE 1:

PLACE #1 - EXAMINED CLOSET W/O RESTRAINT

$$L_{T_1} = L_{SUPP} + \Delta L_{SUPP} + L_{CAPS} + \Delta L_{CAPS} + L_{CLAD} + \Delta L_{CLAD}$$

$$= L_S + \alpha_{ST} L_S \Delta T + L_{CP} + \alpha_{ST} L_{CP} \Delta T + L_{CL} + \Delta L_{CL}$$

$$= L_S (1 + \alpha_{ST} \Delta T) + L_{CP} (1 + \alpha_{ST} \Delta T) + L_{CL} + \Delta L_{CL}$$

$$= (L_S + L_{CP})(1 + \alpha_{ST} \Delta T) + L_{CL} + \Delta L_{CL}$$

CONSIDER ΔL_{CL}

$$\Delta L_{CL} = \alpha_{ST} L_{CL} \Delta T - \frac{P_{CL} L_{CL}}{A_{CL} E_{ST}} = \alpha_U L_U \Delta T + \frac{P_{CL} L_U}{A_U E_U}$$

$L_{CL} = L_U$
$P_{CL} = P_U$ EQUILIBRIUM

$$\alpha_{ST}\Delta T - \frac{P}{A_{CL}E_{ST}} = \alpha_u \Delta T + \frac{P}{A_u E_u}$$

$$(\alpha_{ST} - \alpha_u)\Delta T = P\left(\frac{1}{A_u E_u} + \frac{1}{A_{CL} E_{ST}}\right)$$

$$P = \frac{(\alpha_{ST} - \alpha_u)\Delta T}{\left(\frac{1}{A_u E_u} + \frac{1}{A_{CL} E_{CL}}\right)}$$

Assuming: $E_u \simeq E_{CL} \simeq \bar{E}$

$$P = \frac{\bar{E}(\alpha_{ST} - \alpha_u)\Delta T}{\left(\frac{1}{A_u} + \frac{1}{A_{CL}}\right)}$$

APPLIES TO ALL PIECES.

$$P = \frac{26.4\times10^6\left[(9.65 - 8.56)\times10^{-6}\right](380)}{\left(\frac{1}{11.8} + \frac{1}{1.87}\right)}$$

$$= \frac{10935}{(.085 + .535)}$$

$$= 17{,}637\ \#$$

$$\Delta L_{CL} = (9.65\times10^{-6})(9.5)(380) - \frac{(17637)(9.5)}{(1.87)(26.4\times10^6)}$$

$$= 0.035 - .003$$

$$= 0.032\ \text{IN.}$$

$$L_{T_1} = (5 + \tfrac{1}{2} + \tfrac{1}{2})\left[1 + (9.65\times10^{-6})(380)\right] + 9.5 \pm .032$$

$$= 15.554"$$ SHIELD #1 FREE EXPANSION

PIECE #2 - EXPANDED LENGTH W/O RESTRAINT

SHIELD #2

$$L_{T_{21}} = (L_S + L_{cp})(1 + \alpha_{ST}\Delta T) + L_{Cu} + \Delta L_{Cu}$$

$$P = \frac{(\alpha_{ST} - \alpha_{Cu})\Delta T}{\left(\frac{1}{A_{Cu}} + \frac{1}{A_{Cu}}\right)} = \frac{10935}{\left(\frac{1}{11.8} + \frac{1}{1.71}\right)}$$

$$= 16332\#$$

$$\Delta L_{Cu} = (9.65\times10^{-6})(6.5)(380) - \frac{(16332)(6.5)}{(1.71)(26.4\times10^{6})}$$

$$= 0.024 - .002 = .022"$$

$$L_{T_{21}} = 9.033 + 6.5 + 0.022$$
$$= 15.555"$$

SHIELD #3

$$P = \frac{(\alpha_{ST} - \alpha_{Cu})\Delta T}{\left(\frac{1}{A_{Cu}} + \frac{1}{A_{Cu}}\right)} = \frac{10935}{\left(\frac{1}{3.25} + \frac{1}{0.92}\right)}$$

$$= 7841\#$$

$$\Delta L_{CL} = (9.65\times10^{-6})(6.5)(380) - \frac{(7841)(6.5)}{(0.92)(26.4\times10^{6})}$$

$$= .024 - .002 = .022"$$

$$L_{T2_2} = (8+1)[1+(9.65\times10^{-6})(380)] + 6.5 + .022$$

$$= 9.033 + 6.5 + .022$$

$$= 15.555"$$

SHIELD #4

$$P = \frac{10935}{\left(\frac{1}{2.2} + \frac{1}{0.58}\right)} = 5019\#$$

$$\Delta L_{CL} = (9.65\times10^{-6})(6.5)(380) - \frac{(5019)(6.5)}{(.58)(26.4\times10^{6})}$$

$$= 0.024 - .002 = 0.022"$$

$$L_{T2_3} = 9.033 + 6.5 + .022$$

$$= 15.555"$$

PIECE #3 - FREE TO EXPAND

BASKET STRUCTURE

$$L_{T_3} = L(1 + \alpha_{ST}\Delta T)$$
$$= 15.5\left[1 + (9.65\times10^{-6})(380)\right] = 15.557''$$

EFFECTS OF RESTRAINTS.

THE BASKET EXPANDS AWAY FROM THE #3 & #4 SHIELDING STRUCTURES (FREE TO SLIDE) AND IS SOMEWHAT RESTRAINED BY THE #1 & #2 SHIELDING PIECES (.003" & .002" RESPECTIVELY). IN ALL SHIELDING PIECES THE URANIUM/CLADDING INTERACTION PRODUCES STRESSES AND IN THE #1 & #2 SHIELDING PIECES THE BASKET/SHIELD STRUCTURE INTERACTION PRODUCES ADDITIONAL STRESSES.

URANIUM/CLADDING INTERACTION STRESSES:

$A_{STUD} = .110\ in^2$ ℄ 3/8" ϕ UNTHREADED

SHIELD #1 $P = 17637^{\#}$ (From Pg. 4)

$$\sigma_U = \frac{17637}{11.8} = 1495\ psi\ (t)$$

$$\sigma_{CL} = \frac{17637}{1.87} = 9432\ psi\ (c)$$

$$\sigma_{STUDS} = \frac{17637}{7\times.110} = 22.9\ ksi\ (t)$$

SHIELD #2 $P = 16332^{\#}$ (From Pg. 5)

$$\sigma_U = \frac{16332}{11.8} = 1384\ psi\ (t)$$

$$\sigma_{CL} = \frac{16332}{1.71} = 9550\ psi\ (c)$$

$$\sigma_{STUDS} = \frac{16332}{7\times.110} = 21.2\ ksi\ (t)$$

SHIELD #3 $P = 7841^{\#}$ (From Pg. 5)

$$\sigma_u = \frac{7841}{3.25} = 2413 \text{ psi (t)}$$

$$\sigma_c = \frac{7841}{0.92} = 8523 \text{ psi (c)}$$

$$\sigma_{STUD} = \frac{7841}{2 \times .110} = 35.6 \text{ ksi (t)}$$

SHIELD #4 $P = 5019^{\#}$ (From Pg. 6)

$$\sigma_u = \frac{5019}{2.2} = 2281 \text{ psi (t)}$$

$$\sigma_c = \frac{5019}{0.58} = 8653 \text{ psi (c)}$$

$$\sigma_{STUD} = \frac{5019}{1 \times .110} = 45.6 \text{ ksi (t)}$$

BASKET / SHIELD STRUCTURE INTERACTION STRESSES:
(SHIELD # 1 & #2 ONLY)

THE MAXIMUM INTERFERENCE IS .003", THE MINIMUM IS .002". FOR THIS APPROXIMATION THE MAXIMUM VALUE OF .003" WILL BE USED.

ΔL_T = MAX. INTERFERENCE
= .003"

$$\Delta L_T = \Delta L_{ST} + \Delta L_u + \Delta L_{SUPP}$$

$$= \left(\frac{PL}{AE}\right)_{ST} + \left(\frac{PL}{AE}\right)_u + \left(\frac{PL}{AE}\right)_{SUPP}$$

P IS APPROXIMATELY THE SAME FOR ALL COMPONENTS

ALSO $E = \left(\frac{26.4 + 26.6}{2}\right) \times 10^6$

$= 26.5 \times 10^6$ psi

$.003 = \frac{P}{E}\left[\left(\frac{.45}{40.9}\right) + \left(\frac{8}{6 \times 11.8}\right) + \left(\frac{7.5}{4 \times 18.2 + 2 \times 5.6}\right)\right]$

$= \frac{P}{26.5 \times 10^6}\left(0.38 + .11 + 0.09\right)$

$= 2.2 \times 10^{-8} P$

$P = 137068$ #

STRESSES:

$\sigma_{ST} = \frac{137068}{40.9} = 3351$ psi

$\sigma_U = \frac{137068}{6 \times 11.8} = 1936$ psi

$\sigma_{SUPP} = \frac{137068}{4 \times 18.2 + 2 \times 5.6} = 1632$ psi

$\sigma_{STUDS} = \frac{137068}{.0775[(4)(9) + (2)(7)]}$

$= 35372$ psi

.110

24921

ACTS ON UNTHREADED PORTION OF STUD

COMBINED STRESS SUMMARY @ T = 450°F

TABLE 3

COMPONENT	U/LOAD INT.	BOLT/SHLD INT.	COMBINED[1] OR MAX.
SHELL #1			
URANIUM	1.5 KSI	1.9 KSI	3.4 KSI
CLADDING	9.4	~0	9.4
RIBS	0	1.6	1.6
STUDS	(0) 20.9	(35.4) 24.9	(35.4) 24.9
SHELL #2			
URANIUM	1.4 KSI	1.8 KSI	3.3 KSI
CLADDING	9.6	~0	9.6
RIBS	0	1.6	1.6
STUDS	(0) 21.2	(35.4) 24.9	(35.4) 24.9
SHELL #3			
URANIUM	2.4 KSI	1.9 KSI	4.3 KSI
CLADDING	8.5	~0	8.5
RIBS	0	1.6	1.6
STUDS	(0) 35.6	0	(0) 35.6
SHELL #4			
URANIUM	2.3 KSI	1.9 KSI	4.2 KSI
CLADDING	8.7	~0	8.7
RIBS	0	1.6	1.6
STUDS	(0) 45.6	0	(0) 45.6
BASE SHELL	0	3.4 KSI	3.4 KSI

(1) THE STUD STRESS DO NOT COMBINE FOR THEY ACT ON DIFFERENT PARTS OF THE STUD AND THESE PARTS ARE SEPARATED BY WELDS. THUS THE PORTIONS OF THE STUDS ACT AS SEPARATE MEMBERS FOR STRESS PURPOSES.

CASE 2 - 1000°F (POST DROP, POST FIRE ACCIDENT)

$E_U = 20.1 \times 10^6$ psi
$\alpha_U = 10.8 \times 10^{-6}$ IN/IN-°F

$E_{ST} = 22.5 \times 10^6$ psi
$\alpha_{ST} = 10.1 \times 10^{-6}$ IN/IN-°F

$\Delta T = (1000 - 70) = 930$°F
$\bar{E} = 21.3 \times 10^6$ psi

PIECE #1 SEE FIGURE 1
EXPANDED LENGTH W/O RESTRAINT & CASK/U INTERACTION STRESSES.

$$P = -\frac{\bar{E}(\alpha_{ST} - \alpha_U)\Delta T}{\left(\frac{1}{A_U} + \frac{1}{A_{CL}}\right)}$$

$$= -\frac{(21.3)(10.1 - 10.8)(930)}{(.085 + .535)} = 22365^{\#}$$

$$\Delta L_U = (10.1 \times 10^{-6})(9.5)(930) + \frac{(22365)(9.5)}{(1.87)(21.3 \times 10^6)}$$

$$= .089 + .005 = .094''$$

$$L_{T_1} = (16)[1 + (10.1 \times 10^{-6})(930)] + 9.5 + .094$$

$$= 15.650''$$

$$\sigma_U = \frac{22365}{11.8} = 1895 \text{ psi}$$

$$\sigma_L = \frac{22365}{\text{[illegible]}} = \text{[illegible]}$$

Piece #2

Shield #2

$$P = \frac{(10.1-10.8)(930)(21.3)}{\left(\frac{1}{11.8}+\frac{1}{1.71}\right)} = 20710^{\#}$$

$$\sigma_u = \frac{20710}{11.8} = 1755 \text{ psi}$$

$$\sigma_{cl} = \frac{20710}{1.71} = 12111 \text{ psi}$$

$$\Delta L_a = (10.1\times10^{-6})(6.5)(930) + \frac{(20710)(6.5)}{(1.71)(21.3\times10^{6})}$$

$$= .061 + .004 = .065"$$

$$LT_2 = 9\left[1+(10.1\times10^{-6})(930)\right] + 6.5 + .065$$

$$= 15.650"$$

Shield #3

$$P = \frac{(10.1-10.8)(930)(21.3)}{\left(\frac{1}{3.25}+\frac{1}{0.92}\right)} = 9943^{\#}$$

$$\sigma_u = \frac{9943}{3.25} = 3059 \text{ psi}$$

$$\sigma_{cl} = \frac{9943}{0.92} = 10805 \text{ psi}$$

$$\Delta L_a = (10.1\times10^{-6})(6.5)(930) + \frac{(9943)(6.5)}{(0.92)(21.3\times10^{6})}$$

$$= .061 + .003 = .064$$

$$L_{T_2} = 9[1+(10.1\times10^{-6})(930)]+6.5+.064$$
$$= 15.649"$$

SHIM #4

$$P = \frac{(10.1-10.8)(930)(21.3)}{\left(\frac{1}{5.2}+\frac{1}{0.58}\right)} = 6365\#$$

$$\sigma_u = \frac{6365}{2.2} = 2893 \text{ psi}$$

$$\sigma_a = \frac{6365}{0.58} = 10974 \text{ psi}$$

$$\Delta L_a = (10.1\times10^{-6})(6.5)(930)+\frac{(6365)(6.5)}{(0.58)(21.3\times10^{6})}$$
$$= .061+.003 = .064"$$

$$L_{T_4} = 15.649"$$

PIECE #3 EXPANDED LENGTH W/O RESTRAINT

$$L_{T_3} = 15.5\,(10.1\times10^{-6})(930)+15.5$$
$$= 15.646"$$

STRUCTURE / SHIELDING INTERACTION STRESSES.

THE MAXIMUM INTERFERENCE IS .004"
ALL SHIELD PIECES ARE EFFECTED IN COMPRESSION.

$$\Delta L_T = \Delta L_{ST} + \Delta L_U + \Delta L_{SUPP} = .004$$

$$\frac{P}{E}\left[\left(\frac{L_{ST}}{A_{ST}}\right)+\left(\frac{L_U}{A_U}\right)+\left(\frac{L_{SUPP}}{A_{SUPP}}\right)\right] = .004"$$

$$\frac{P}{21.3\times10^6}\left[\left(\frac{15.5}{40.9}\right)+\left(\frac{8}{6\times11.8+4\times3.25+4\times2.2}\right)+\right.$$

$$\left.+\left(\frac{7.5}{4\times18.2+2\times5.6+4\times1.5+4\times1.1}\right)\right] = .004$$

$$\frac{P}{21.3\times10^6}\left(.38+.09+.08\right) = .004$$

$$P = 154909\#$$

STRESSES:

$$\sigma_{ST} = \frac{154909}{40.9} = 3788 \text{ psi}$$

$$\sigma_U = \frac{154909}{92.6} = 1673 \text{ psi}$$

$$\sigma_{SUPP} = \frac{154909}{94.4} = 1641 \text{ psi}$$

COMBINED STRESS SUMMARY @ T=1000°F

TABLE 4

COMPONENT	U/CLAD INT.	BKT/SHLD. INT.	COMB'D.
SHIELD #1			
URANIUM	1.9 ksi	1.7 ksi	3.6 ksi
CLADDING	12.0	~0	12.0
RIBS	0	1.6	1.6
SHIELD #2			
URANIUM	1.8 ksi	1.7 ksi	3.5 ksi
CLADDING	12.1	~0	12.1
RIBS	0	1.6	1.6
SHIELD #3			
URANIUM	3.1	1.7 ksi	4.8 ksi
CLADDING	10.8	~0	10.8
RIBS	0	1.6	1.6
SHIELD #4			
URANIUM	2.9	1.7 ksi	4.6 ksi
CLADDING	11.0	~0	11.0
RIBS	0	1.6	1.6
BKT. STRUCT.	0	3.8 ksi	3.8 ksi

SEE FIGURE 1

CASE 3 — $-40^{\circ}F$ (COLD CONDITION)

$E_U = 30.2 \times 10^6$ PSI
$\alpha_U = 7.65 \times 10^{-6}$ IN/IN/°F

$E_{ST} = 29.6 \times 10^6$ PSI
$\alpha_{ST} = 8.4 \times 10^{-6}$ IN/IN/°F

$\Delta T = 70 + 40 = 110^{\circ}F$
$E = 29.6 \times 10^6$ PSI

PIPE #1 - SHROUD #1

From previous case

$$P = \frac{E(\alpha_{ST} - \alpha_U)\Delta T}{\left(\frac{1}{A_U} + \frac{1}{A_{CL}}\right)}$$

$$= \frac{(29.6)(8.4 - 7.65)(110)}{\left(\frac{1}{11.8} + \frac{1}{1.87}\right)}$$

$$= 3542^{\#}$$

$$\Delta L_{CL} = (8.4 \times 10^{-6})(95)(110) - \frac{(3542)(95)}{(1.87)(29.6 \times 10^6)}$$

$$= .009 - .0007 = .0083$$

$$L_1 = 6\left[1 - (8.4 \times 10^{-6})(110)\right] + 9.5 - .0083$$

$$= 15.486''$$

PIECE #2 - SHIELD #2

$$P = \frac{(29.6)(0.75)(110)}{\left(\frac{1}{11.8} + \frac{1}{1.71}\right)} = \frac{2442}{(.085 + .585)}$$

$$= 3645\ \#$$

$$\Delta L_{c_2} = .009 - \frac{(3645)(6.5)}{(1.71)(29.6\times10^6)}$$

$$= .009 - .0005 = .0085$$

$$L_{T_2} = 9\left[1 - (8.4\times10^{-6})(110)\right] + 6.5 - .0085$$

$$= 15.483"$$

- SHIELD #3 -

$$P = \frac{2442}{\left(\frac{1}{3.75} + \frac{1}{0.92}\right)} = 1751\ \#$$

$$\Delta L_{c_3} = .005 - \frac{(1751)(6.5)}{(.92)(29.6\times10^6)}$$

$$= .005 - .0004 = .0086$$

$$L_{T_3} = 9\left[1 - (8.4\times10^{-6})(110)\right] + 6.5 - .0086$$

$$= 15.483"$$

— SHIELD #4 —

$$P = \frac{3442}{\left(\frac{1}{22} + \frac{1}{.59}\right)} = 1121\ \#$$

$$\Delta L_{cu} = .009 - \frac{(1121)(6.5)}{(.92)(29.6\times10^6)}$$

$$= .009 - .0003 = .0087$$

$$L_{T_{24}} = 9[1-(8.4\times10^{-6})(110)]+6.5-.0087$$

$$= 15.483"$$

PIECE #3 - BOLT STRUCTURE

$$L_{one} = 15.5\left[1-(8.4\times10^{-6})(110)\right]$$

$$= 15.486"$$

Summary of Lockups (expansion w/o restraint)
TABLE 5

COMPONENT	COLD LOCKUP
SHIELD 1	15.486
SHIELD 2	15.483
SHIELD 3	15.483
SHIELD 4	15.493
B/L STRUCTURE	15.496

AS IS SEEN IN TABLE 5 THE MAXIMUM INTERFERENCE IS .003" BETWEEN THE BASKET STRUCTURE & SHELL #2.

$$\Delta L = \Delta L_{ST} + \Delta L_u + \Delta L_{supp} = .003"$$

$$= \frac{P}{E}\left[\left(\frac{L}{A}\right)_{ST} + \left(\frac{L}{A}\right)_u + \left(\frac{L}{A}\right)_{supp}\right] = .003$$

$$= \frac{P}{29.6\times10^6}\left[\left(\frac{15.5}{40.9}\right) + \left(\frac{65}{2\times11.8}\right) + \left(\frac{9}{2\times5.6}\right)\right] = .003$$

$$= \frac{P}{29.6\times10^6}\left[0.38 + .28 + 0.8\right] = .003$$

$$P = 60822\#$$

BASKET/STRUCTURE INTERACTION STRESSES

$$\sigma_{ST} = \frac{60822}{40.9} = 1487 \text{ psi}$$

$$\sigma_u = \frac{60822}{2\times11.8} = 2577 \text{ psi}$$

$$\sigma_{supp} = \frac{60822}{2\times5.6} = 5431 \text{ psi}$$

$$\sigma_{studs} = \frac{60822}{14\times0.0175} = 56.1 \text{ ksi}$$

URANIUM/CLADDING INTERACTION
STRESS DUE TO DIFFERENTIAL EXPANSION.

SHIELD #1

$P = 3542^{\#}$ (FROM PAGE 16)

$\sigma_u = \frac{3542}{11.5} = 334$ psi (C)

$\sigma_a = \frac{3542}{1.87} = 1893$ psi (T)

SHIELD #2

$P = 3645^{\#}$ (FROM PAGE 17)

$\sigma_u = \frac{3645}{11.8} = 309$ psi (C)

$\sigma_a = \frac{3645}{1.71} = 2132$ psi (T)

SHIELD #3

$P = 1751^{\#}$ (FROM PAGE 17)

$\sigma_u = \frac{1751}{3.25} = 539$ psi (C)

$\sigma_a = \frac{1751}{0.02} = 9013$ psi (T)

SHELL #4

$P = 1121^{\#}$

$\sigma_u = \frac{1121}{2.2} = 510$ psi (C)

$\sigma_{cc} = \frac{1121}{0.58} = 1933$ psi (T)

Combined Stress Summary @ T = 40°F

TABLE 6

Component	U/Cold Inst.	Beltline/Shut. Inst.	Combined
Shell #1			
Uranium	0.3 ksi	~0	0.3 ksi
Cladding	2.1	~0	2.1
Ring	0	~0	0
Stud	0	~0	0
Shell #2			
Uranium	0.3 ksi	2.6 ksi	2.9
Cladding	2.1	~0	2.1
Ring	0	5.4	5.4
Stud	0	56.1 *	56.1 *
Shell #3			
Uranium	0.5 ksi	0	0.5 ksi
Cladding	1.9	0	1.9
Ring	0	0	0
Stud	0	0	0
Shell #4			
Uranium	0.5	0	0.5 ksi
Cladding	1.9	0	1.9
Ring	0	0	0
Stud	0	0	0
Basket Structure	0	1.5 ksi	1.5 ksi

* THIS VALUE CANNOT BE REACHED SINCE THE THERMAL STRESS WILL SELF-RELIEVE AS S_{YD} IS REACHED (S_{YD} = 33.5 ksi)

STRESS ANALYSIS OF SHIELDING UNDER END DROP CONDITIONS.

A. TOP END DROP (HEAD)

DESIGN LOAD = 280 "G" x DLF
= 280 x 2.0
= 560 "G"

FOR THIS ANALYSIS THE MAXIMUM DLF (2.0) WILL BE USED.

SHIELD ASSY #1

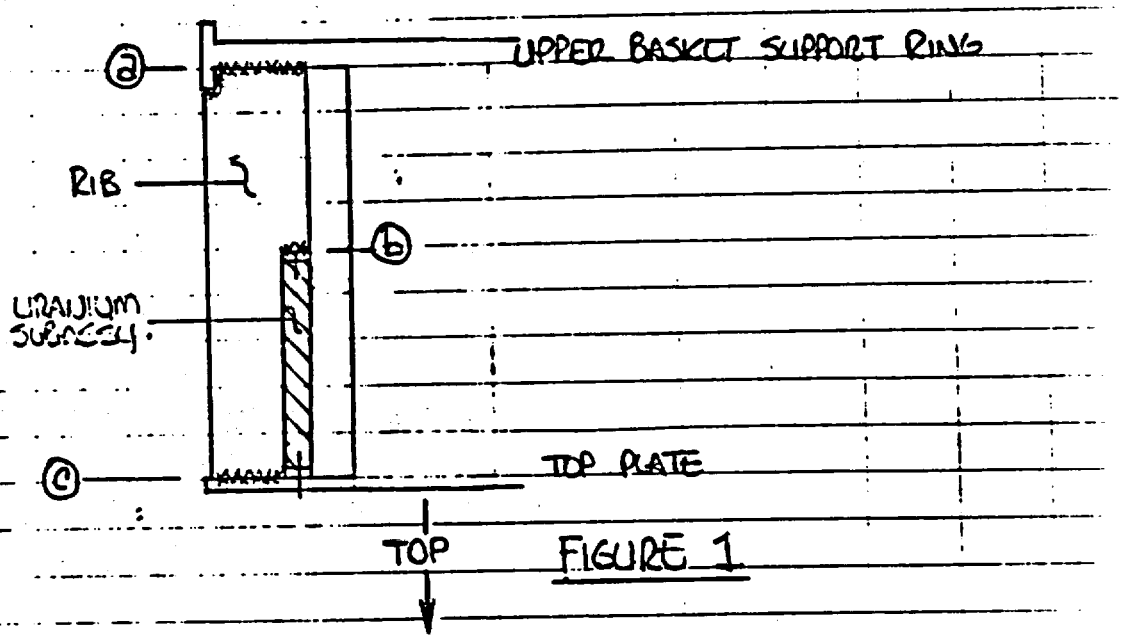

FIGURE 1

SHIELD ASSY. # 1 (CONT.)

WEIGHTS:

CLADDING	= 9 #
URANIUM	= 76
RIBS	= 47
	132 #

a. RIB-TO-SUPPORT RING (NO CREDIT FOR TOP PLATE).

FULL PULLTATION WILD

DESIGN LOAD = 132 # × 560

= 73.9 K

AREA = (1")(2)(2") + (3)(4.9375)(3/4")

= 15.1 IN²

TENSILE STRESS = 73.9 / 15.1 = 4.9 KSI ←

b. RIB-TO-SHIELDING SUBASSY.

SINCE THE SHIELDING SUBASSY IS CAPTURED BETWEEN THE UPPER BOLT SUPPORT RING AND THE TOP PLATE THE STRESS AT (b) IS NEGLIGIBLE.

C. SHIELD/RIB-TO-TOP PLATE.

i. THE RIB-TO-TOP PLATE WELD MUST BE CAPABLE OF TRANSMITTING THE SHIELD SUBASSY LOAD IF WELD AT (b) OR THE STUD/CLAD SHEAR AT JUST BELOW (b).

$F = (9^{\#} + 76^{\#})560$

$= 47.6$ KIPS

WELD AREA $= \frac{\pi}{4}[(3)(3.8125")]$

$= 8.6 in^2$

WELD STRESS $= \frac{47.6}{8.6} = 5.5$ KSI

ii. THE TOP PLATE MUST BE CAPABLE OF SUSTAINING THE SHIELDING SUBASSY IN SHEAR

$F = 47.6$ KIPS

SHEAR AREA = ONE SIDE LENGTH x THK

$= 11.3125 \times 0.5$

$= 5.7 in^2$

SHEAR STRESS $= \frac{47.6}{5.7} = 8.4$ KSI

SHEAR STN 304 $= .577 \times 20.1 = 11.6$ KSI

SHELL ASSY #2

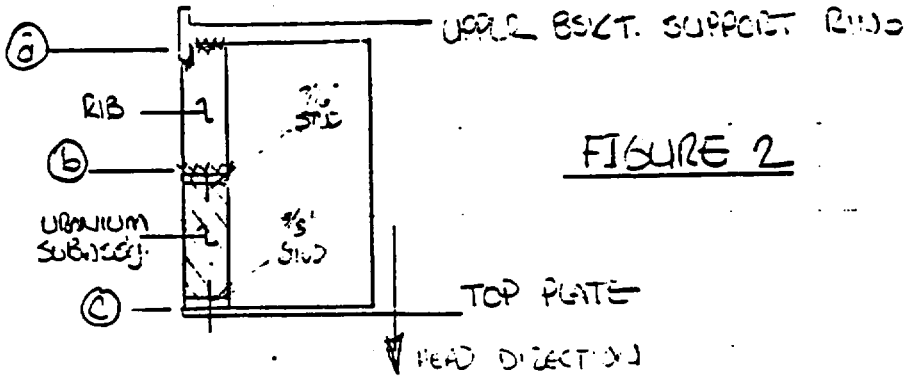

FIGURE 2

WEIGHTS:

CLADDING	= 7#
URANIUM	= 52#
RIBS	= 11#
	70#

6. SUPPORT RIBS-TO-SUPPORT RING. (NO TOP PLATE CIRCUIT.

FULL PENETRATION WELDS.

DESIGN LOAD = 70 × 500
= 35.2 KIPS

WELD AREA = $\frac{3}{4}[(2)(1.5)+(2)(2)]$

= $5.25 in^2$

TENSILE STRESS = $\frac{35.2}{5.25}$ = 7.5 KSI

b. SUPPORT RIB-TO-URANIUM SUBASSY (NO TOP PLATE CREDIT)

$F = (52+7)560 = 33$ KIPS

WELD AREA $= 4 \times 1.125 \times .75$
$= 3.375\ in^2$

$\text{STRESS} = \frac{33.0}{3.375} = 9.8$ KSI

c. STUD AT CLADDING

CLADDING WELD AREA $= .707\ t\ell$
$= .707\,[(.06)(24)+(.0675)(2)]$
$= 1.28\ in^2$

STUD AREA $= 7 \text{ STUDS} \times .0775\ in^2$
$= .542\ in^2$

TOP PLATE SHEAR AREA $= .875 \times .5 \times 2$
$= .875\ in^2$

TOTAL AREA $= 1.29 + .542 + .875$
$= 2.70\ in^2$

$\text{STRESS} = \frac{30.1\ K}{2.70} = 11.1$ KSI

SHIELD ASSY #3

SEE FIGURE 2 FOR TYPICAL LAYOUT.
BUT 7/ STUDS TOP & BOTTOM.

WEIGHTS:

CLADDING = 3#
URANIUM = 14#
RIB = 3#
20#

a. SUPPORT RIB-TO-SUPPORT RING

DESIGN LOAD = 20# X 560
= 11.2 KIPS

WELD AREA = 2" X 0.75
= 1.5 IN²

WELD STRESS = $\frac{11.2}{1.5}$ = 7.5 KSI ←

b. SUPPORT RIB-TO-URANIUM SUBASSY

DESIGN LOAD = (3+14)(560)
= 9.5 KIPS

WELD AREA = 1.125 X 0.75
= .843 IN²

WELD STRESS = $\frac{9.5}{.843}$ = 11.3 KSI ←

(NO CREDIT FOR TOP PLATE SHEAR)

C. STUD AND CLADDING.

$F = 9.5$ kips

CLAD WELD AREA $= .707[(.06)(7.5) + (.182)(2)]$
$= 0.6\ in^2$

NO. STUDS = 2 (3/8" studs)
STUD AREA $= 2 \times .0775$
$= .16\ in^2$

$$\text{STRESS} = \frac{9.5}{0.6 + .16} = 12.5 \text{ ksi}$$

(NOTE: NO CREDIT TAKEN FOR SHEAR IN TOP PLATE).

SHIELD ASSY. #4

SEE FIGURE 2 FOR TYPICAL LAYOUT. BUT W/STUDS TOP AND BOTTOM.

WEIGHTS:

CLADDING	$= 1.8^{\pm}$
URANIUM	$= 9.7^{\pm}$
RIBS	$= 1.3^{\#}$
	$12.8^{\#}$

a. SUPPORT RIB-TO-SUPPORT RING

DESIGN LOAD $= 12.8 \times 560$
$= 7.2$ kips

FULL PENETRATION WELD

$$\text{WELD AREA} = \frac{3}{5} \times \frac{3}{4} \times 2$$
$$= 0.5625 \text{ in}^2$$

SHEAR AREA IN TOP PLATE

$$L = .875'' + 2.25'' + .75$$
$$= 3.875$$

$$A = 3.875'' \times 0.5$$
$$= 1.9 \text{ in}^2$$

$$\text{TOTAL STRESS AREA} = 0.6 + 1.9$$
$$= 2.5 \text{ in}^2$$

$$\text{STRESS} = \frac{7.2^k}{2.5}$$
$$= 2.9 \text{ ksi} \leftarrow$$

b. SUPPORT RIB -TO- SHIELDING SURFACE

$$\text{WELD LOAD} = (1.8'' + 9.7'')\,560$$
$$= 6.44 \text{ kips}$$

$$\text{WELD AREA} = \frac{3}{4} \times \frac{3}{4} \times 2$$
$$= 1.125 \text{ in}^2$$

From (a), top plate shear area = 1.9 in²

Total shear area = 1.9 + 1.125
= 3.025

Shear stress = $\frac{6.44}{3.025}$
= 2.1 ksi

C. Studs, clad and top plate

Clad weld area = .707 [(.06)(5) + (.19)(2)]
= 0.48 in²

3/8 ϕ stud area = 0.0775 in²

Top plate shear area = 1.9 in²

Σ shear areas = 2.46 in²

Stress = $\frac{6.44 \text{ kips}}{2.46 \text{ in}^2}$

= 2.6 ksi

B. Bottom End Drop

Design Load = 287 "G" x DLF
= 287 x 2.0
= 574 "G"

For this analysis a DLF = 2.0, the maximum possible, will be used.

In all cases the components will be in compression. The minimum cross sections of the support ribs are the critical locations and only these will be analyzed.

Shell Assy #1 (See Page 1)

For conservatism assume all 5 ribs have the same x-sect. area as the smallest.

$$A = 1.125 \times .75 \times 5 \text{ ribs}$$
$$= 4.2 \text{ in}^2$$

$$F = 85 \times 574$$
$$= 48.8 \text{ kips}$$

$$\sigma_{comp} = \frac{48.8 k}{4.2 in^2} = 11.6 ksi \ (C) \longleftarrow$$

SHIELD ASSY #2

$A = 1.125 \times .75 \times 4$
$= 3.4\ in^2$

$F = 59^{\#} \times 574$
$= 33.9\ kips$

$STRESS = \frac{33.9}{3.4} = 10\ ksi\ (c)$

SHIELD ASSY #3

$A = 1.125 \times .75$
$= .84\ in^2$

$F = 17^{\#} \times 574$
$= 9.8\ kips$

$STRESS = \frac{9.8}{0.84} = 11.6\ ksi\ (c)$

SHIELD ASSY #4

$A = 0.75 \times 0.75 \times 2$
$= 1.125\ in^2$

$F = 11.5^{\#} \times 574$
$= 6.6\ kips$

$STRESS = \frac{6.6}{1.125} = 5.9\ ksi\ (c)$

12

Hawker Siddeley Canada LTD
ORENDA DIVISION
Ref: 3368

APPENDIX

IMPACT TESTING OF CHARPY V-NOTCH TEST SPECIMENS

FOR

ELDORADO NUCLEAR LIMITED

RECEIVED
NOV 30 1976
ROSS

1.0 MATERIAL

Six (6) Charpy V-Notch Impact Test Specimens were submitted to the Materials Services Laboratory to determine impact strength.

2.0 CHARPY IMPACT TEST

The results of impact testing at -40°F on the six (6) test specimens were as follows:-

IDENTIFICATION	MATERIAL	IMPACT STRENGTH (FT/LBS)
368A	Depleted Uranium	8.0
368A	" "	9.5
368A	" "	9.0
385B	" "	9.0
385B	" "	6.0
385B	" "	9.0.

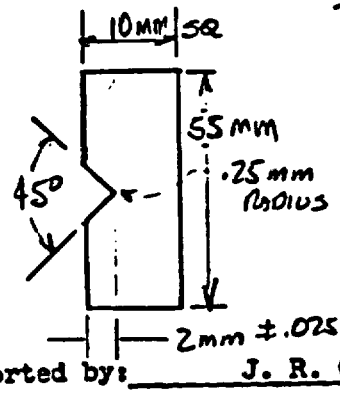

CHARPY V-NOTCH
PER
ASTM E23

Reported by: J. R. Geldart

Approved by: J. B. Mrozek
Materials Services Supervisor

FIGURE WITHHELD UNDER 10 CFR 2.390

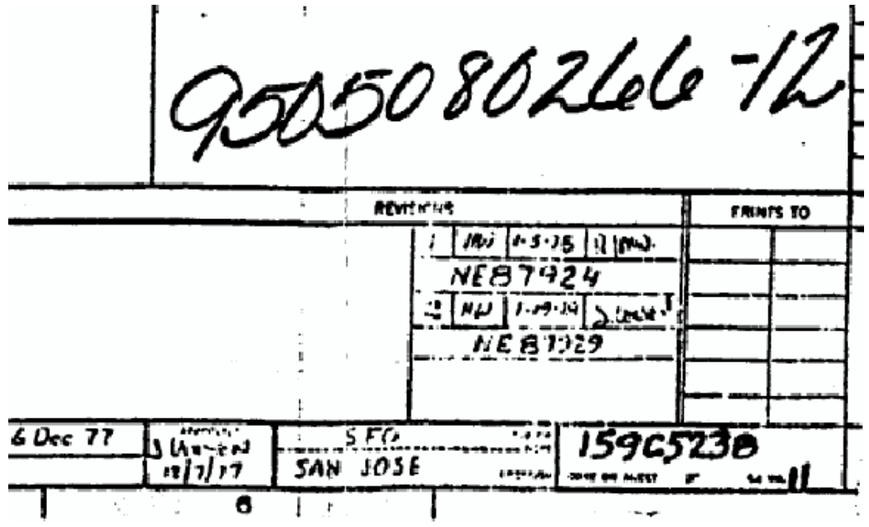

FIGURE WITHHELD UNDER 10 CFR 2.390

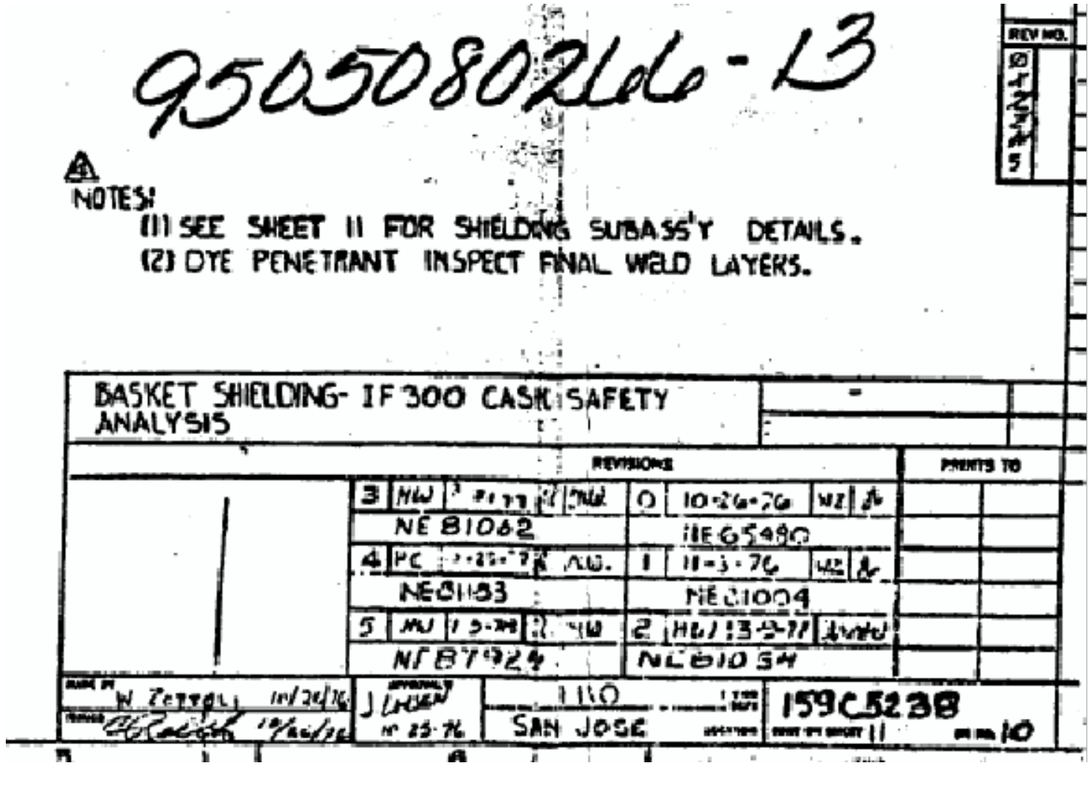

FIGURE WITHHELD UNDER 10 CFR 2.390

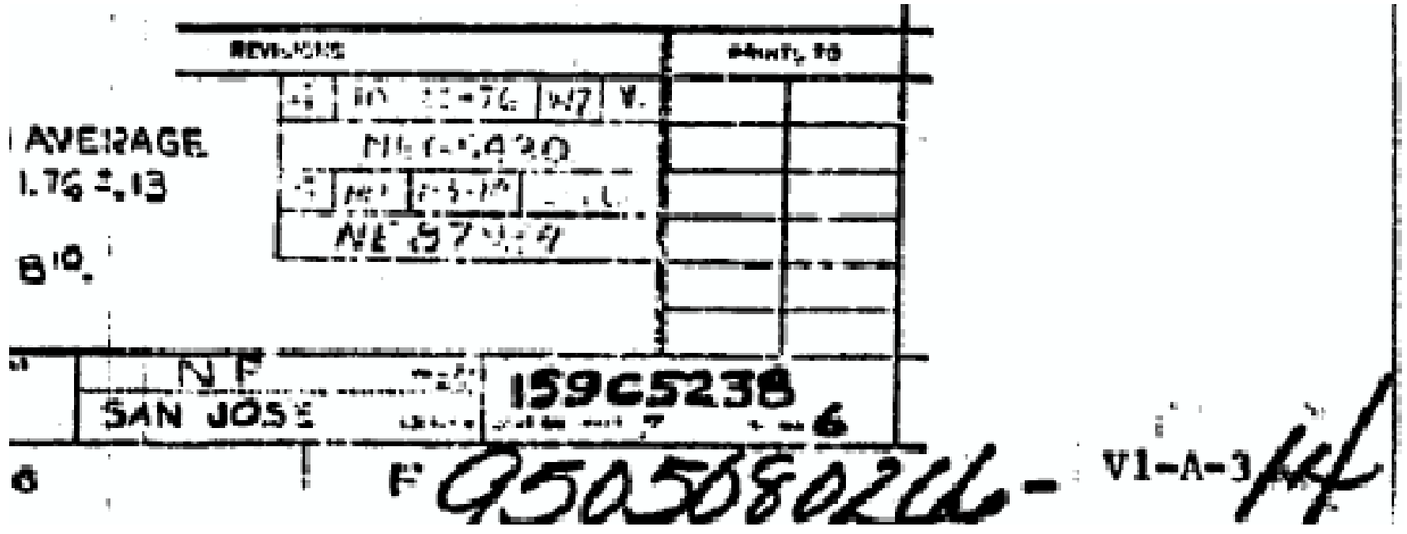

APPENDIX V-2

STRUCTURAL ANALYSES OF IF-300 CASK FOR SHIPMENT OF GROUP II BWR AND PWR FUELS

TABLE OF CONTENTS

TABLE OF CONTENTS continued

1. INTRODUCTION[1]

This report presents the results of the analyses of the IF-300 cask for shipment of current generation BWR and PWR fuels. The cask was analyzed for the limiting standard accident cases, viz., 30-foot side drop, and 30-foot end drop. Preliminary analyses were performed to investigate the influence of variation in parameters on the response of the cask-fuel rod system. This included the investigation of the influence of the depleted uranium shielding on the response of fuel rods. At the end of the detailed analyses for the three accident cases, secondary analyses were also performed to further investigate the influence of the variation of additional parameters (which were considered to be of importance on the basis of the detailed analyses) on the response of the system. This included the investigation of the influence of the depleted uranium shielding on the response of fuel rods. At the end of the detailed analyses for the two accident cases, secondary analyses were also performed to further investigate the influence of the variation of additional parameters (which were considered to be of importance on the basis of the detailed analyses) on the response of the system. This included the investigation of the influence of the following effects on the response of the fuel rods: the flexural effects for the end drop case, and the effects of the cask ovalling, and basket spacer disk in-plane vibrations for the side drop case.

A description of the cask-fuel rod system is presented in Chapter 2. Assumptions and model properties used in the analyses for the side and end drop cases are presented in Chapter 3. Chapter 4 describes the analyses for the 30-foot side drop case, and includes a description of the analytical model, the analysis procedures, and the results. Chapter 5 presents a similar description for the 30-foot end drop case.

---

[1] Material in these sections has been developed from the work performed by Engineering Design Analysis Company (EDAC) under contract to General Electric Co.

A general discussion of results, comparison of these results against failure test results, and conclusions are presented in Chapter 6. Appendix A presents a discussion of preliminary and secondary analyses.

2. DESCRIPTION OF THE CASK-FUEL ROD SYSTEM

CASK

The IF-300 cask body, as shown in Figure 2-1, consists of an inner cylinder of stainless steel, 37.5-inch inside diameter with 0.5-inch thick wall, having its bottom end sealed with a 1.5-inch thick stainless steel plate. The upper end is welded to the closure flange. Surrounding the inner cavity is the depleted uranium metal shielding material. This heavy metal assembly consists of annular castings, each with a 38.5-inch inner diameter and a 4-inch thick wall. Sections are interlocked, end to end, using an overlapping joint which holds the stack together and prevents radiation streaming. This assembly is shrink-fitted to the inner cavity to ensure good thermal contact for heat transfer purposes. The bottom end shield is a 3.75-inch thick uranium metal casting. The outer body shell is also a stainless steel cylinder with a 46.5-inch inner diameter and a 1.5-inch thick wall. The outer shell is also shrink-fitted to the uranium to ensure good heat transfer characteristics.

The cylindrical portion of the cask is encircled by a thin-walled, corrugated stainless steel water jacket, extending axially from the upper valve box to a point slightly above the cask bottom, thus masking the active fuel zone. Welded to the outer shell outside diameter are four 7-inch high and 1.25-inch thick circumferential fins. These rings serve as lifting rings and impact fins. They are also used to support the water jacket sections. The overall length of the cask body from fins to flange face is 184 3/16 inches. The cask cavity depth from the flange face is 169.5 inches. The flange is a stainless steel machined forging whose face contains 32 equally-spaced studs, each of which is 1.75 inches in diameter. The studs protrude 6.75 inches from the face and are made of 17 4PH stainless steel.

CASK HEADS

The IF-300 cask can be equipped with two different heads. These heads provide two alternate cask cavity lengths to match the particular dimensions of the fuel being shipped. With the short head in place, the overall cavity length is 169.5 inches. The long head increases the cavity length to 180.25 inches. Most PWR fuel is shipped using the short head. BWR fuel necessitates using the extended head. Shielding in the head consists of three inches of uranium. The outer shell and flange form a single stainless steel machined casting. A circular stainless steel plate is welded in place to form the head cover. Each head has 32 radially-mounted fins on the end, 16 of which protrude 9.5 inches from the surface. Because of variation in fuel lengths, it is necessary to provide a spacing scheme. There are five spacer assemblies for the two heads. These spacers are mounted on circular plates which bolt to the top of the head cavity. Basket spacers with several different lengths are provided to elevate short bundles.

FUEL BASKETS

Two different fuel baskets are used in the IF-300 cask: a 7-cell PWR unit and an 18-cell BWR unit. The 7-cell basket holds the various PWR assemblies and the 18-cell basket holds the standard BWR fuel clusters. Each basket cell is a square, thin-walled stainless steel tube, the walls of which are slotted to provide coolant flow to the contained fuel. Cells are held in place by nine circular spacers placed along the basket length. The basket cells run the full length of the fuel. When the cask is horizontal, the weight of the fuel assemblies is carried by the spacer discs. Cells are not principal load-carrying members; they function as guides for use in fuel loading. Criticality control in each fuel basket is provided by boron carbide-filled stainless steel tubes located in the gaps exterior to the basket cells. Each basket is keyed into the cask to prevent rotation during shipment.

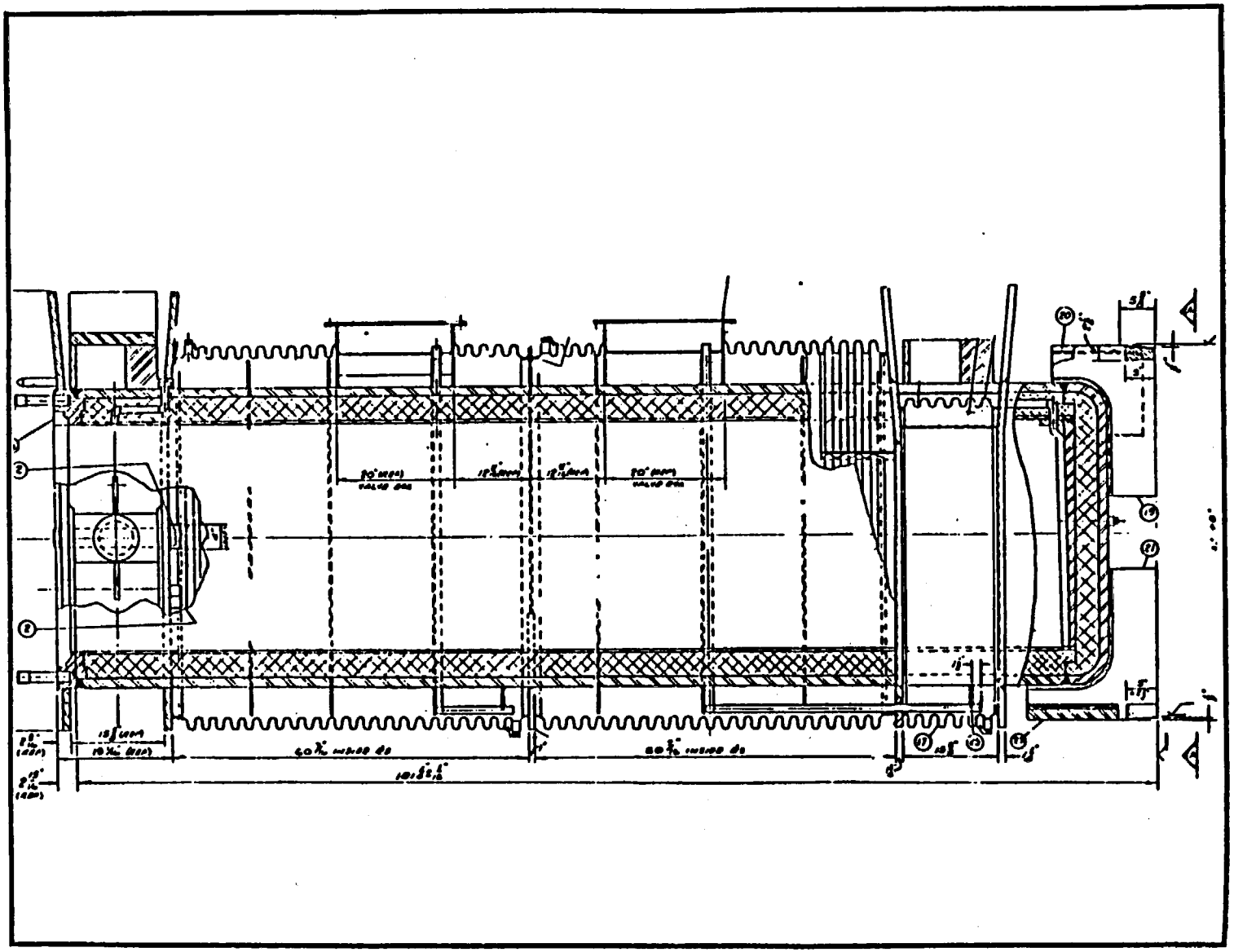

FIGURE 2-1 SECTIONAL VIEW OF CASK BODY

3. ASSUMPTIONS AND PROPERTIES USED IN THE ANALYSES

ASSUMPTIONS

The following is a list of assumptions used in the analyses:

1. The cask was assumed to be a simply-supported beam for the 30-foot side drop analysis. This assumption was based on the behavior of the cask at impact when the two fins at each end first hit the rigid surface and the cask spans between them as a simply-supported beam.

2. The moment-curvature and force-deflection relationships for the cask and the fuel rods were assumed to be bilinear.

3. The fuel rods were assumed to act independently of each other because of lack of transfer of shear between individual rods. It was assumed that the influence of friction on shear transfer was negligible. Therefore, properties such as the moment of inertia, area, yield moment, weight per unit length, etc., were computed for a single rod and then multiplied by the number of rods.

4. Spacer disks were assumed to be rigid and of zero thickness for the 30-foot side drop analysis.

5. The fuel rods were assumed to rest directly upon basket spacer disks as continuous beams for the 30-foot side drop analysis.

6. The weight of the water in the cask was included as part of the total cask weight; however, its influence on damping was not included. For the 30-foot end drop analysis, the weight of water was lumped at the bottom end of the cask.

7. With the exception of the heads and the BWR basket shielding, the mass of the cask was assumed to be uniformly distributed.

8. A conservative value of two percent of critical damping was used, because of lack of damping data for Zircalloy. For steel, USNRC Regulatory Guide 1.60 recommends a value of three percent of critical damping.

9. The gaps between the fuel rods themselves and between the fuel rods and the basket cells were assumed to be negligible for the 30-foot side drop analysis.

10. The stiffness and strength of basket cells were not included in the analyses.

11. The weight of the depleted uranium shielding was included as part of the cask weight in the analyses, but the effects of its stiffness and strength were ignored for the 30-foot side drop analysis. It was found that this was a conservative assumption. (See Appendix A).

12. For the 30-foot end drop analyses, the cask uranium shielding was assumed to be capable of carrying compressive load only, due to the fact that it is cast in sections. Furthermore, due to a lack of detailed data on post yield properties of uranium, the shielding was assumed to be elastic-perfectly plastic.

13. The steel shells of the cask were assumed to share loading according to their cross-sectional areas, with equal strains, for the 30-foot end drop analysis.

14. The stiffness and strength of fuel pellets were not included in the analysis; however, their weight was included. For the 30-foot side drop analyses, the weight was uniformly distributed; for the 30-foot end drop analysis, it was lumped at the bottom of the cask.

15. The energy-absorbing effects of fuel bundle stainless steel appurtenances were ignored for the 30-foot end drop analysis.

16. A maximum value of 0.75 inches was used for the gap between the end of the fuel rod and the inside of the cask for the 30-foot end drop analysis.

PROPERTIES

Thirty-Foot Side Drop Analysis

The following cask and fuel rod properties were used for the 30-foot side drop analysis:

Cask: The cask stiffness and strength defined in terms of a moment-curvature relationship and are shown in Figure 3-1 (Ref. 1). The weights of the cask used are presented in Table 3-1.

Fuel Rods: The stress-strain curve for Zircalloy was based on static loading and is shown in Figure 3-2. The corresponding moment-curvature relationships for the BWR and PWR cases are shown in Figures 3-3 and 3-4, respectively. Other properties relevant to the analyses are presented in Table 3-2. These properties correspond to the fuel rods which were selected as the critical ones out of all the combinations on the basis of preliminary hand calculations.

Thirty-Foot End Drop Analysis

The following cask and fuel rod properties were used for the 30-foot end drop analyses.

Cask: The cross-sectional areas of 59.7 square inches, 226.0 square inches, and 534.0 square inches were used for the inner steel shell, outer steel shell, and depleted uranium shielding, respectively. The stress-strain curve for stainless steel, shown in Figure 3-5, is based on the moment-curvature relationship of the cask. Material data for the depleted uranium was supplied by GE (Ref. 9). As noted in the assumptions, the depleted uranium shielding was assumed to carry no tension

because it is built in sections. An elastic-perfectly plastic compression relationship was assumed for uranium and is shown in Figure 3-6. Stress-strain properties of different materials used for the analyses are summarized in Table 3-3.

The weights of the cask are summarized in Table 3-1.

Fuel Rods: The stress-strain curve for Zircalloy is shown in Figure 3-2. The stress-strain properties are presented in Table 3-3. Other properties used were the same as for the side drop analysis.

TABLE 3-1

WEIGHTS OF THE IF-300 CASK

Component	Weight (Pounds) BWR Case	PWR Case
Cask Body, including Steel Shells, Uranium Shielding, End Fins, and Miscellaneous	99,900	99,900
Removable Head	9,450	6,850
Baskets	4,900	4,500
Basket Shielding	900	--
Inner Cavity Water	4,000	4,000

TABLE 3-2

FUEL ROD PROPERTIES

Property	Case	
	BWR	PWR
Cladding O.D.	0.483 in.	0.374 in.
Cladding Thickness	0.032 in.	0.0225 in.
Cross-Sectional Area of Fuel Pellet	0.132 in.	0.0817 in.
Weight of Pellet	0.052 lb/in.	0.0323 lb/in.
Weight of Cladding	0.011 lb/in.	0.00589 lb/in.
Total Rod Weight	0.063 lb/in.	0.038 lb/in.

TABLE 3-3

MATERIAL PROPERTIES

Property	Stainless Steel	Depleted Uranium	Zircalloy
Modulus of Elasticity	30×10^6 psi	26×10^6 psi	9.3×10^6 psi
Compressive Yield Stress	60,000 psi	30,000 psi	65,000 psi
Tensile Yield Stress	60,000 psi	1 psi	65,000 psi

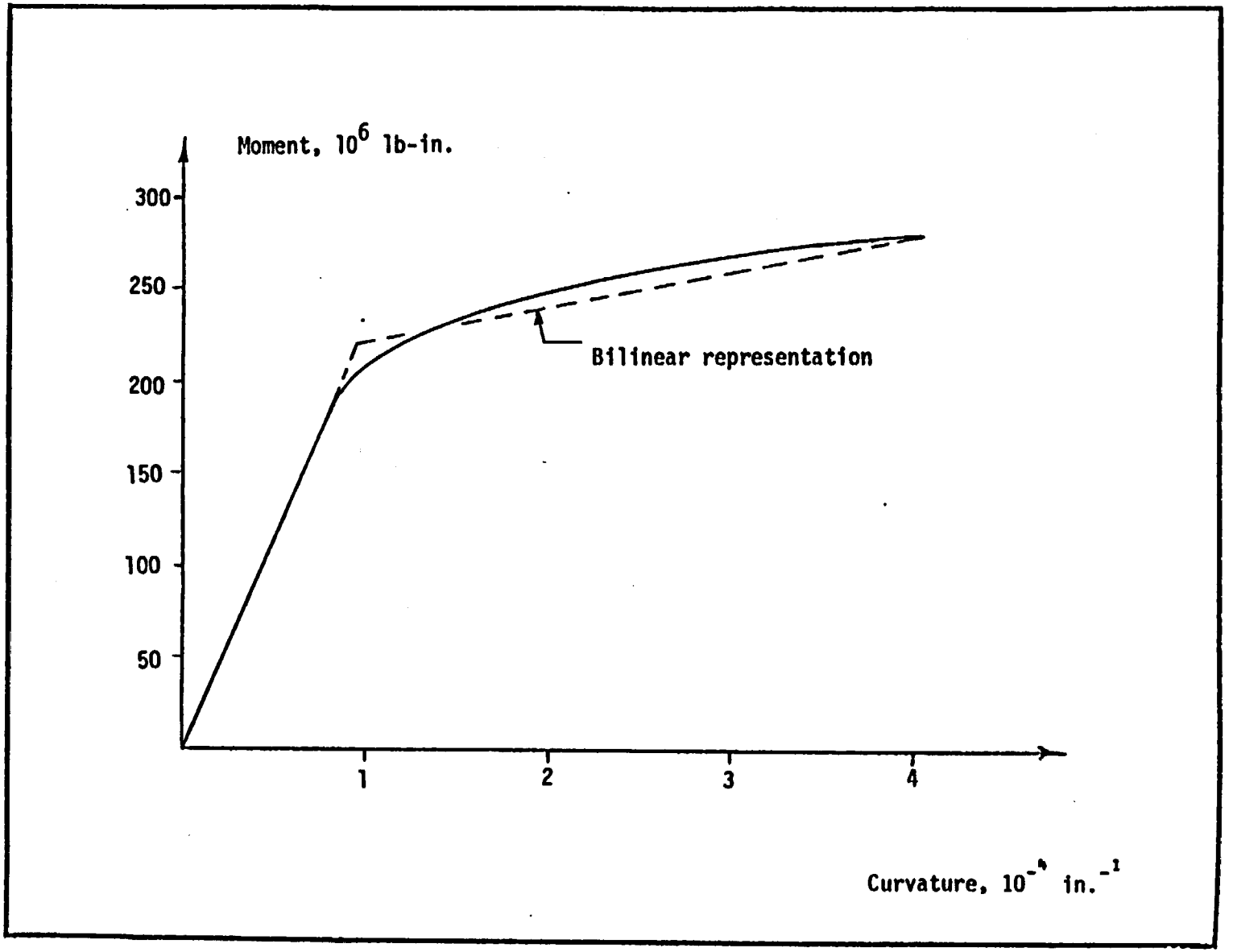

FIGURE 3-1 CASK BODY MOMENT-CURVATURE RELATIONSHIP

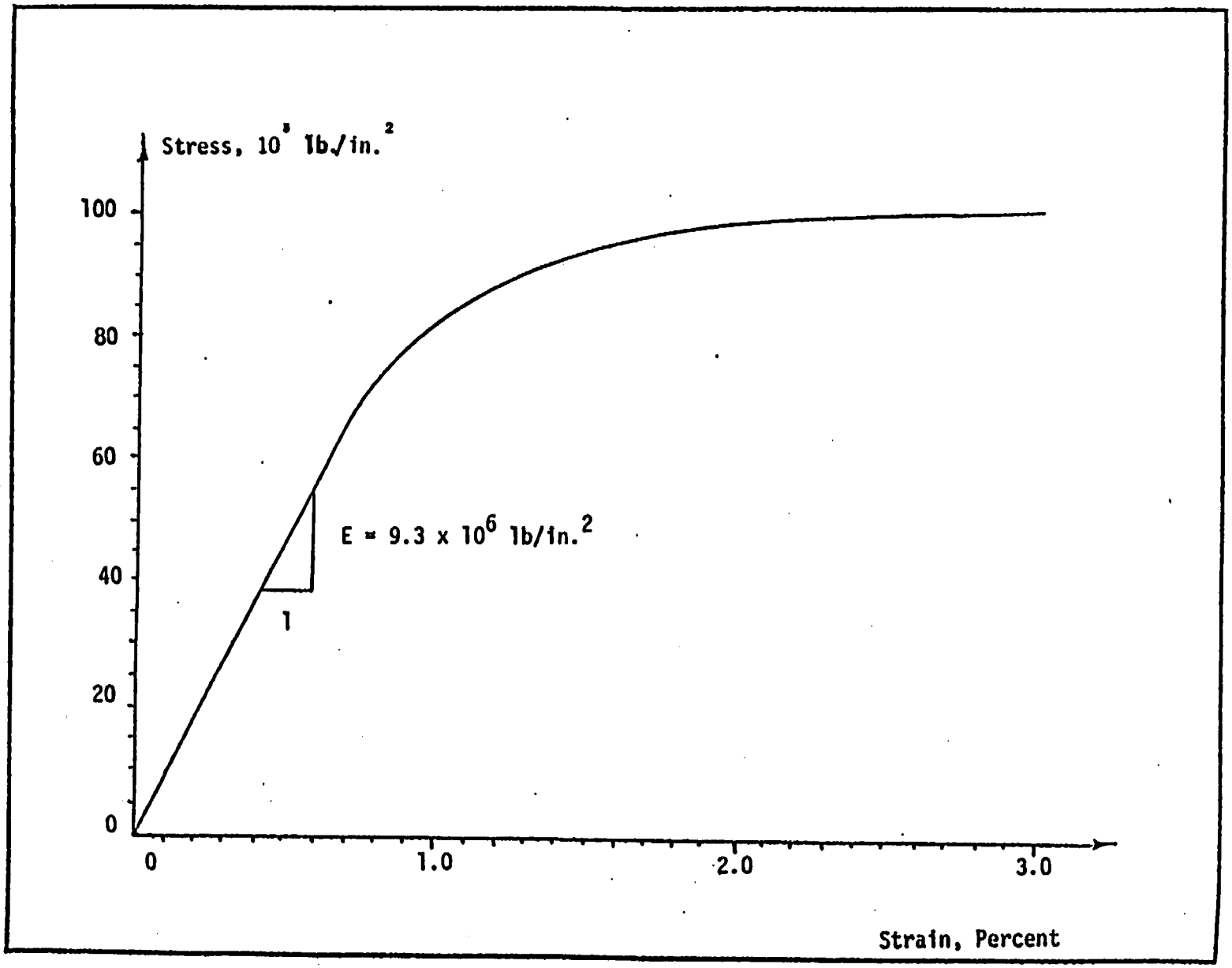

FIGURE 3-2 STRESS-STRAIN RELATIONSHIP FOR ZIRCALLOY

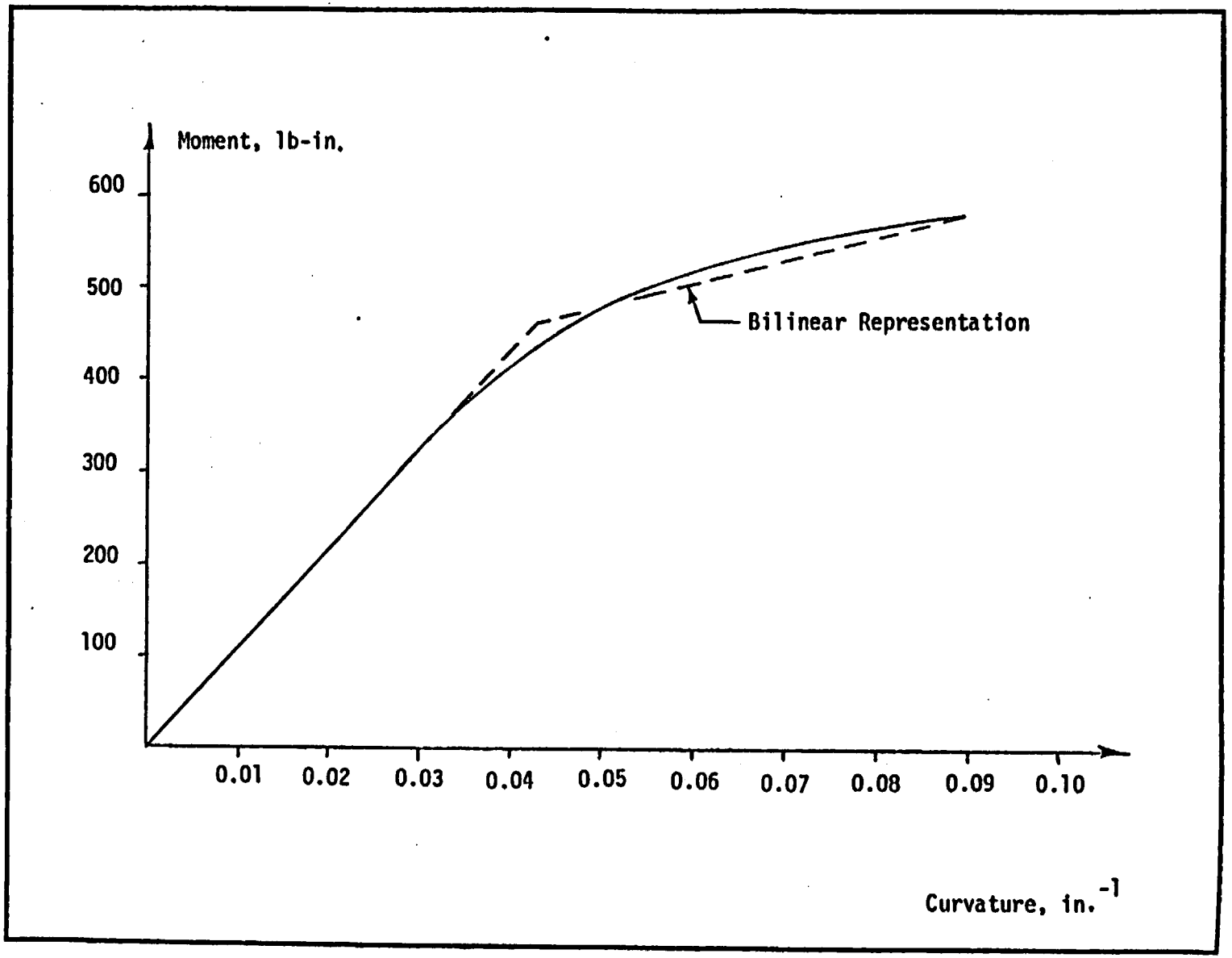

FIGURE 3-3 BWR FUEL ROD MOMENT-CURVATURE RELATIONSHIP

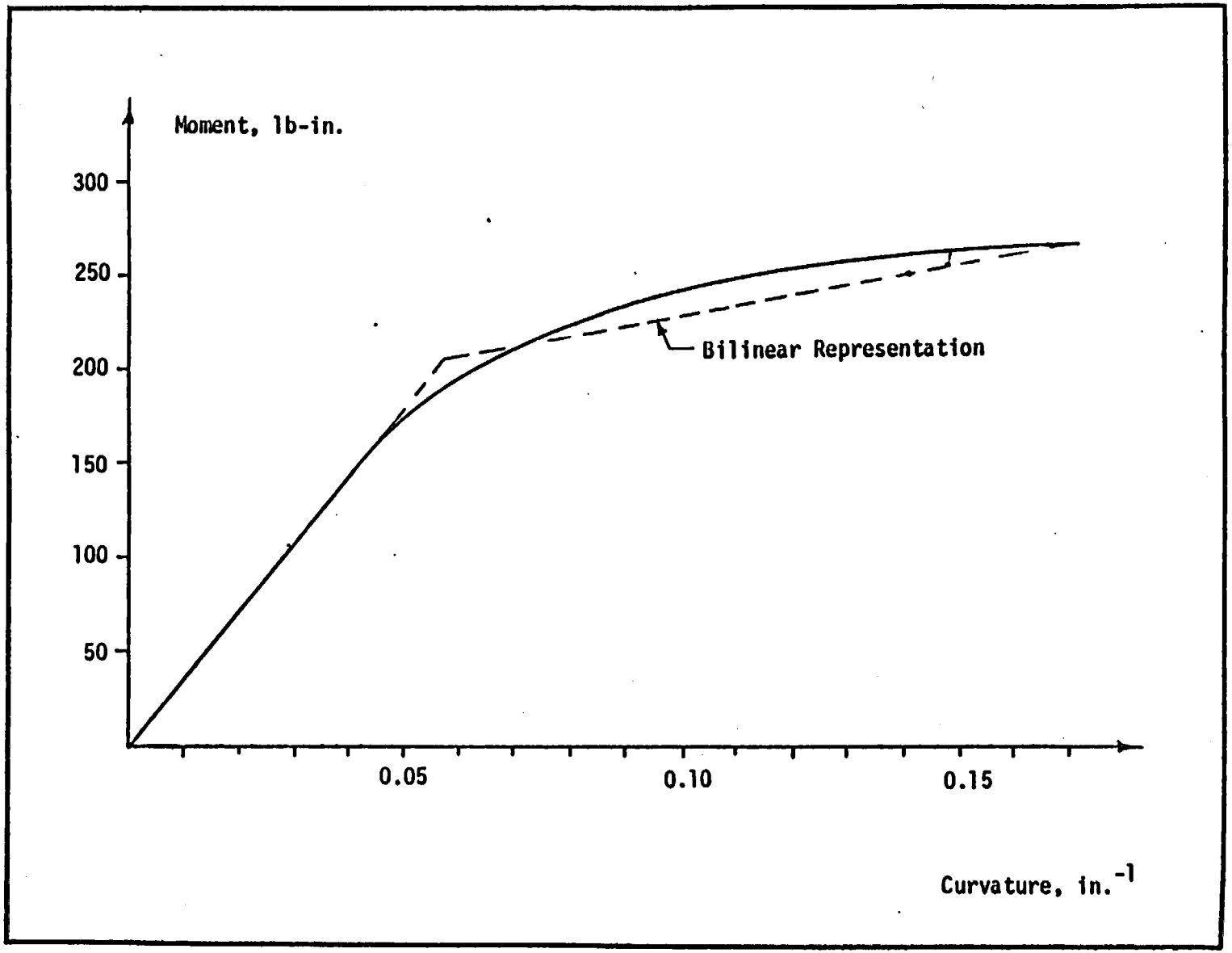

FIGURE 3-4 PWR FUEL ROD MOMENT-CURVATURE RELATIONSHIP

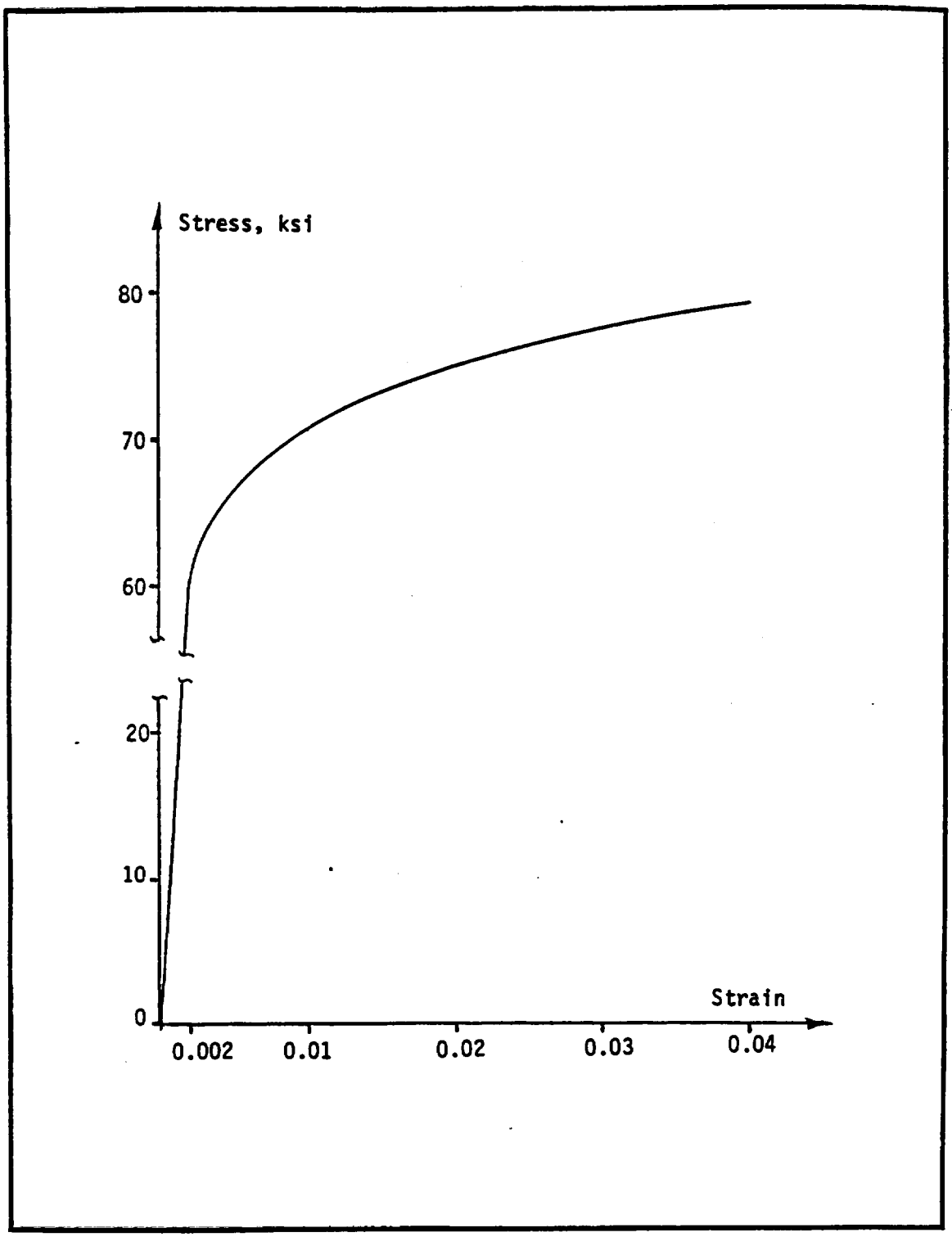

FIGURE 3-5 ASSUMED STRESS-STRAIN CURVE FOR STAINLESS STEEL

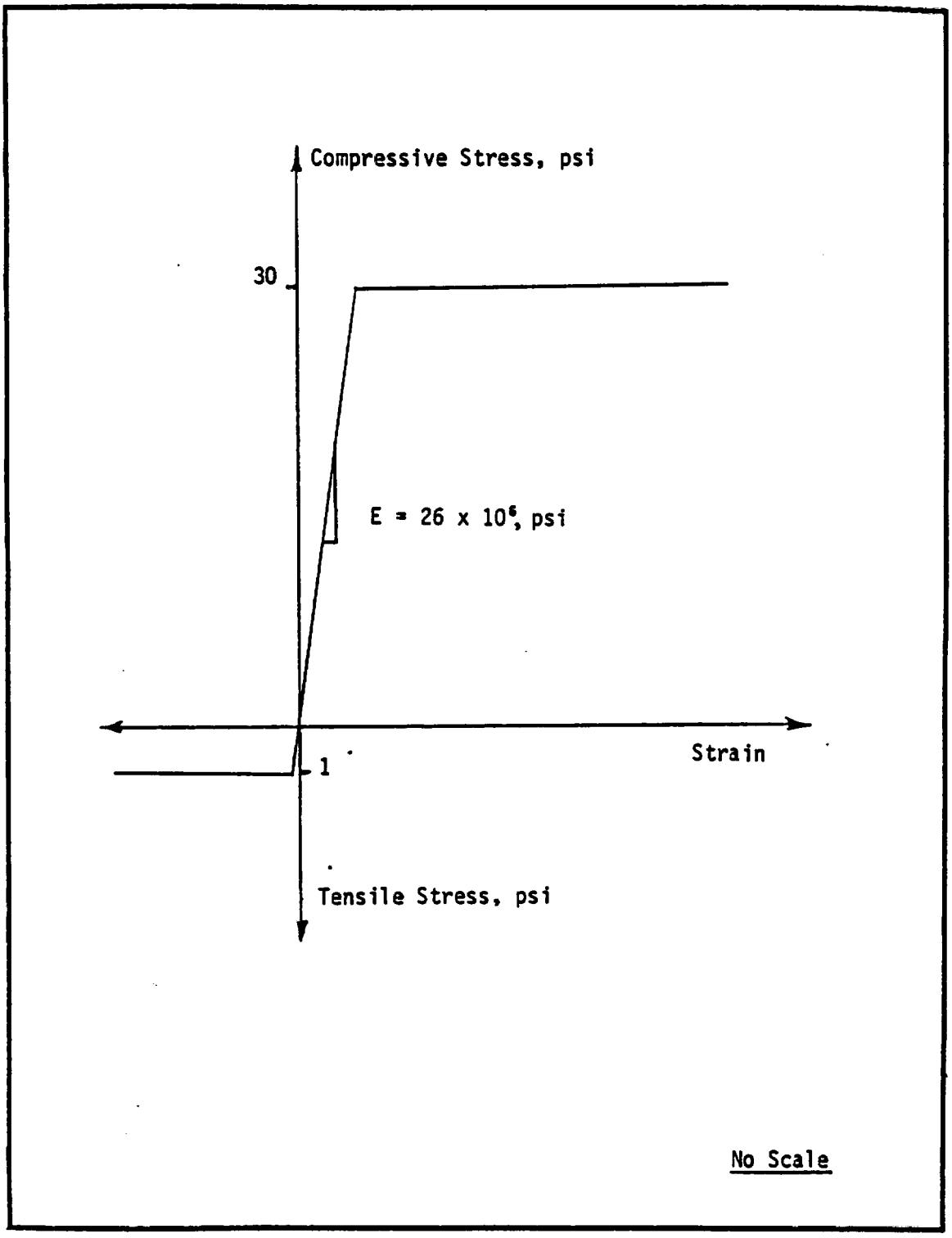

FIGURE 3-6 ASSUMED STRESS-STRAIN CURVE FOR DEPLETED URANIUM

4. ANALYSIS FOR 30-FOOT SIDE DROP

INTRODUCTION

The 30-foot side drop analyses were performed for BWR and PWR configurations. The input loading consisted of an initial velocity of 44.0 feet per second and a force-time relationship shown in Figure 4-1. The downward initial velocity was applied at all the nodal points of the cask-fuel system. The upward force-time relationship representing the impact fin deformation was applied at the locations of supports, assumed to be half-way between the two impact fins near each end of the cask.

ANALYTICAL MODELS

The analytical models for the PWR and BWR cases used in the analyses are shown in Figures 4-2 and 4-3. The dimensions for these models, are shown in Figures 4-4 and 4-5 (Ref. 2).

The cask was modeled as a simply-supported beam. The fuel rods were modeled as a continuous beam. The centerlines of the cask and the fuel rods were connected by rigid truss elements representing the basket spacers.

The mass of the cask was assumed to be uniformly distributed, except for the heads and the BWR basket shielding (concentrated near the head). The fuel mass was assumed to be distributed over the active fuel length only, as shown in Figures 4-4 and 4-5.

ANALYSIS PROCEDURES

Natural frequencies for the cask-fuel rod systems were first computed using the computer program EDAC/ISAS (Integrated Structural Analysis Sys-

tem). Nonlinear dynamic analyses were then performed using the computer program EDAC/ANSR-II. Each of these programs were originally developed at the University of California, Berkeley, and have been modified by EDAC engineers. Benchmark analysis examples for these computer programs are on file.

The nonlinear dynamic analyses were performed using a direct integration method based on constant acceleration technique. The time step size used for the analyses was 0.00002 seconds. Maximum values of displacement were computed for each nodal point, and maximum values of internal forces (bending moments and shears) were computed for each element. Time histories of displacements and forces were computed for selected locations only. Maximum strains were computed for each element of the fuel rods.

RESULTS

Tables 4-1 and 4-2 present summaries of the natural frequencies computed for the two analytical models. It should be noted that the cask modes start appearing with the eighth mode for the BWR configuration and the ninth mode for the PWR configuration, and have similar frequencies for each configuration

Figures 4-6 and 4-7 show typical displacement time histories for the BWR and PWR cases, respectively. A summary of maximum displacements obtained from the nonlinear dynamic analyses is presented in Table 4-3. Figures 4-8 and 4-9 show schematically the displacements of the cask with time for the BWR and PWR configurations. Two facts are evident from the figures. First, the cask behaves almost as a rigid body. Second, the retarding forces at the supports are not balanced, and the cask rotates as it rebounds. Results of maximum bending moments are presented in Table 4-4. Comparison with moment-curvature relationships showed that plastic hinges formed in the fuel rods in each case. The cask also underwent slight inelastic deformations.

Maximum fuel rod strains are summarized in Table 4-5 and are plotted in Figures 4-10 and 4-11 for the BWR and PWR configurations. It should be noted that the values shown represent absolute maxima, and do not necessarily occur at the same time.

TABLE 4-1

NATURAL FREQUENCIES OF THE CASK-FUEL ROD SYSTEM

BWR CONFIGURATION

Mode	Frequency (Hz)	Mode Type
1	27.7	Fuel
2	35.0	Fuel
3	40.5	Fuel
4	48.0	Fuel
5	56.3	Fuel
6	61.9	Fuel
7	64.4	Fuel
8	80.3	Cask
9	105.4	Fuel
10	131.5	Fuel
11	138.9	Fuel
12	150.3	Fuel
13	162.9	Cask
14	164.8	Fuel
15	178.4	Fuel
16	189.8	Fuel
17	190.9	Cask
18	198.2	Fuel
19	207.6	Cask
20	230.2	Fuel
21	295.4	Fuel

TABLE 4-1 continued

NATURAL FREQUENCIES OF THE CASK-FUEL ROD SYSTEM

BWR CONFIGURATION

Mode	Frequency (Hz)	Mode Type
22	305.4	Fuel
23	309.2	Cask
24	327.5	Fuel
25	349.4	Fuel
26	354.2	Cask
27	366.6	Fuel
28	381.2	Fuel
29	394.5	Cask
30	402.2	Fuel

TABLE 4-2

NATURAL FREQUENCIES OF THE CASK-FUEL ROD SYSTEM

PWR CONFIGURATION

Mode	Frequency (Hz)	Mode Type
1	24.7	Fuel
2	29.0	Fuel
3	32.7	Fuel
4	37.7	Fuel
5	43.5	Fuel
6	49.7	Fuel
7	55.3	Fuel
8	56.2	Fuel
9	74.3	Cask
10	95.4	Fuel
11	111.9	Fuel
12	118.4	Fuel
13	127.1	Fuel
14	137.3	Fuel
15	148.0	Fuel
16	158.0	Fuel
17	166.0	Fuel
18	175.1	Cask
19	200.4	Cask
20	209.4	Fuel
21	247.3	Fuel

TABLE 4-2 continued

NATURAL FREQUENCIES OF THE CASK-FUEL ROD SYSTEM

PWR CONFIGURATION

Mode	Frequency (Hz)	Mode Type
22	255.7	Fuel
23	268.0	Fuel
24	276.2	Cask
25	281.4	Fuel
26	287.7	Fuel
27	314.4	Cask
28	316.0	Fuel
29	325.3	Fuel
30	360.9	Fuel

TABLE 4-3

MAXIMUM DISPLACEMENTS

Case	Location	Node	Displacement* (in)	Time (ms)
BWR Configuration	Fuel Midspan	7	-4.92	14.2
BWR Configuration	Cask Support	12	-3.04	14.1
BWR Configuration	Fuel Midspan	27	-3.58	9.2
BWR Configuration	Cask Midspan	50	-3.47	13.8
BWR Configuration	Cask Support	80	-3.43	15.9
PWR Configuration	Fuel Midspan	7	-5.31	15.6
PWR Configuration	Cask Support	12	-3.52	15.9
PWR Configuration	Fuel Midspan	27	-4.06	11.3
PWR Configuration	Cask Midspan	41	-3.46	13.4
PWR Configuration	Cask Support	82	-2.64	11.3

* These displacements are "total" displacements, not "relative" displacements, and are referenced from the level of the fixed supports.

TABLE 4-4

MAXIMUM BENDING MOMENTS

Case	Location	Node	Moment (lb-in.)
BWR Configuration	Cask Midspan	41	239,200,000
BWR Configuration	Fuel Support	58	619,100
PWR Configuration	Cask Midspan	41	256,800,000
PWR Configuration	Fuel Support	40	460,000

TABLE 4-5

MAXIMUM FUEL ROD STRAINS

Case	Node	Strain (percent)	Time (ms)
BWR Configuration	58	1.94	10.4
PWR Configuration	40	2.66	9.4

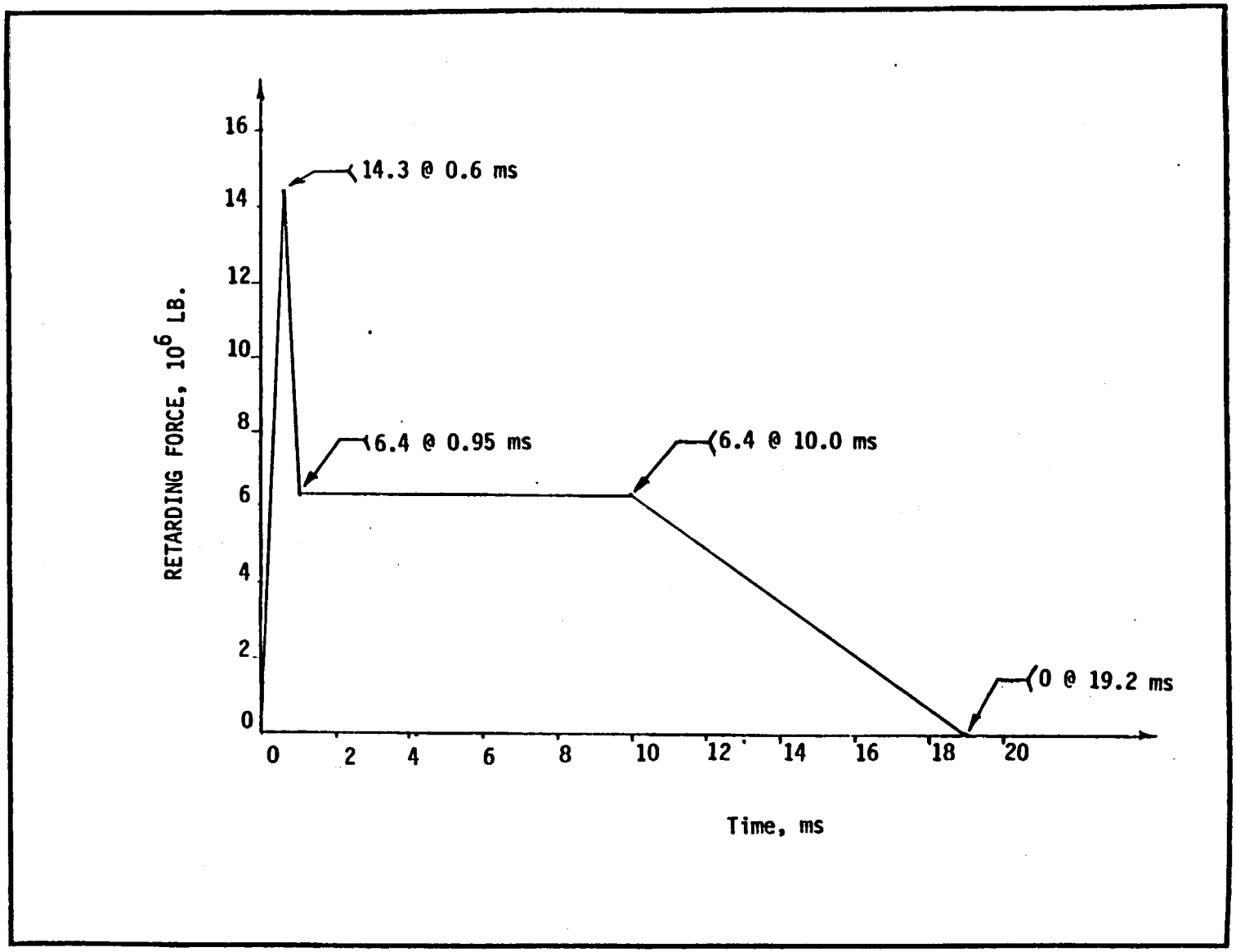

FIGURE 4-1 FORCE VERSUS TIME INPUT -- 30-FOOT SIDE DROP

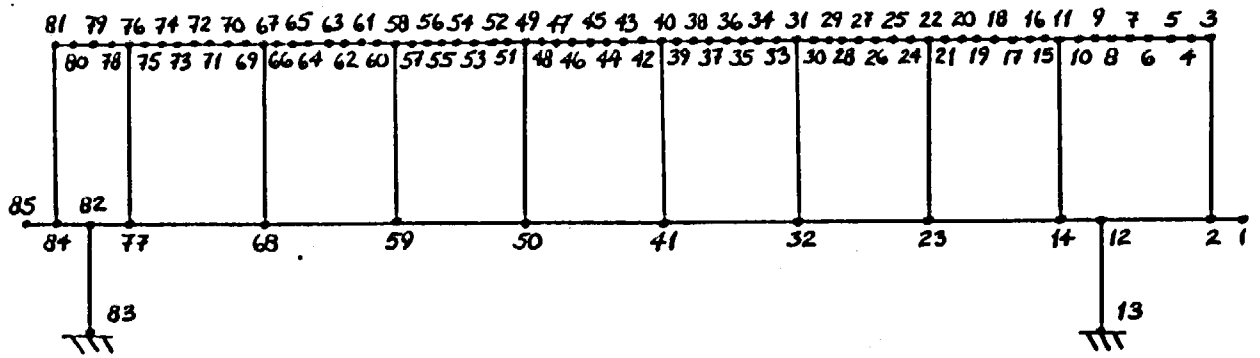

FIGURE 4-2 PWR ANALYTICAL MODEL

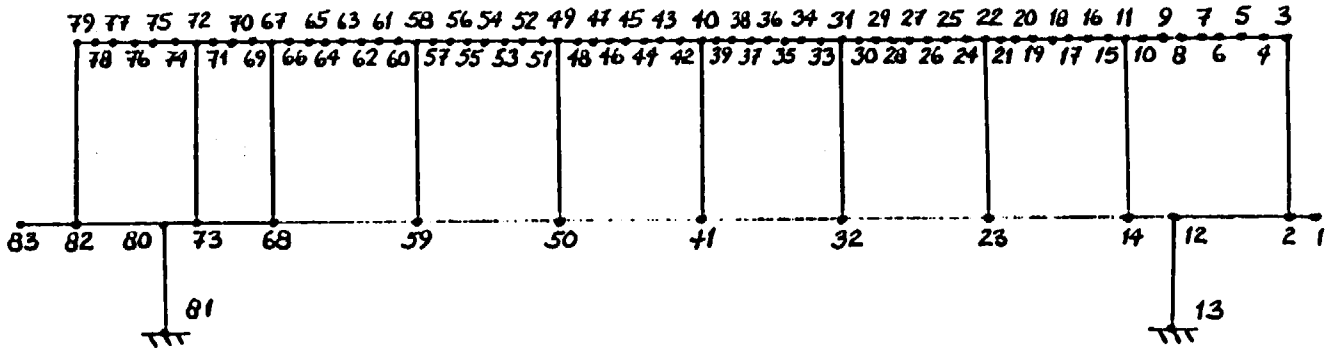

FIGURE 4-3 BWR ANALYTICAL MODEL

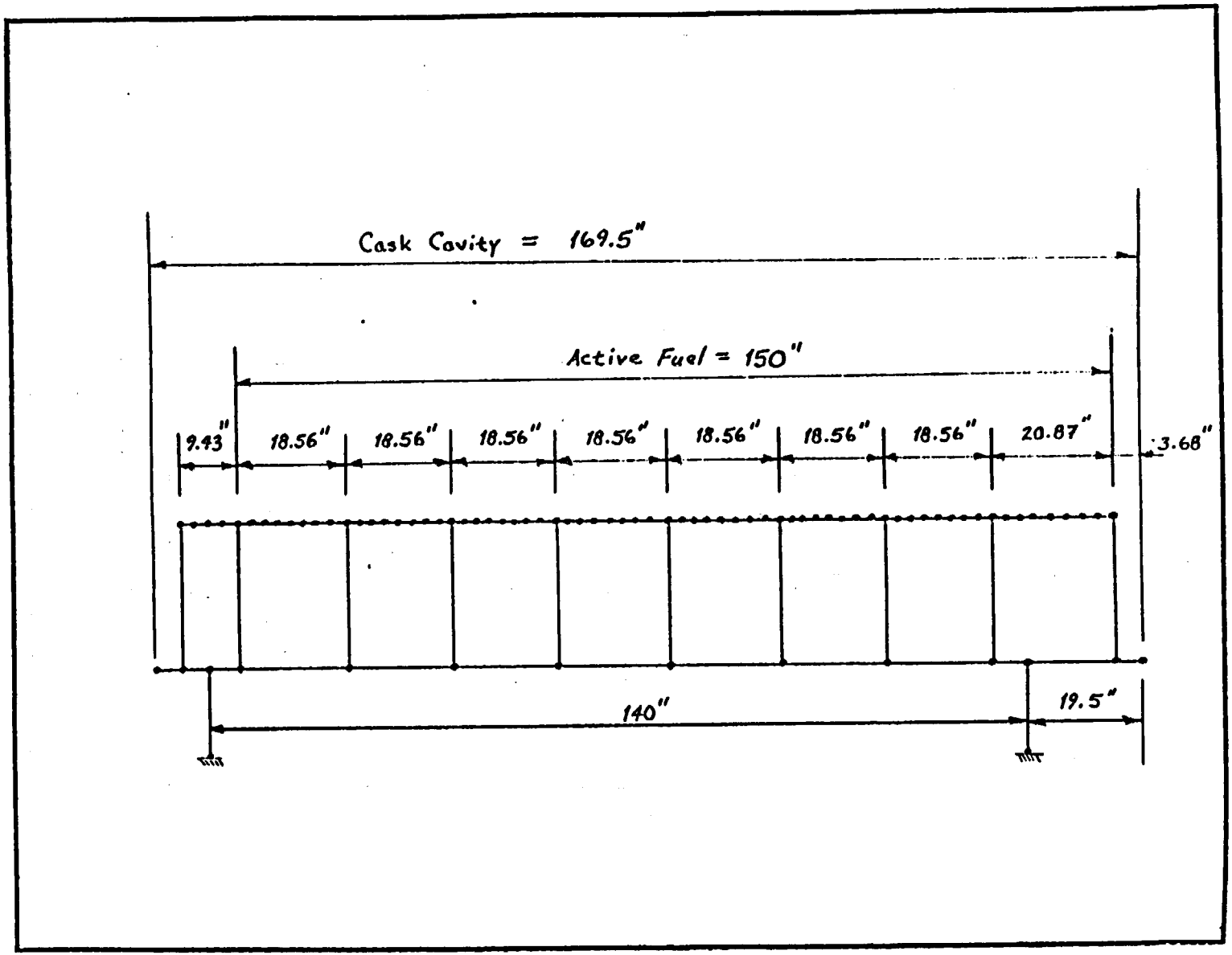

FIGURE 4-4 PWR MODEL DIMENSIONS

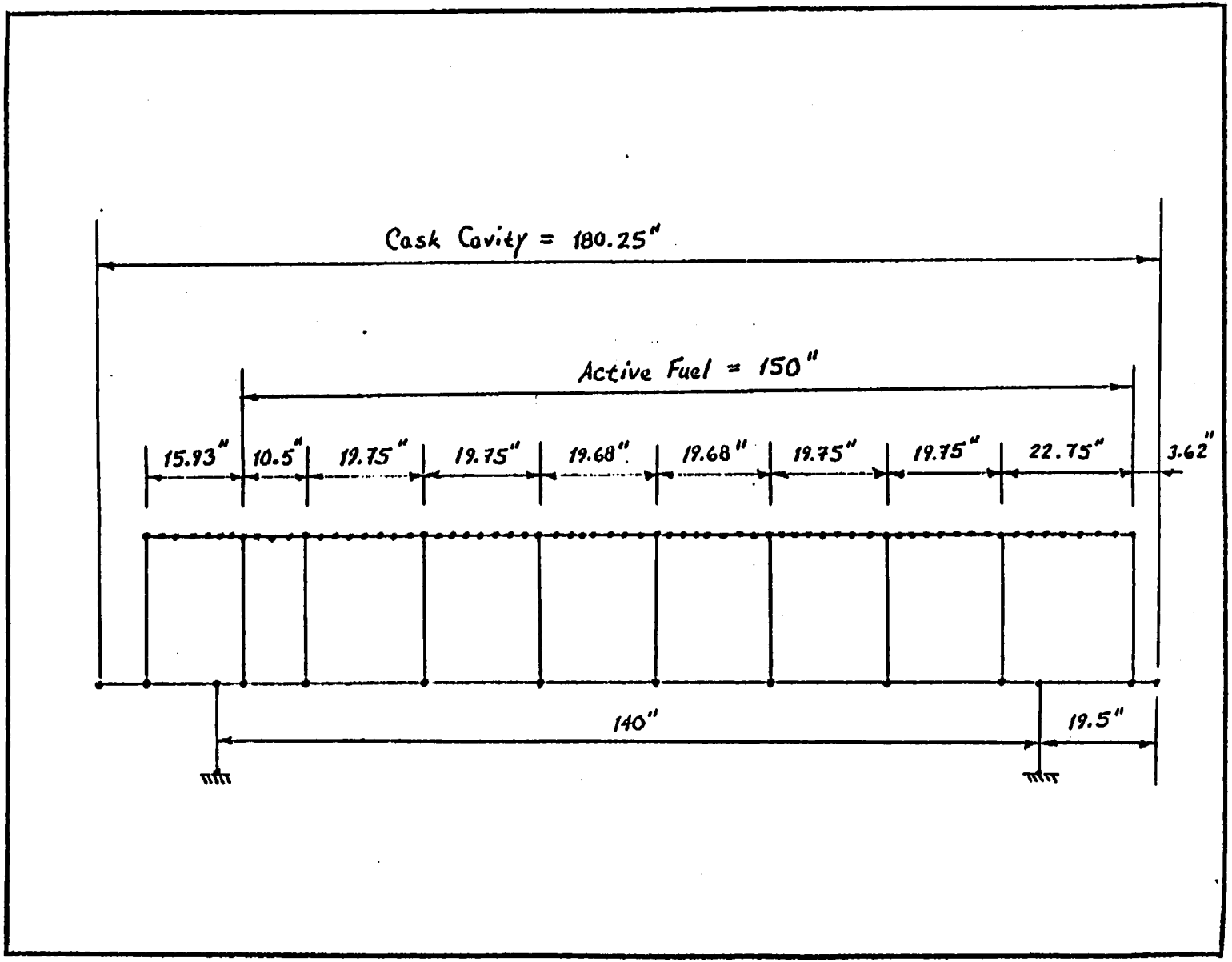

FIGURE 4-5 BWR MODEL DIMENSIONS

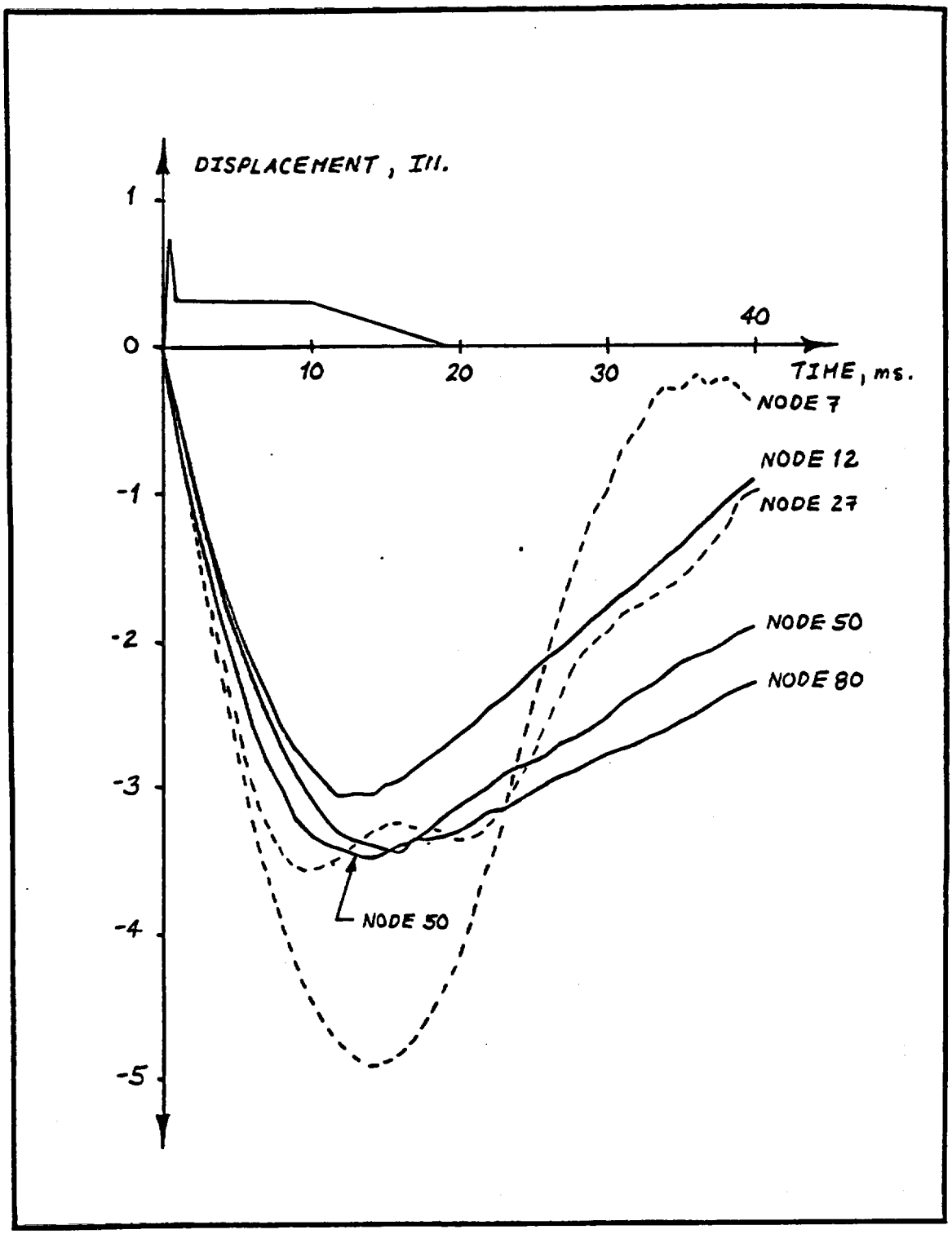

FIGURE 4-6 TYPICAL DISPLACEMENT TIME HISTORIES

BWR CONFIGURATION

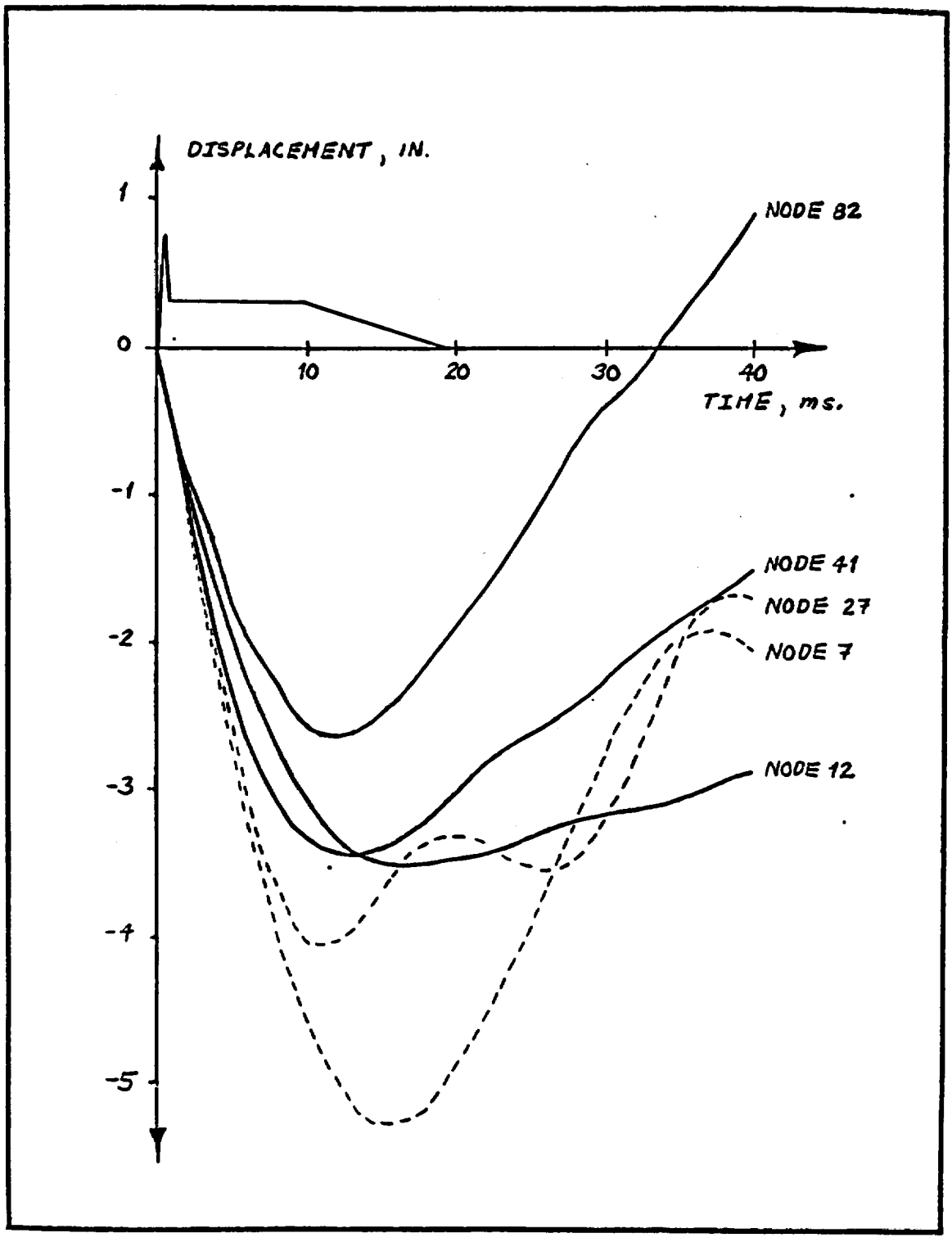

FIGURE 4-7 TYPICAL DISPLACEMENT TIME HISTORIES

PWR CONFIGURATION

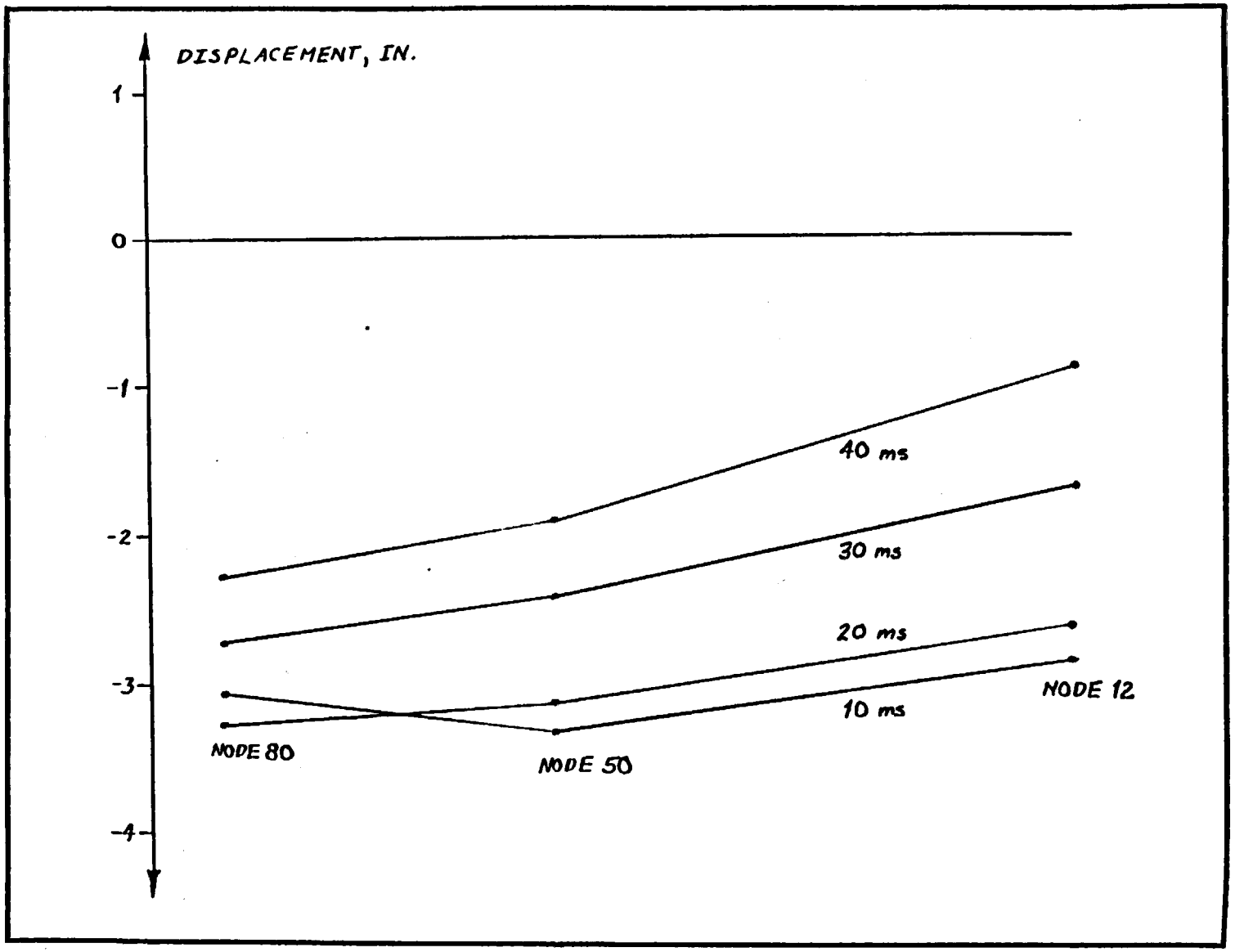

FIGURE 4-8 SCHEMATIC DIAGRAM OF CASK DISPLACEMENT VERSUS TIME

BWR CONFIGURATION

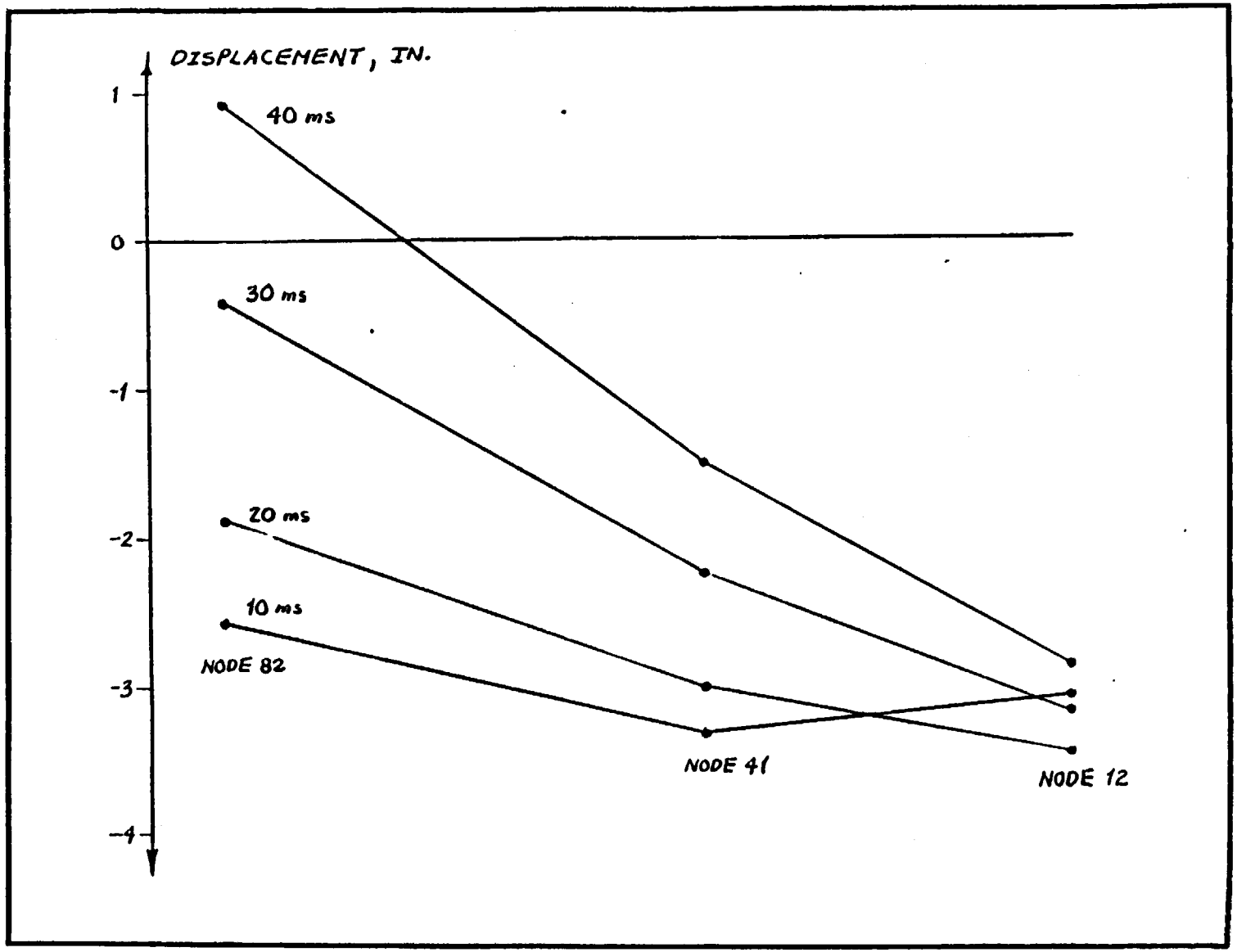

FIGURE 4-9 SCHEMATIC DIAGRAM OF CASK DISPLACEMENT VERSUS TIME

PWR CONFIGURATION

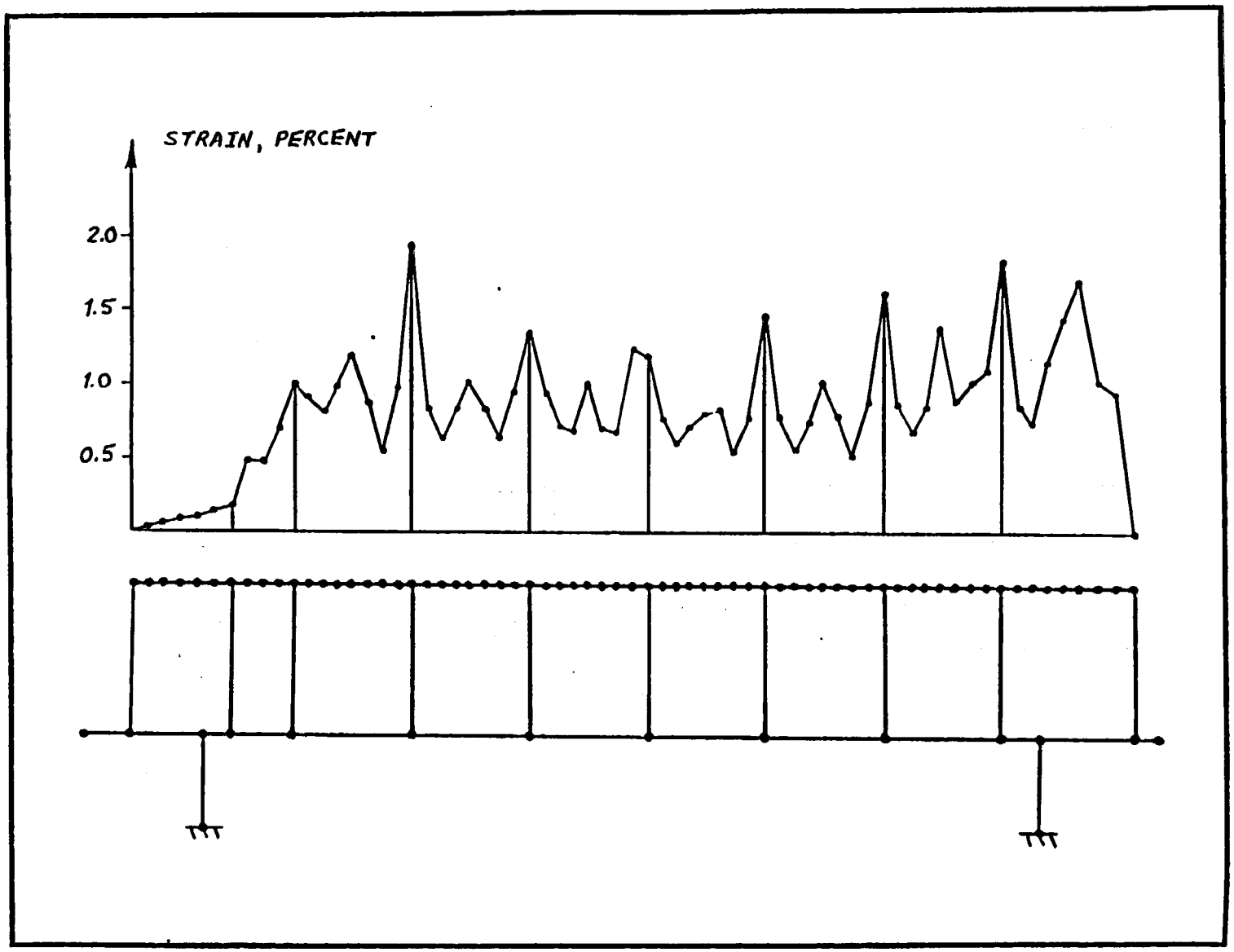

FIGURE 4-10 MAXIMUM FUEL ROD STRAINS

BWR CONFIGURATION

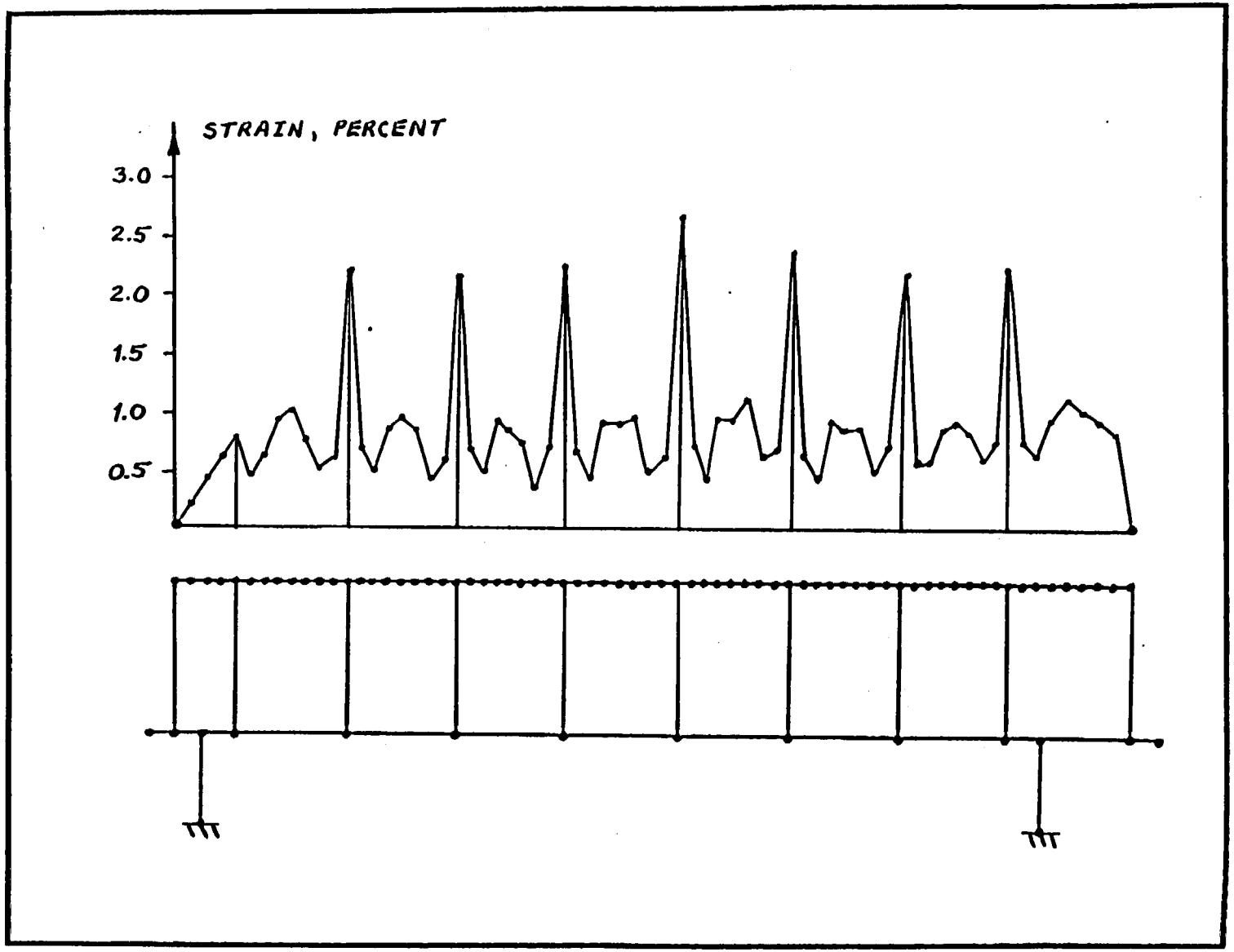

FIGURE 4-11 MAXIMUM FUEL ROD STRAINS

PWR CONFIGURATION

5. ANALYSIS FOR 30-FOOT END DROP

INTRODUCTION

The 30-foot end drop analyses were performed for BWR and PWR configurations. The input loading consisted of an initial velocity of 44.0 feet per second and a force-time relationship as shown in Figure 5-1. The downward initial velocity was applied at all the nodal points of the caskfuel system. The upward force-time relationship was applied at the bottom of the cask.

ANALYTICAL MODELS

The analytical models for the the BWR and PWR cases are shown in Figure 5-2. The dimensions for these models are based on drawings 159C5238 (Ref. 2). The common numbering system emphasizes the similarity of the BWR and PWR cases.

The cask was modeled by vertical beam elements connecting Nodes 2 through 42. Each pair of successive nodes was connected by two beam elements, representing the steel shells and the depleted uranium shielding, respectively. The fuel rods were modeled by vertical beam elements connecting Nodes 3 through 53. A nonlinear "gap" element was used to model the axial clearance between the end of the fuel rod and the inside of the cask cavity, and connected Nodes 2 and 3. This element was very flexible in tension and very stiff in compression. It should be noted that although this gap element is illustrated as being horizontal, it was actually a vertical member with a nominal length of 0.01 inches when the gap between the cask and the fuel rods was closed. At all the nodes for all the elements, only axial degrees of freedom were included. Lateral degrees of freedom were not considered. However, flexural analyses were performed to investigate the influence of flexural deformations on the stresses in the fuel rods. These secondary analyses are presented in Appendix A.

The mass of the cask was assumed to be uniformly distributed, except at the heads (Nodes 2 and 42). The weight of the basket and water in the cask was lumped at the base (Node 2). The mass of the fuel cladding was assumed to be uniformly distributed, with the mass of the pellets lumped at the base of the rods (Node 3). This implies that for axial loading the pellet column acts independently of the cladding so that the pellet mass can be lumped at the base of the rods.

ANALYSIS PROCEDURES

Natural frequencies for the cask-fuel rod systems were first computed using the computer program EDAC/ISAS. For these computations, element properties corresponding to compression in the elastic range were used.

Nonlinear dynamic analyses were then performed using the computer program EDAC/ANSR-II. These analyses employed a direct integration method based on constant acceleration technique. The time step size used for the analyses was 0.00001 seconds. Maximum values of displacement were computed for each nodal point, and maximum values of axial force were computed for each element. Time histories of displacements and forces were computed for selected locations only.

RESULTS

Tables 5-1 and 5-2 present summaries of the natural frequencies computed for the BWR and PWR configurations. Both the cask and fuel rod modes are identified.

Tables 5-3 and 5-4 present the results for maximum axial stresses in the cask steel shells, the cask uranium shielding, and the fuel rods for the BWR and PWR configurations. The results clearly indicate that the maximum stresses in the fuel rods as well as the cask steel shells were considerably smaller than the corresponding yield stresses.

TABLE 5-1

NATURAL FREQUENCIES OF THE CASK-FUEL ROD SYSTEM

BWR CONFIGURATION

Mode	Frequency (Hz)	Mode Type
1	170.5	Cask
2	189.8	Fuel
3	510.4	Cask
4	569.0	Fuel
5	847.3	Cask
6	946.6	Fuel
7	1179.3	Cask
8	1321.6	Fuel
9	1504.4	Cask
10	1692.9	Fuel
11	1820.6	Cask
12	2059.7	Fuel
13	2126.1	Cask
14	2419.2	Cask
15	2420.8	Fuel
16	2698.1	Cask
17	2775.2	Fuel
18	2961.1	Cask
19	3122.1	Fuel
20	3206.7	Cask
21	3433.6	Cask

TABLE 5-1 continued

NATURAL FREQUENCIES OF THE CASK-FUEL ROD SYSTEM

BWR CONFIGURATION

Mode	Frequency (Hz)	Mode Type
22	3460.3	Fuel
23	3640.3	Cask
24	3789.1	Fuel
25	3825.6	Cask
26	3988.5	Cask
27	4107.6	Fuel
28	4127.9	Cask
29	4243.2	Cask
30	4333.5	Cask

TABLE 5-2

NATURAL FREQUENCIES OF THE CASK-FUEL ROD SYSTEM

PWR CONFIGURATION

Mode	Frequency (Hz)	Mode Type
1	175.8	Cask
2	189.1	Fuel
3	526.3	Cask
4	566.7	Fuel
5	873.8	Cask
6	942.9	Fuel
7	1,216.1	Cask
8	1,316.4	Fuel
9	1,551.3	Cask
10	1,686.3	Fuel
11	1,877.4	Cask
12	2,051.6	Fuel
13	2,192.5	Cask
14	2,411.2	Fuel
15	2,494.7	Cask
16	2,764.3	Fuel
17	2,782.3	Cask
18	3,053.5	Cask
19	3,109.8	Fuel
20	3,306.9	Cask
21	3,446.7	Fuel
22	3,540.8	Cask

TABLE 5-2 continued

NATURAL FREQUENCIES OF THE CASK-FUEL ROD SYSTEM

PWR CONFIGURATION

Mode	Frequency (Hz)	Mode Type
23	3,753.9	Cask
24	3,774.3	Fuel
25	3,945.0	Cask
26	4,091.4	Fuel
27	4,113.0	Cask
28	4,256.8	Cask
29	4,375.7	Cask
30	4,397.4	Fuel

TABLE 5-3

MAXIMUM AXIAL STRESSES

BWR CONFIGURATION

Location	Stress (psi)	Static Yield Stress (psi)	Time (ms)
Cask Steel Shells	40,980	60,000	6.5
Cask Uranium Shielding	30,000	30,000	5.0
Base of Fuel Rods	47,730	65,000	10.4

TABLE 5-4

MAXIMUM AXIAL STRESSES

PWR CONFIGURATION

Location	Stress (psi)	Static Yield Stress (psi)	Time (ms)
Cask Steel Shells	47,030	60,000	8.3
Cask Uranium Shielding	30,000	30,000	7.7
Base of Fuel Rods	29,990	65,000	5.0

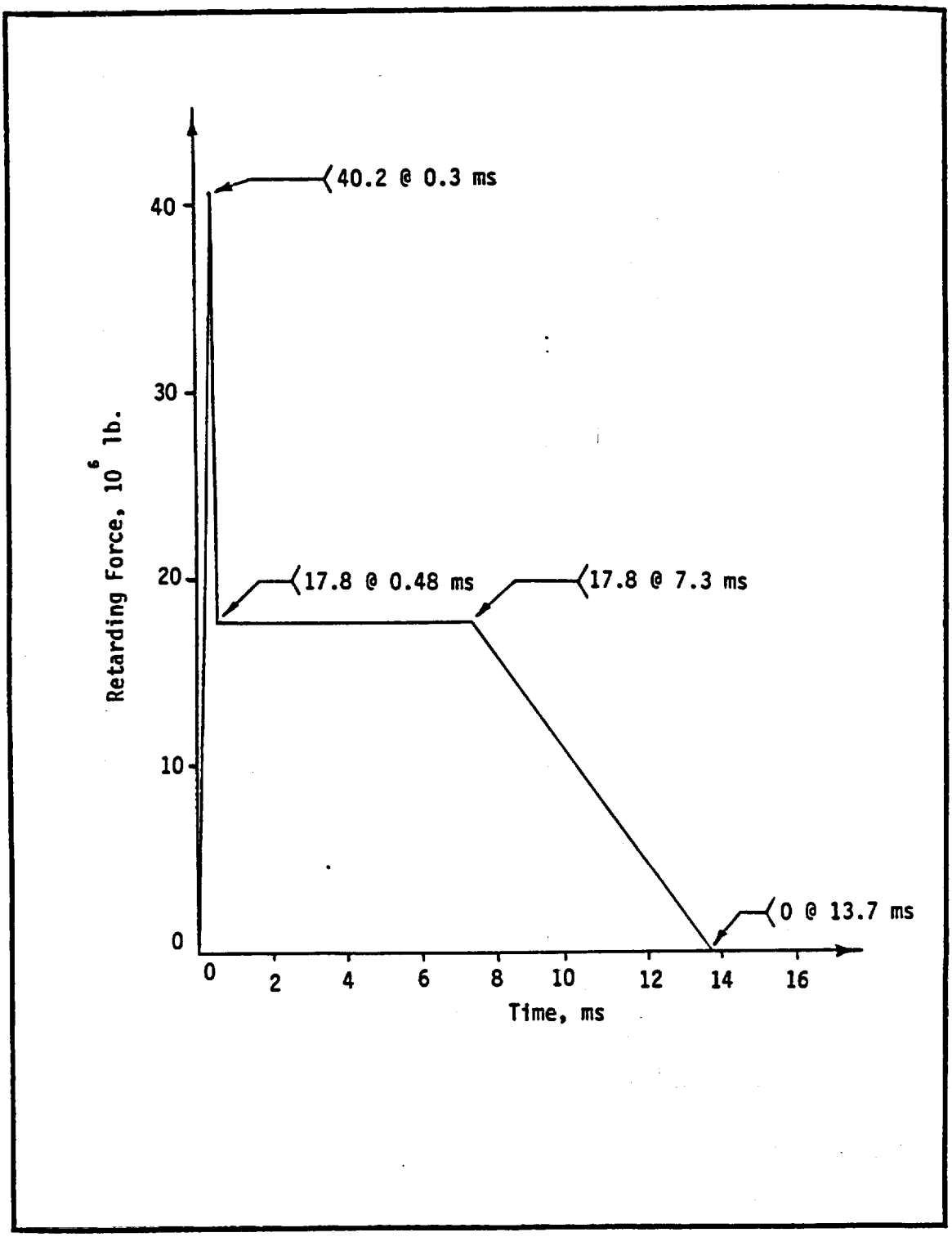

FIGURE 5-1 FORCE VERSUS TIME INPUT -- 30-FOOT END DROP

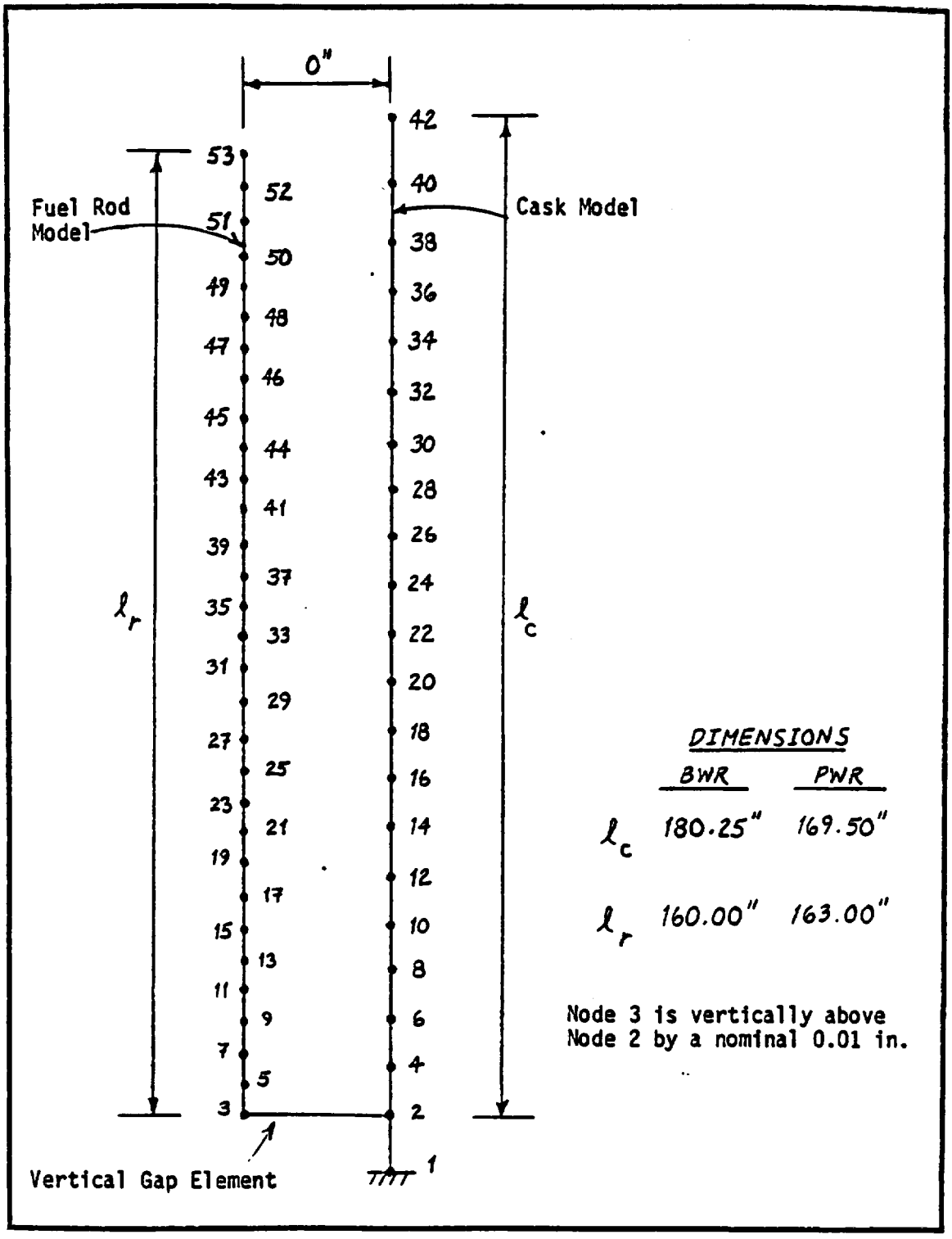

FIGURE 5-2 ANALYTICAL MODEL

computed at all nodal points along the length of the fuel rods for the PWR and BWR configurations. It was found that for the PWR configuration, the stress ratios varied from a minimum of 4.8 to a maximum of 11.0, with the majority of the values being in the range of 7.0 to 8.0. Similarly, very high values of stress ratios were obtained for the BWR configuration.

It was also found that at locations where the stress ratios were low, the values of strains were very low, considerably less than the yield strains, and therefore insignificant. A typical plot showing the variation of bending moments and the corresponding flexural strains is presented in Figure 6-4. The plot clearly shows that the strain decreases rapidly from the peak value at the support as a function of location. This indicates that at points of maximum strains, the stress ratios are very high, as discussed above. However, at locations where the stress ratios are low, the strains are also low and therefore not critical. It can therefore be stated on the basis of this discussion that fracture strains should be used as criterion for comparison for this problem if tests other than GE bending tests are also to be considered.

INFLUENCE OF TEMPERATURE ON CRITERION STRAINS

Figures 6-1, 6-2, and 6-3 show plots of test results for all temperatures. The results tend to fall on a single straight line, indicating that these test results are uncorrelated with temperature. It is evident on the basis of these three plots that the influence of temperature (in the range of consideration here) on the criterion strains is insignificant. It can be concluded on the basis of this observation that the GE bending test results, obtained at room temperature, are also applicable for higher temperatures, and are therefore directly applicable for comparison against the analysis results presented in this report regardless of the temperature.

COMPARISON OF THE RADIUS OF CURVATURE OF THE FUEL RODS AGAINST THE RADIUS OF THE GE BENDING TEST FIXTURE

Figure 6-4 shows a schematic layout of a basket spacer with one fuel rod. At the location of maximum strain (over a basket support), the radius of curvature of the rod was found to be approximately 7.03 inches from the analyses for the 30-foot side drop case. The radius of the fixture about which the fuel rods were bent for the GE bending tests was about 2.75 inches. This demonstrates that the calculated curvatures are considerably less than the GE test curvatures.

CONSERVATIVE ASSUMPTIONS IN THE ANALYSES

The analyses described in this report were based on numerous conservative assumptions discussed in Chapter 3. These included the assumptions that the basket spacer disks were rigid and of zero thickness, the fuel rods rested directly on basket spacer disks (actually they are supported along their lengths by guide channels), the enclosed water provided no damping to the system, the stiffness and strength of the guide channel were not included in the side drop analysis, the stiffness and strength of the fuel pellets were not included, and the crushing effects of fuel bundle appurtenances were not considered for the end drop analysis. The analyses were therefore very conservative, and it is quite likely that the strains obtained from these analyses are considerably higher than strains actually encountered during these postulated accidental drop cases.

CONCLUSIONS

It can be concluded on the basis of the above discussions that the fuel rod strains obtained from the analyses of the cask-fuel rod systems for the PWR and BWR configurations for the postulated accident cases, viz., 30-foot side drop and 30-foot end drop were found to be smaller than the criterion strains obtained from the available test results. Thus no fuel rod failures would be expected.

6. FINDINGS, ACCEPTANCE CRITERIA, AND CONCLUSIONS

GOVERNING CASE

The results of the analyses of the cask-fuel rod system for the 30-foot side drop and the 30-foot end drop cases were presented in Chapters 4 and 5, respectively. For the 30-foot side drop case, it was found that the fuel rods yielded and the corresponding maximum strains were 2.66 percent for the PWR configuration and 1.94 percent for the BWR configuration. For the 30-foot end drop case, it was found that the fuel rods did not yield. The results for this case are compared against the test results in the following paragraphs.

COMPARISON OF ANALYSIS RESULTS AGAINST BENDING TEST RESULTS

Table 6-1 presents the results of the bending tests of fuel rods performed by GE (Ref. 1). The tests were performed on actual sections of fuel rods containing uranium irradiated to high exposures. These are the most relevant and directly applicable tests available for comparison against the results of the analyses for the 30-foot side drop. As the table indicates, the test results, performed at room temperature, showed strains of 8.6 percent without cracking and rupture for most cases. For a few cases the strains were of the order of 6.0 percent to 8.0 percent. These strains are considerably higher than the maximum strains of 2.66 percent and 1.94 percent for the BWR and PWR configurations, respectively, obtained from the 30-foot side drop analyses.

COMPARISON OF ANALYSIS RESULTS AGAINST OTHER TEST RESULTS

In addition to the bending tests performed by GE and discussed above, other test results on irradiated Zircalloy fuel rods are available which

may be indirectly of interest to the cask drop problem. They include the tube tensile and tube burst tests from the NRC/Battelle-Columbus program and Japanese data of varying stress ratios (Ref. 3). A summary of these results, which include uniform strains and fracture strains at different temperatures, is presented in Figures 6-1 through 6-3. These figures are plotted on probability paper, where the ordinates represent the strains, and the abscissa represent the corresponding probabilities of exceedance. Figure 6-1 shows a plot of uniform strains for tensile tests for all temperatures, Figure 6-2 shows a similar plot for fracture strains, and Figure 6-3 shows a similar plot for fracture strains for tensile tests along with GE bending test data.

If the results of the analyses for the 30-foot side drop case are compared against these results, it is clear that if uniform strains (Fig. 6-1) are used as the criterion of comparison, the strains from the 30-foot side drop analyses will have approximately a 20 percent probability of exceeding the criterion uniform strains. However, if fracture strains are used as the criterion of comparison, the strains from the 30-foot side drop analyses will always be smaller than the criterion fracture strains. A discussion on the validity of fracture strains versus uniform strains is presented below, where it is concluded that the fracture strains should be used as criterion for comparison for this problem. The strains obtained for the 30-foot side drop analyses will therefore be always smaller than the test strains, even if tests other than GE bending tests are considered.

VALIDITY OF FRACTURE STRAINS VERSUS UNIFORM STRAINS

If the stress ratio, α, defined as the ratio of the longitudinal bending stress to the hoop stress is high (approximately higher than 2.0), the fracture strain criterion governs (Ref. 3). If, on the other hand, the stress ratio is low (approximately lower than 2.0), the uniform strain criterion governs. Accordingly, stress ratios were

TABLE 6-1

FUEL ROD BENDING TEST RESULTS FROM GENERAL ELECTRIC COMPANY

Specimen No.	Burn-up MWd/T	Ram Deflection Reached, in.	Estimated Outer Surface Strain %	Residual 13" Deflection in.	Comments
G28/D1-1A	12,000	>2	8.6	90° deflection	Failed
G28/D1-1B	12,500	>1	8.6	>5	No cracking
G28/D1-2A	14,000	1-1/8	8.6	6	No cracking
G28/D1-2B	14,300	1-3/8	8.6	>9	No cracking
G28/D1-2C	14,500	1-1/8	8.6	6	No cracking
G11/E2-2A	15,500	5/8	6-8	>3	No cracking
G11/E2-2B	16,000	1-1/8	8.6	>5	No cracking
G11/E2-2C	16,300	1-1/8	8.6	6	No cracking
G11/E2-3A	16,500	5/8	6-8	>2-1/8	Failed
G11/E2-3B	16,800	1-1/4	8.6	>6	No cracking
G11/E2-3C	17,050	5/8	6-8	>2-1/8	No cracking

The strain rate applied in these tests was estimated as 2×10^{-3} - 4×10^{-3} in/in/sec.

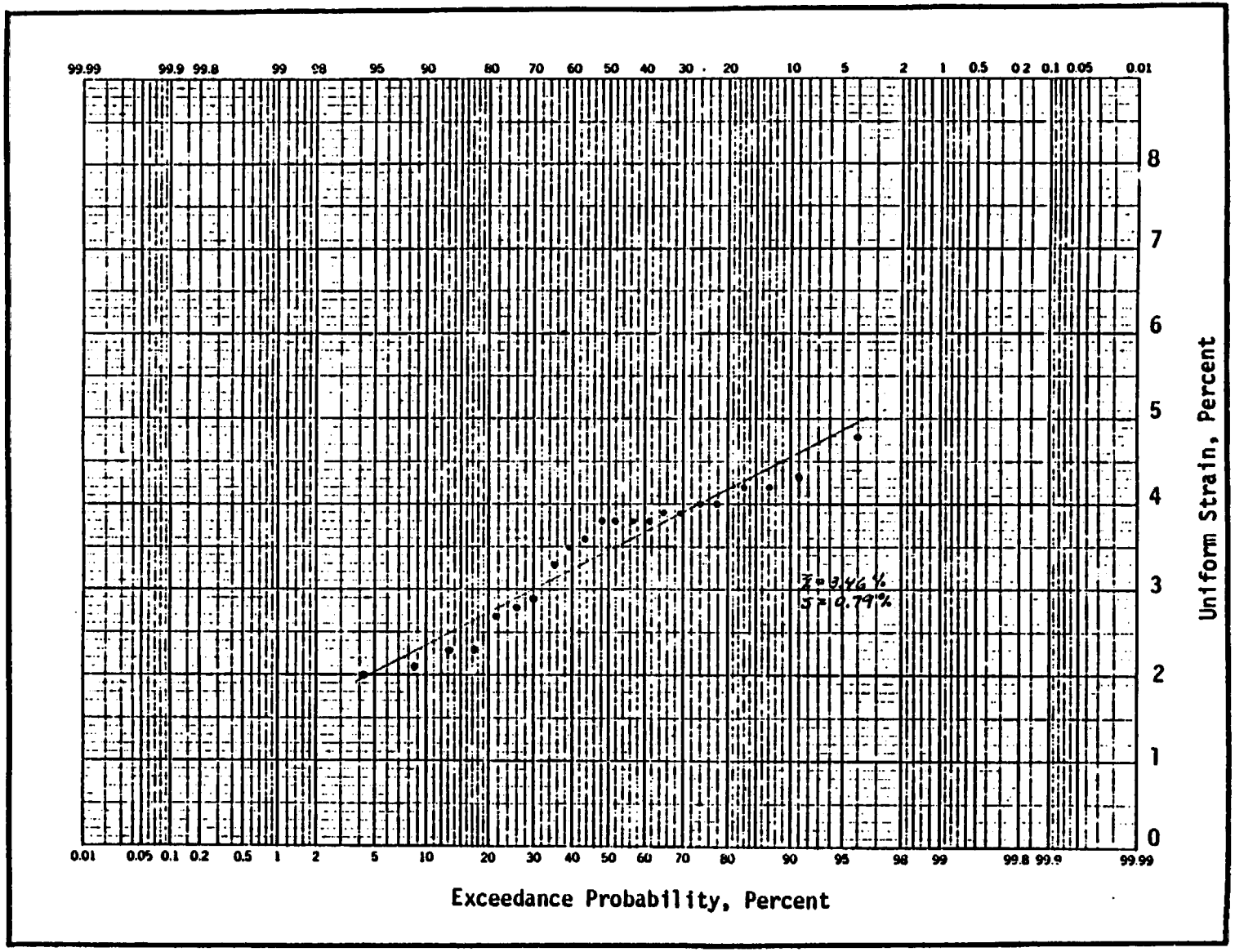

FIGURE 6-1 PLOT OF UNIFORM STRAIN FOR ALL TEMPERATURES

(TENSILE TESTS, GE BENDING TESTS NOT INCLUDED)

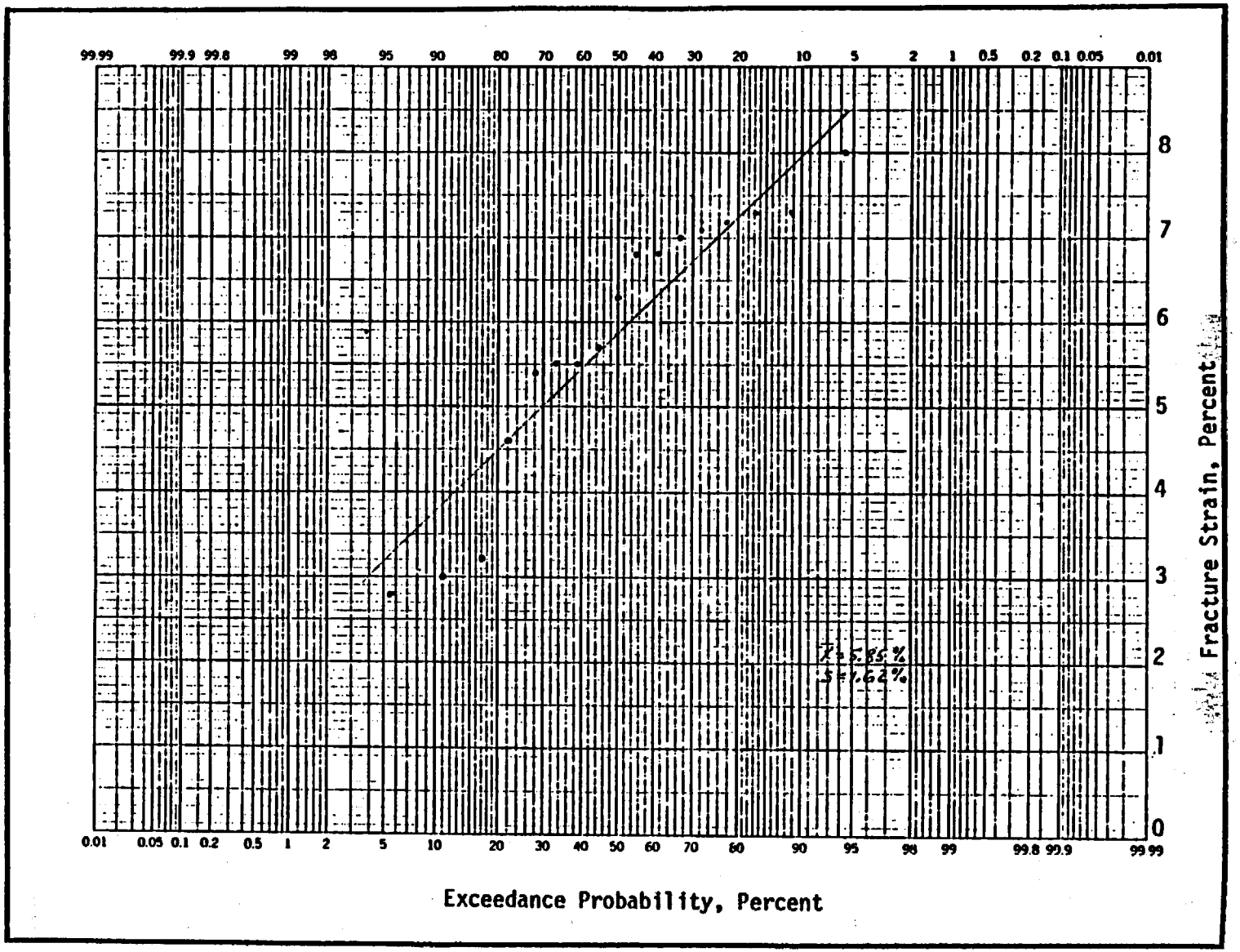

FIGURE 6-2 PLOT OF FRACTURE STRAIN FOR ALL TEMPERATURES

(TENSILE TESTS, GE BENDING TESTS NOT INCLUDED)

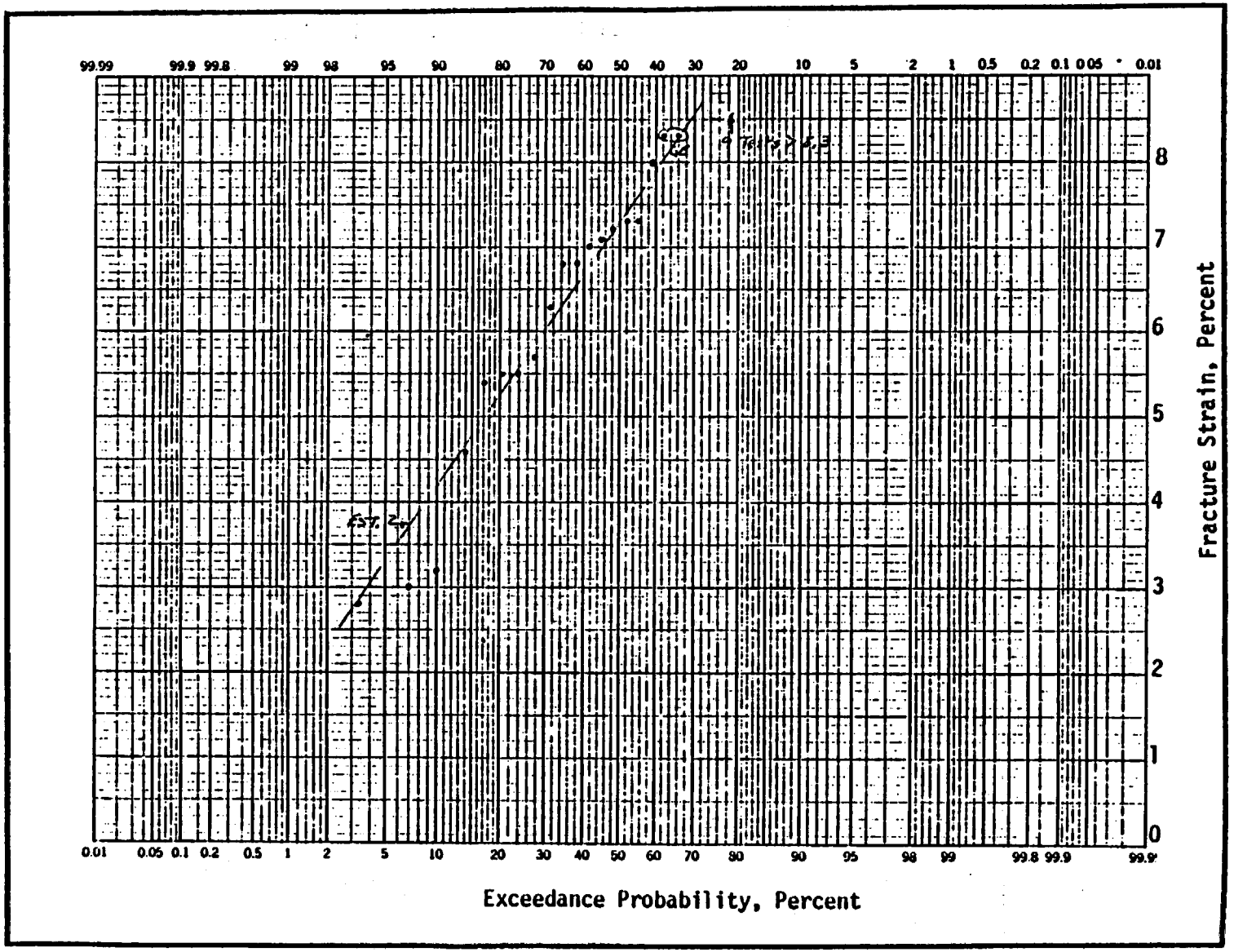

FIGURE 6-3 PLOT OF FRACTURE STRAINS FOR ALL TEMPERATURES

(TENSILE TESTS AND GE BENDING TESTS)

REFERENCES

1. IF300 Shipping Cask - Consolidated Safety Analysis Report - Chapter 5.6.5.A (NEDO-10084-2), October 1979.

2. IF300 Shipping Cask - Consolidated Safety Analysis Report - Chapter 4 (NEDO-10084-2), October 1979.

3. Letter Report to General Electric from Pacifica Technology, R.E. Nickell, dated May 16, 1978.

APPENDIX V-2

APPENDIX A

PRELIMINARY AND SECONDARY ANALYSES

APPENDIX A'

PRELIMINARY AND SECONDARY ANALYSES

PRELIMINARY ANALYSIS -- INVESTIGATION OF THE INFLUENCE OF THE DEPLETED URANIUM SHIELDING STIFFNESS ON THE RESPONSE OF FUEL RODS -- 30-FOOT SIDE DROP CASE

Preliminary analyses were performed to investigate the influence of the depleted uranium shielding in the cask shell on the response of the fuel rods. Analyses were performed for the BWR and PWR configurations, using the 122.0g rectangular acceleration input time history originally used (Ref. 1). The following table shows the results.

Configuration	Depleted Uranium Shielding Included?	Maximum Fuel Rod Strain (percent)
BWR	No	1.43
BWR	Yes	1.42
PWR	No	3.60
PWR	Yes	3.30

The above results show that the influence of depleted uranium shielding on the fuel rod response is negligible. The strains for the analysis cases without the depleted uranium shielding are slightly higher than those with the depleted uranium shielding. For the final analyses (described in Chapter 4), therefore, the depleted uranium shielding was not included.

SECONDARY ANALYSES

Flexural Analyses for the 30-Foot End Drop Case

The analyses for the 30-foot end drop case, described in Chapter 5, assumed that the fuel rods can deform only axially. Lateral degrees of freedom were not included in the analytical models.

To determine the influence of flexural deformations not considered in the 30-foot end drop analyses, flexural models were developed for the BWR and PWR fuel rod configuration. A typical model (for PWR configuration) is shown in Figure A-1. It was assumed that the fuel rods would deform until they come in contact with the guide tubes. The analyses were performed for this bent configuration with maximum posible deflections. The maximum axial forces obtained from the 30-foot end drop analyses were applied as vertical loads for these flexural analyses. The stresses obtained are presented below:

Configuration	Flexural Stress (psi)
BWR	51,590
PWR	16,210

The above flexural stresses were added to the axial stresses obtained from the end drop analyses described in Chapter 5. The total stresses so obtained are presented below, along with the corresponding maximum strains. The strains were obtained approximately by equating the areas under the elastic and elastic-plastic stress-strain curves, similar to Figure 6-1.

Configuration	Total Stress (psi)	Yield Stress (psi)	Strain (percent)
BWR	99,320	65,000	1.08
PWR	46,200	65,000	0.50

Investigation of the Cask Ovalling and Basket Spacer Disc In-plane Vibrations on the Response of the Cask-fuel Rod System

To investigate the influence of the cask ovalling and basket spacer disc in-plane vibrations on the response of the cask-fuel rod system, their respective frequencies were calculated. It was found that the fundamental cask ovalling frequency was about 212.0 cps, and the first two in-plane frequencies of the spacer discs were about 282.0 cps and 512.0 cps for the BWR configuration, and 278.0 cps and 1,040.0 cps for the PWR configuration. If these frequencies are compared against the frequencies of the cask and the fuel rods for the 30-foot side drop case, presented in Tables 4-1 and 4-2, it would be clear that there will be no interaction between the frequencies of the cask ovalling and spacer discs with the first few most significant frequencies of the cask-fuel rod system. It needs to be pointed out here that the contribution of the second, third, and higher modes of the cask, as compared to the first mode, to the response of the cask-fuel rods system, especially the fuel rods, is insignifcant. It can therefore be concluded that the influence of cask ovalling and spacer disc in-plane vibrations on the response of the cask-fuel rod system will be negligible.

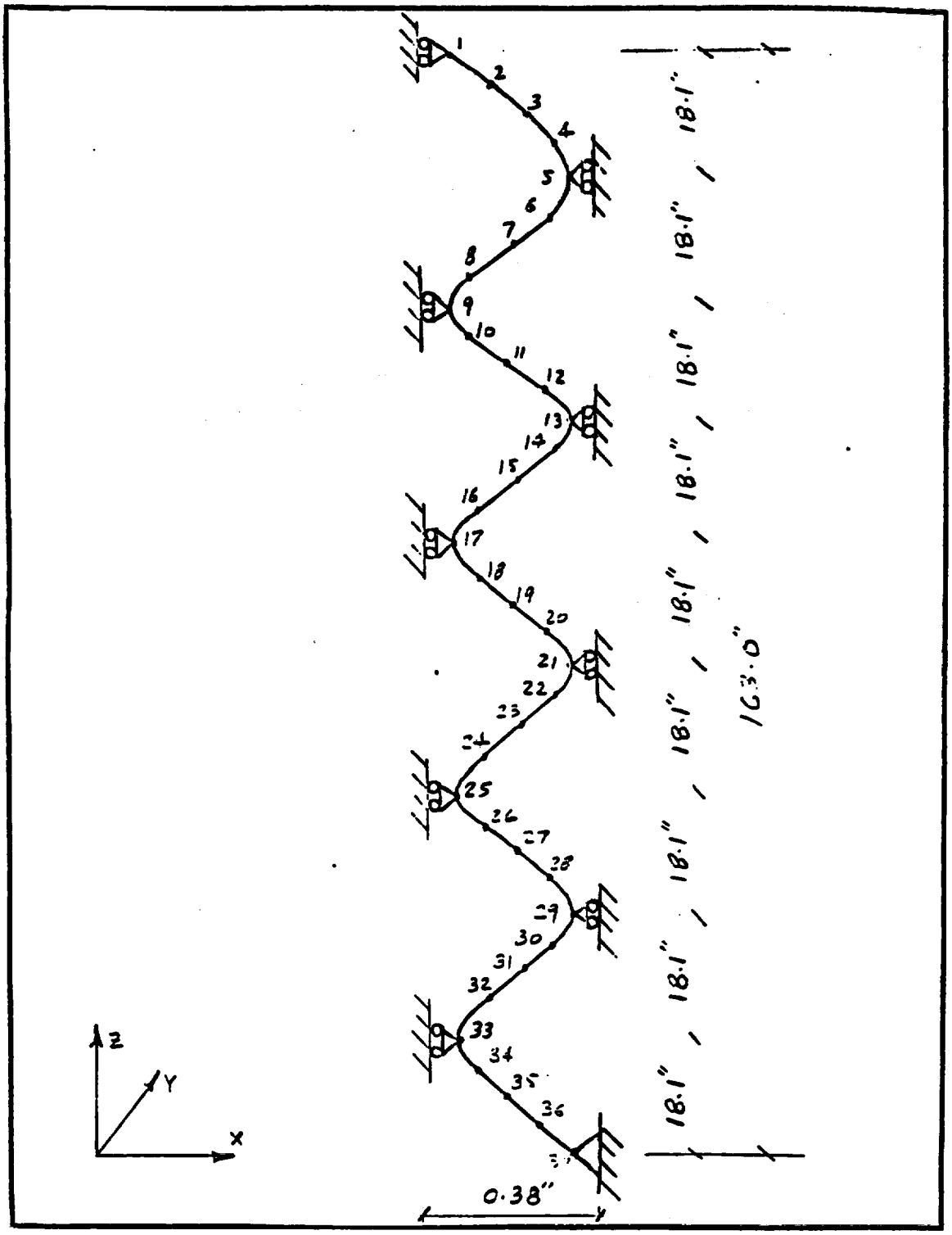

FIGURE A-1 FLEXURAL FUEL ROD MODEL FOR END-DROP CASE -- PWR CONFIGURATION

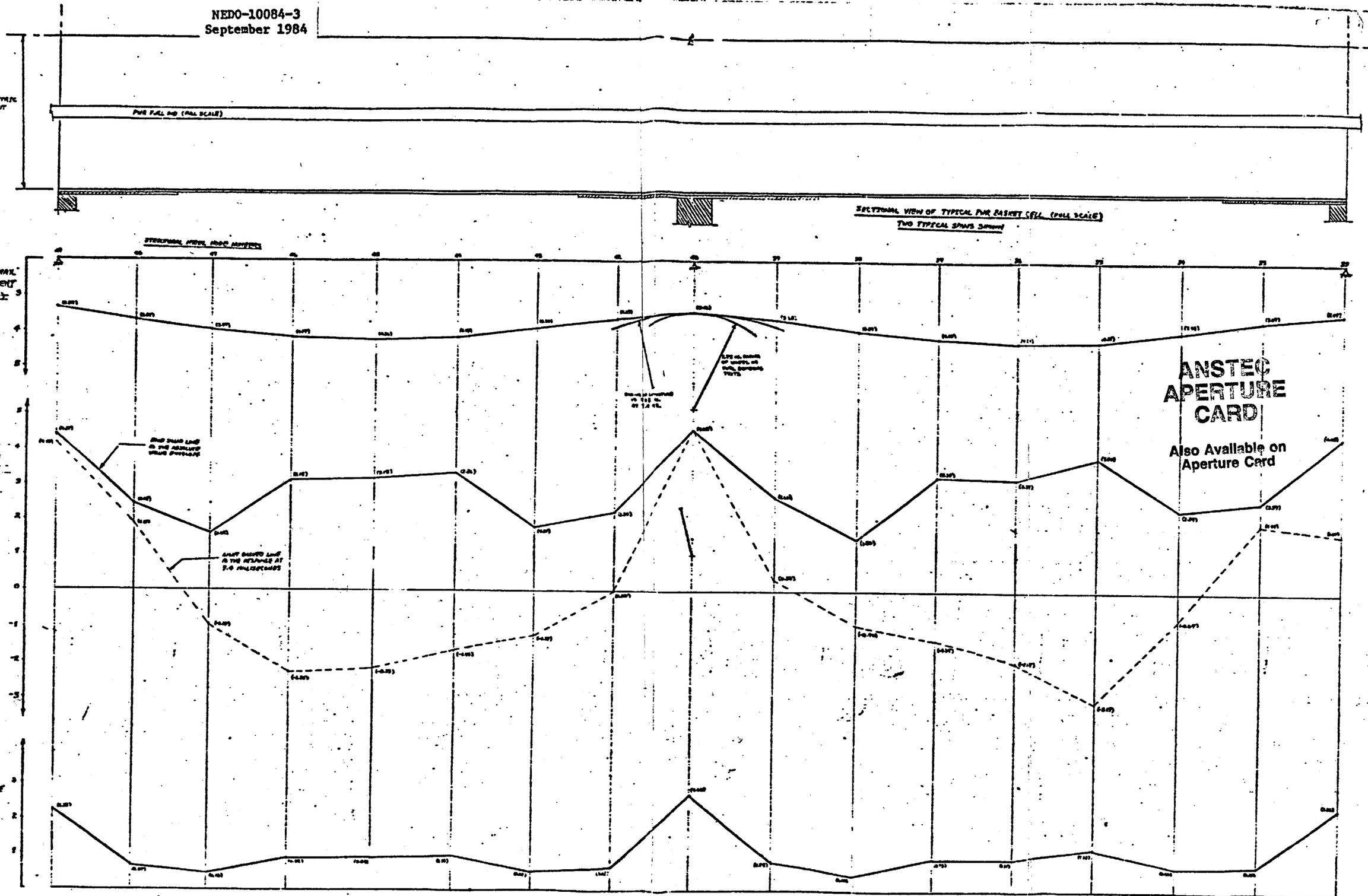

FIGURE 6-4 LAYOUT OF A BASKET SPACER AND A FUEL ROD AND THE CORRESPONDING MAXIMUM BENDING MOMENT AND MAXIMUM STRAIN CURVES

APPENDIX V-3

IF-300 BWR FUEL BASKET
HORIZONTAL DROP ANALYSIS

JANUARY 1983

NEDO-10084-3
September 1984

RSFA 83-07

DRF No. 137-0010

IF-300 BWR FUEL BASKET

HORIZONTAL DROP ANALYSIS

January 1983

Prepared By: K. E. OBERMILLER — DATE 1/21/83

Prepared By: G. C. MOK — DATE 1/21/83

Approved By: S. RANGANATH — DATE 1/21/83

NUCLEAR POWER SYSTEMS ENGINEERING DEPARTMENT

GENERAL ELECTRIC COMPANY, SAN JOSE, CALIFORNIA

Summary

This report presents an analytical study of the consequence of a thirty-foot drop of the IF300 irradiated fuel shipping cask. Specifically, the study assessed the structural integrity of the BWR fuel basket which supports the eighteen BWR fuel bundles transported inside the cask. The evaluation was performed for a horizontal drop (i.e., cask dropping parallel to the ground) under different orientations. Based on a static structural analysis, it was concluded that the 0 degree drop was the most severe one from the viewpoint of deformation and potential instability. Then, an elastic-plastic dynamic finite element evaluation was performed to determine the maximum dynamic loadings and to evaluate the structural consequences of the prescribed 30 foot drop.

The results of the analysis showed minimal yielding and nonsignificant deformations, and stresses were well below those required for buckling. It is therefore concluded that the structural integrity of the basket will be maintained following a postulated 30 foot cask drop.

1.0 Introduction

This report presents an analytical study of the consequences of a thirty-foot drop of the IF-300 irradiated fuel shipping cask. Specifically, the study assesses the structural integrity of the BWR fuel basket which supports the eighteen BWR fuel bundles transported inside the cask. The drop considered herein is a horizontal one; i.e., it occurs with the longitudinal axis of the cask parallel to the ground.

A cutaway view of the cask is depicted in Figure 1. A schematic drawing of the cask and BWR fuel basket is shown in Figure 2. A BWR spacer disk is shown in Figure 3.

The spacer disks and the top plate bear all the fuel load. The highest loaded spacer disk (based on a static analysis, Ref. 1) was selected for the detailed dynamic analysis described here. Deceleration versus time histories for different drop orientations (from Reference 2) were used in the dynamic analysis. Specifically three cases, namely, landing on the top (0 degree) of the unit, at 45 degrees and at 90 degrees from the top, were considered. All the deceleration-time histories show a short-duration ($\sim$1 msec), high-amplitude triangular pulse at the beginning, followed by a relatively long-duration ($\sim$15 msec), low-magnitude constant deceleration. A comparison of the three cases shows the highest overall deceleration in the 0 degree drop, therefore the zero degree drop can be expected to produce the most limiting stresses. A finite element static analysis of the spacer disk using the peak deceleration load for the three drop orientations confirms this. Accordingly, the 0 degree drop case was selected for a detailed dynamic finite element analysis.

Dynamic evaluation of a complex configuration like this is extremely difficult since it involves not only transient analysis but also the effects of geometric and material nonlinearity. The analysis presented here is comprehensive and considered all aspects of the problem--dynamic effects of

the basket components, effects of nonlinear material behavior, geometric nonlinearity due to yielding of the cask following impact and structural instability due to buckling. It represents a major effort involving state-of-the-art analysis, and required extensive computational work for model development, verification and analysis.

The dynamic analysis was carried out using the finite element computer program ANSYS, and included the inertial effects of all major basket components. The analysis also considered material yielding and the nonlinear effects of the radial gap between the outer rim of the spacer disk and the inner surface of the cask. The spacer disk material is A216 stainless steel that has a nominal yield strength of 58.4 ksi at the operating temperature of 200°F. Sufficiently small time steps were used to assure convergence. Analysis was performed for the entire period for which deceleration time history was available. Each run required approximately 100 NBU of computer time.

The results of the analysis showed minimal yielding in the disk. Stresses were well below those required for buckling and deformations were not significant. It is therefore concluded that the structural integrity of the basket is maintained for any drop orientation and that the cask can withstand a 30 foot drop successfully.

2.0 Analytical Approach

An evaluation of the structural integrity of a BWR fuel basket subjected to the impact force of a horizontal drop involves four major analytical steps:

(i) to identify the most critical component of the basket for a detailed finite element dynamic analysis

(ii) to define the most critical impact load for the analysis

(iii) to construct a finite element model for the critical component and carry out the analysis

(iv) to review the analysis results for indications of structural instability and/or excessive deformation.

2.1 Selection of the Limiting Spacer Disk

The fuel basket is a circular cylindrical frame structure which fits into the inner cavity of the shipping cask to provide lateral support for the fuel bundles. The structural strength of the basket is provided by 9 circular spacer disks and 4 tie rods which are welded to the disks as shown in Figures 2, 3 and 4. Each spacer disk of the BWR fuel basket has an array of 18 square holes or fuel cells which are partitioned by disk ligaments and cell spacers. The disk ligaments are integral members of the spacer disk plane. The cell spacers are continuous members, running the length of the fuel basket, which separate the 9 rectangular holes on the spacer disk into 18 fuel bundle locations. The orientation of the fuel basket with respect to the cask is always the same due to a keyway in the basket and a key in the cask which prevents the basket from rotating relative to the cask.

A fuel bundle is placed within a cell defined by a thin-walled channel and a cell spacer, both of which run through all 9 spacer disks. The fuel channels are not load bearing members. They serve only as guides for the

fuel bundles as they are lowered into the basket. Thus, in a horizontal position, the weight of the fuel bundles is directly transmitted through the spacer disks onto the inner wall of the cask.

The distribution of the fuel weight on the disk is determined by the disk spacings and by the beam action of the fuel basket. Treating the basket as a continuous beam supported laterally as the spacer disks and at the top plate of the cask, an earlier finite element static analysis under self weight (Reference 1) has shown that the second spacer disk from the bottom of the cask would experience the highest load. This spacer disk is subjected to a load of 2365 pounds when the basket is fully loaded with all 18 BWR fuel bundles and was, therefore, selected for detailed analysis.

2.2 Applied Loading

Figure 5 shows the deceleration time histories for the 0°, 45°, and 90° impact cases. (See Figure 3 for orientation definitions.) Of these three cases, the 0°drop clearly shows the highest overall deceleration and can therefore be expected to produce the most critical stresses. To confirm this a finite element static analysis of the spacer disk was performed using the peak deceleration loads for all three cases. (See Figure 6 for the model used.) The results of this comparison are shown in Table 1. It is seen that the maximum axial stress in a cell spacer for the 0° drop is approximately equal to that of the 90° drop and is about 38% greater than that of the 45° drop. A similar comparison of the stresses in the disk ligaments shows the 0° drop results to be significantly higher than those of the 90° and the 45° drops. It is, therefore, conservative to investigate only the 0° drop case in detail for the horizontal drop analysis of the fuel basket.

To convert the deceleration to an impact force in this analysis, the maximum static load (2365 pounds) of the spacer disk was used. Since the static load is equivalent to one G acceleration, the total impact load on the disk is simply the total static load multiplied by the deceleration expressed

TABLE 1

Static Analysis Results

Member (See Figure 6)		0° Drop Stresses	45° Drop Stresses	90° Drop Stresses
Cell Spacer	1	-40.9	-23.0	--
	2	-40.9	-18.2	--
	3	--	--	-21.2
	4	--	-23.8	-31.9
	5	--	-29.5	-41.9
Disk Ligament	1	-85.0	-46.5	--
	2	-49.4	-19.0	--
	3	-66.6	-37.5	--
	4	-66.6	-32.2	--
	5	-49.4	-20.2	--
	6	-16.1	--	--
	7	-32.9	-18.6	--
	8	-32.9	-14.6	--
	9	-16.1	--	--

All stresses in ksi. Only significant compressive stresses are shown.

in G's. An amplification factor of 1.05 on the deceleration was also used in this analysis to account for a slight deviation of the cask from rigid body motion.

The actual loading of the model was accomplished by applying pressure on the inside surfaces of the cells where the fuel bundles are supported. The static load on the most heavily loaded spacer disk (2365 lb) was determined as described in the previous section. This load was first converted to a pressure and then converted to a dynamic load by multiplying by the appropriate deceleration. Although this total wieght is not concentrated solely in the fuel cells, it was assumed that each of the eighteen fuel cells would support one-eighteenth of that weight. This would concentrate the total weight in the most critical area of the spacer disk as an added measure of conservatism. The following equation was used to calculate the pressures in each of the fuel cells.

$$\text{pressure} = \frac{\frac{2365 \text{ lb}}{18}}{A} \times G$$

where A = the total area of the supporting member
G = the deceleration, in G's, of the spacer disk (including the 5% increase to account for the structural response of the cask).

2.3 Dynamic Analysis

A dynamic analysis of the most highly loaded spacer disk was performed using the finite element computer program ANSYS. The program capabilities used in this analysis have been properly verified in accordance with an established GE internal QA procedure for engineering computer programs.

The finite element model used is shown in Figure 7. Only one-half of the spacer disk is modeled due to the symmetry of the problem. The spacer disk is modeled with the 2-D 4-node isoparametric finite element with incompatible modes (ST1F42). The rim of the spacer disk was modeled with elements 4 inches deep. The cell spacers run the length of the cask but only a 4 inch deep portion was modeled. The mass of the additional material, however, was added to the cell spacer elements by increasing their densities. Similarly, elements 30 and 36 have higher densities to account for the mass of the tie rods which also run the entire length of the cask. These greater densities were used so that a more realistic dynamic response of the spacer disk would be obtained. All other elements are one inch deep and have unaltered densities.

Each spacer disk fuel cell, for the most highly loaded disk, supports 105 pounds of fuel bundle and fuel cell channel weight. This mass was uniformly distributed over the side of the cell which supports it. The following equation was used to calculate the masses to be assigned to the nodes along the applicable side of each cell.

$$\text{mass} = \frac{a}{A} \times \frac{105 \text{ lb}}{g}$$

where a = the area of the supporting member surrounding a node (the mass supported by this area will be assigned to that node)

A = the total area of the supporting member

$g = 386.4 \text{ in/sec}^2$

When the disk is loaded it will deform and make contact with the cask wall which has a slightly larger diameter than the disk (37.5 inches versus 37.31 inches). Contact will only be made, however, after a finite amount of movement has occurred. For this reason, gap elements were added to the model. These elements consist of two nodes which travel relative to each

other in a specified direction. The nodes are initially separated and travel with no resistance until they contact each other. At this point the "outside" node resists any further motion of the "inside" node by acting as a very stiff spring. These elements were positioned around the outside of the spacer disk rim radially opposite each node that could deform enough to contact the cask wall. The radial distance that each node could move before making contact with the cask wall was calculated and entered as the gap size for the gap element corresponding to that node. This removes any uncertainties about the contact area between the spacer disk and cask wall.

Figure 8 shows the bilinear stress-strain curve that was used for the material in the analysis. These properties were obtained from data supplied by Allegheny Ludlum for Type 216 stainless steel at 200°F, the design temperature. Von Mises Kinematic hardening was assumed. Except for plastic flow, it has been conservatively assumed that the material has no other damping.

The spacer disk was assumed to be at rest initially and was subsequently subjected to a dynamic load based on the deceleration versus time history of the 0° Drop case. Loading was applied as a uniform pressure on the bottom surface of each of the eighteen fuel cells as described in the previous section. Since the mass and inertial force of the fuel overshadow the contributions from other components, this method of applying the dynamic load is an adequate approximation.

e

To aid the interpretation of results and the selection of time steps an elastic frequency analysis was performed. When the spacer disk is fixed at its impact point (i.e., at the lowest point of its outer rim) the lowest natural frequency was calculated to be 120.6 Hz. This result changes less than 0.5 H, if the effect of the stiff spring representing the cask is included in the analysis. This fact confirms that the cask cavity wall in the model is adequately rigid compared to the spacer disk.

Based on a parametric study using various integration time steps, the time stop of 0.005 milliseconds was found to be adequate. The stiffness of the model was reformed at each time step due to the nonlinearity of the problem.

3.0 Analytical Results

While evaluating the results, two possible failure modes were postulated:

(i) buckling of the weaker members such as the disk ligaments and the cell spacers under compressive loads

(ii) excessive plastic deformation.

For each finite element in the analysis model, the computer program calculates a set of stress values corresponding to the centroid location of the element. Plots of the axial stress for various elements versus time are shown in Figures 9 through 13. A review of the axial stresses in the disk ligaments and cell spacers shows the following:

(i) Higher stresses tended to occur in members located closer to the impact point (i.e., the lowest point of the finite element model in Figure 7.)

(ii) The stresses in the vertical members are generally compressive while those of horizontal members are usually tensile. Thus if buckling was to occur, it would be in a vertical member.

(iii) The stress-time histories always show sinusoidal oscillations of several frequencies. For the highly-stressed members, however, a dominant frequency is apparent and is near the lowest natural frequency of the spacer disk (120.6 Hz). Figures 9 and 10 show two of these time histories, one of which is for the most highly stressed disk ligament (elements 168, 169 and 172 in Figure 7) and the other is for the most

highly stressed cell spacer (elements 98, 99 and 100). Clearly, the primary dynamic response of the spacer disk is dominated by the lowest vibration mode.*

(iv) As shown in the time histories of Figures 9 and 10, the peak stress value of the time history is always attained early in the transient. This observation confirms the belief that the triangular load pulse at the beginning of the load history governs the dynamic response.

From the results shown in these figures the maximum compressive stress is 41.5 ksi in the disk ligaments and is 23.0 ksi in the cell spacers. Both of these values are lower than the corresponding static buckling capability--52 ksi for the disk ligaments and 45 ksi for the cell spacers. (See Appendix A for details.) Therefore, buckling of these spacer disk members is not predicted. The maximum displacement that occurred during the response was 0.06 inches. This is not large enough to interfere with or cause any damage to the fuel bundles.

Furthermore, only two of the elements (Nos. 96 and 167 in Figure 7) have plastic deformation. The maximum Von Mises permanent strain is less than 0.6%. This result indicates that the impact loading causes only minor, highly-isolated permanent deformation in the spacer disk.

*This suggests that the response can be approximately described in terms of a single-degree-of-freedom system. Using this approximation and the readily-available information on the dynamic response of a single-degree-of-freedom system to a triangular force pulse, it can be shown that the dynamic load amplification factor for this problem is less than unity. This result means that, in this case, the impact load behaves much like a very-short-duration impulse, i.e., it cannot produce a response that exceeds the static response. A comparison of the actual results of the finite element static and dynamic analysis confirms that the stresses are less severe under dynamic loading and that the amplification factor is less than one.

4.0 Conclusion

The nonlinear dynamic analysis of the most critically loaded spacer disk subjected to the limiting impact loads showed no appreciable permanent deformations in the disk. The peak compressive dynamic stresses in the disk ligament and the cell spacer do not exceed the buckling strength and structural stability is maintained. It is therefore concluded that structural integrity of the basket will be maintained following a postulated 30 foot cask drop.

References

1. Spent Fuel Services Operation E. C. #C5467-334.

2. NEDO-10084-2 Appendix 5-1, Figure 5 and Table 7.

Appendix A

Static Buckling Analysis of Cell Spacers and Disk Ligaments

To determine the axial stress which will induce buckling in the cell spacers and disk ligaments, the ADINA finite element program was used. The model shown in Figure A1 uses 23 three-dimensional beam elements with an initial eccentricity of 0.03 inches. The end conditions were conservatively assumed to be pinned-pinned and the updated Langrangran formulation was used to account for large deformations. Effects of geometric nonlinearity were included by reformulating the stiffness matrix after each load step. The analysis was done elastically with a Young's modulus of 26.2×10^6 psi. An axially compressive load was incrementally applied to the top of the model until the beam became unstable. The same procedure and model was used for the cell spacer and the disk ligament. The only difference between the two was the dimensions of the cross-section. The load versus lateral deflection curves for both the cell spacer and disk ligament are shown in Figures A2 and A3. The critical buckling load was defined to be the point at which the lateral deflection is twice as large as the initial linear portion of the curve would predict. This results in a critical buckling stress of 45.0 ksi for the cell spacers and 52.0 ksi for the disk ligaments.

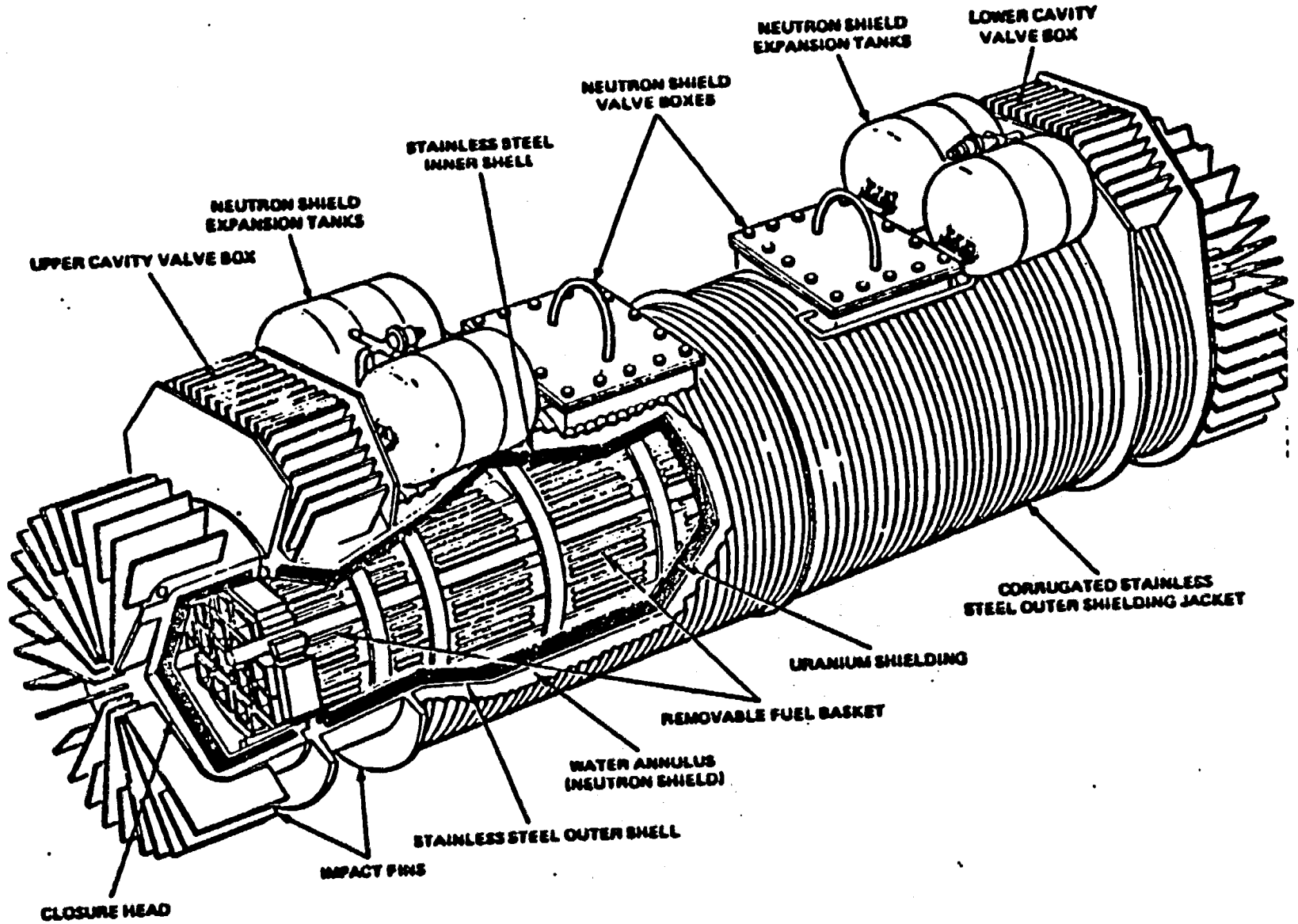

Figure 1 IF-300 Cask. Cutaway View

FIGURE WITHHELD UNDER 10 CFR 2.390

Figure 2 - BWR Fuel Basket Schematic

FIGURE WITHHELD UNDER 10 CFR 2.390

Figure 3 - BWR 18 CELL FUEL BASKET

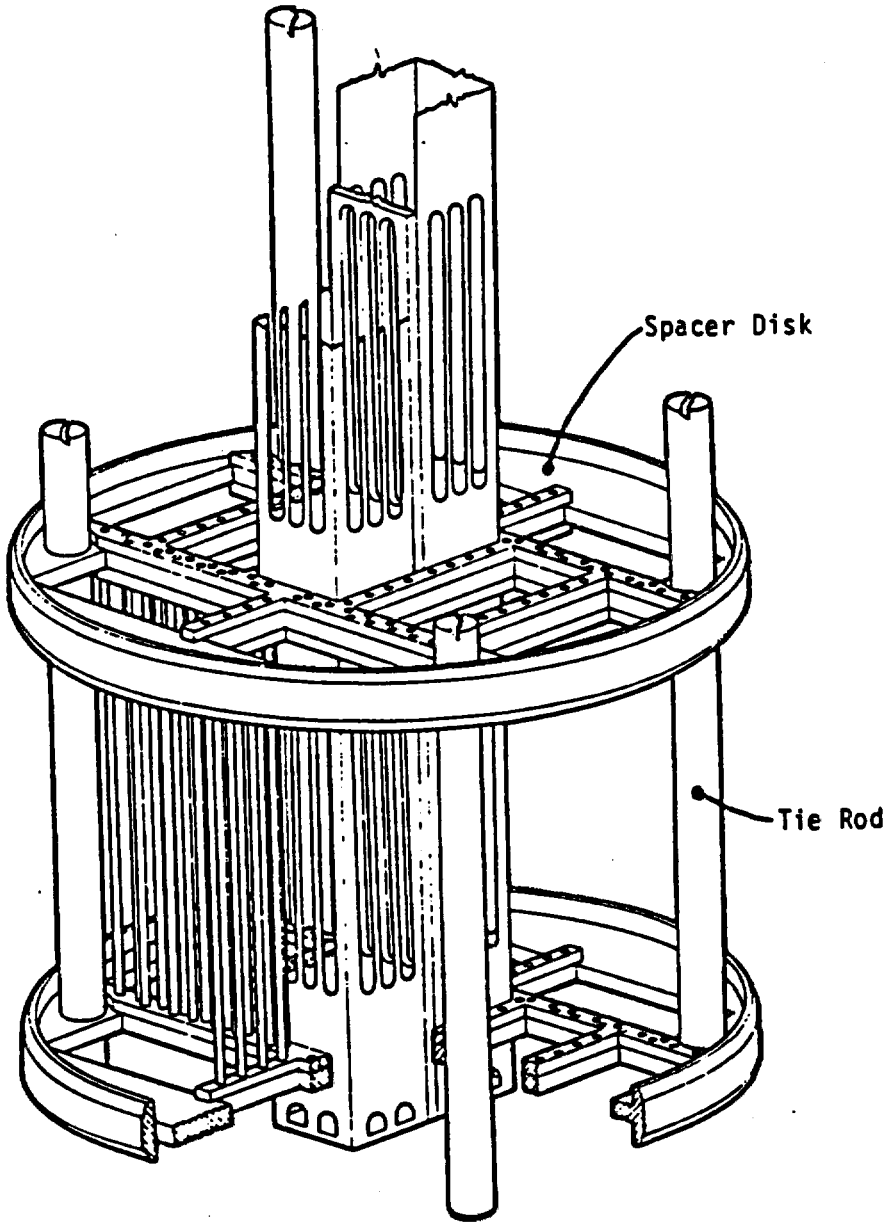

Figure 4 - BWR Fuel Basket Assembly

#	Cask Orientation	Peak G's	Plateau G's
1	0 degrees	204	91
2	45 degrees	153	68
3	90 degrees	133	59

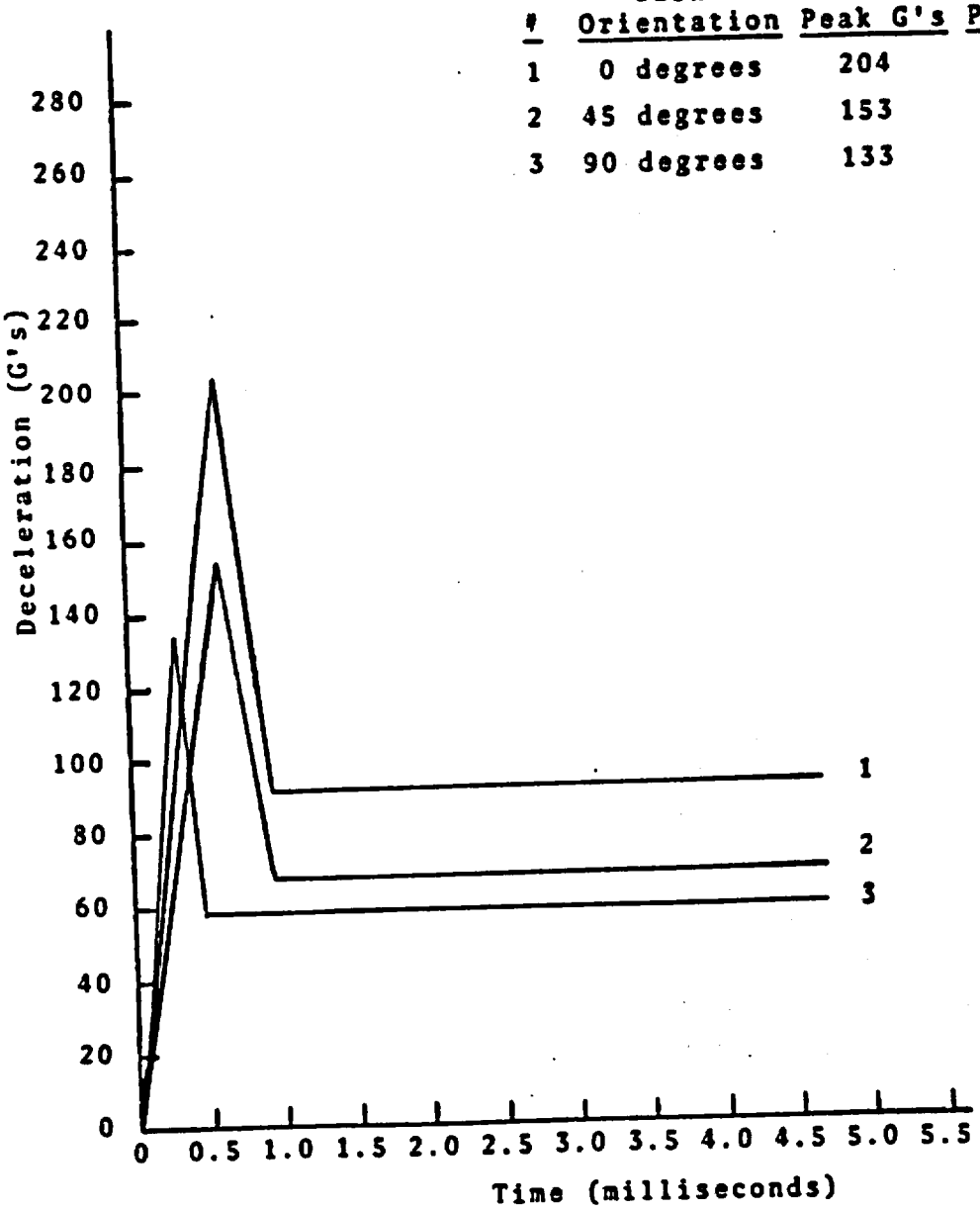

Figure 5 - Deceleration Time Histories

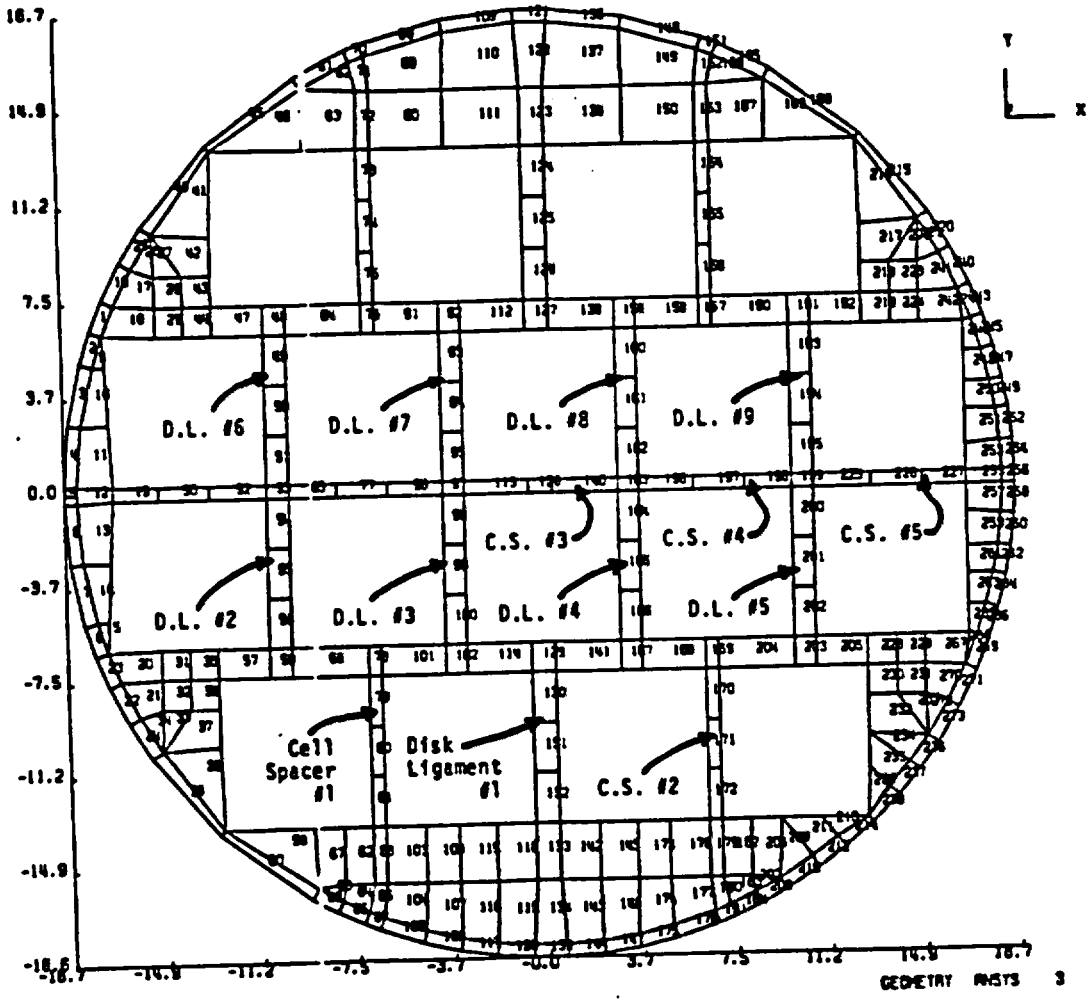

Figure 6 - Static Finite Element Model
(with element numbers)

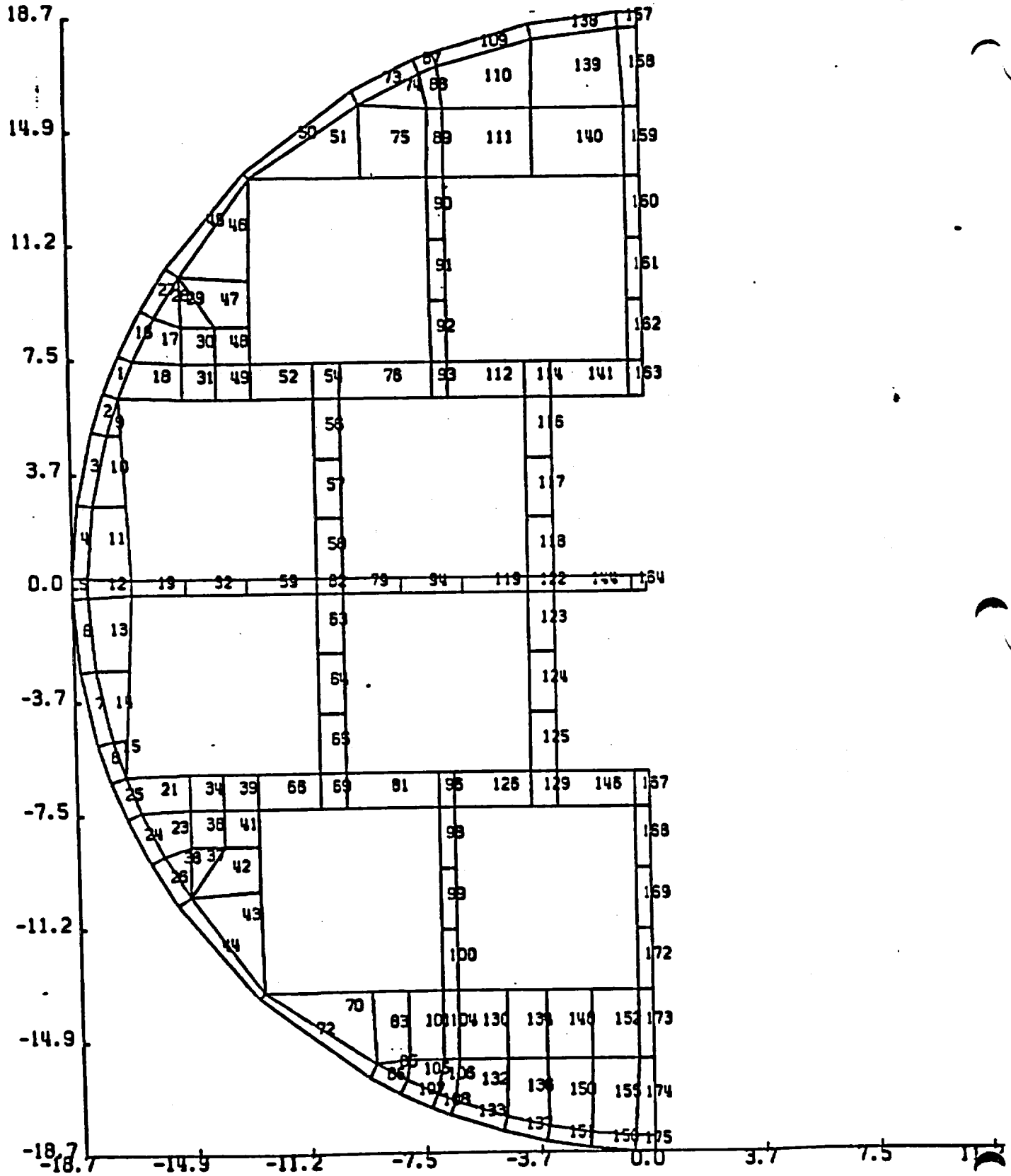

Figure 7 - Dynamic Finite Element Model

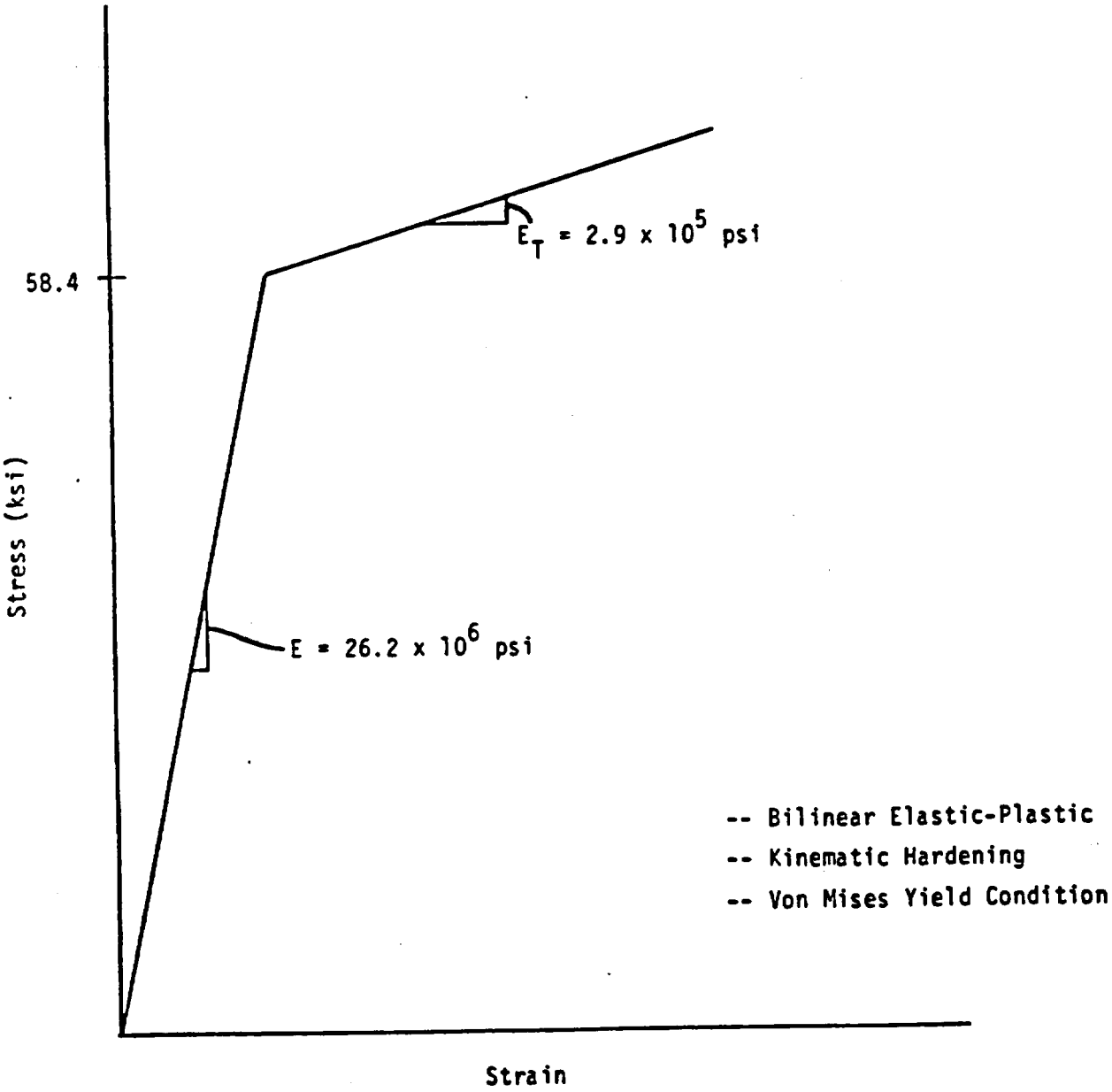

FIGURE 8

Stress-Strain Curve of Spacer Disk Material

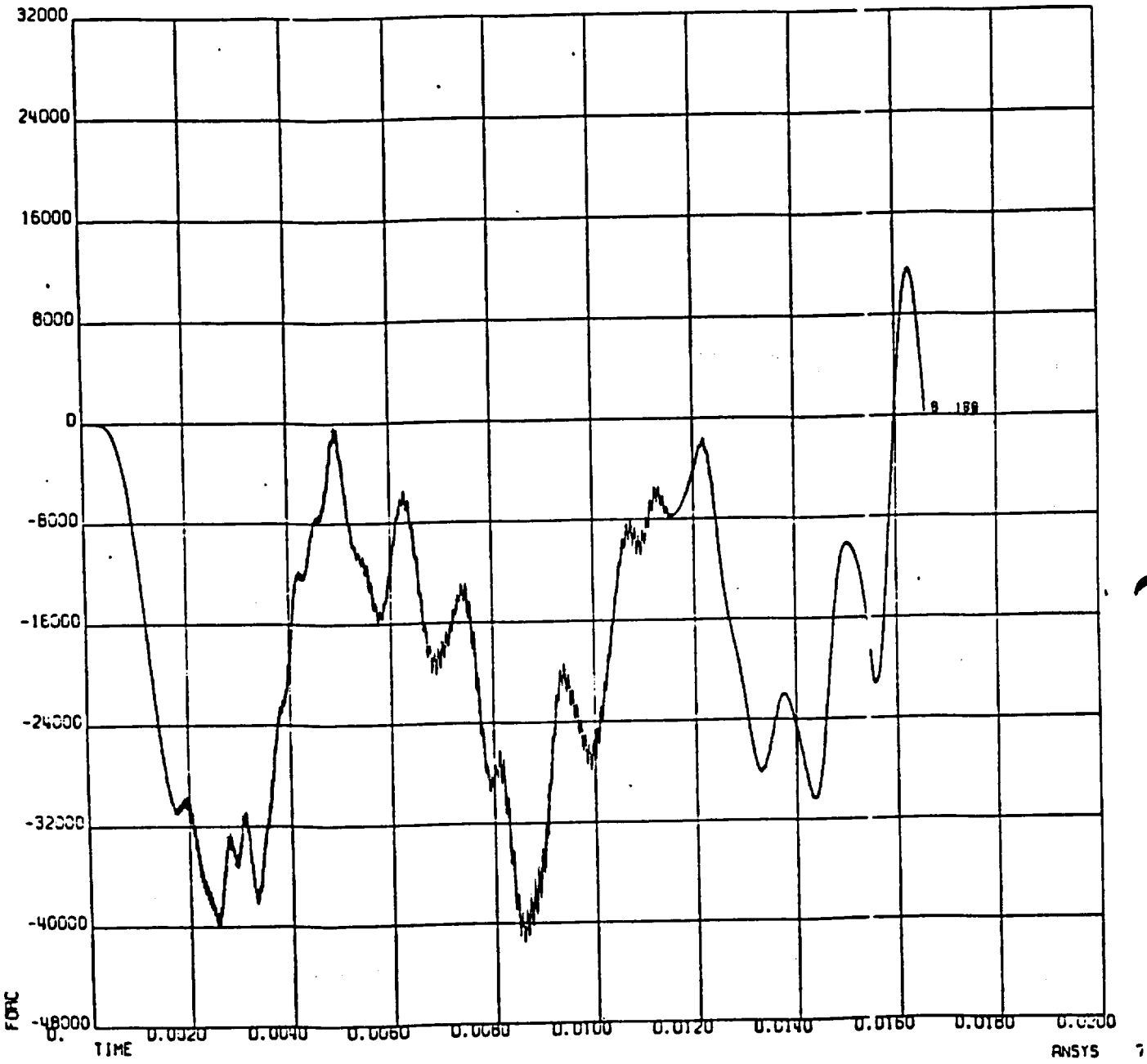

Figure 9 - Axial Stress vs. Time for Elements 168, 169, 172

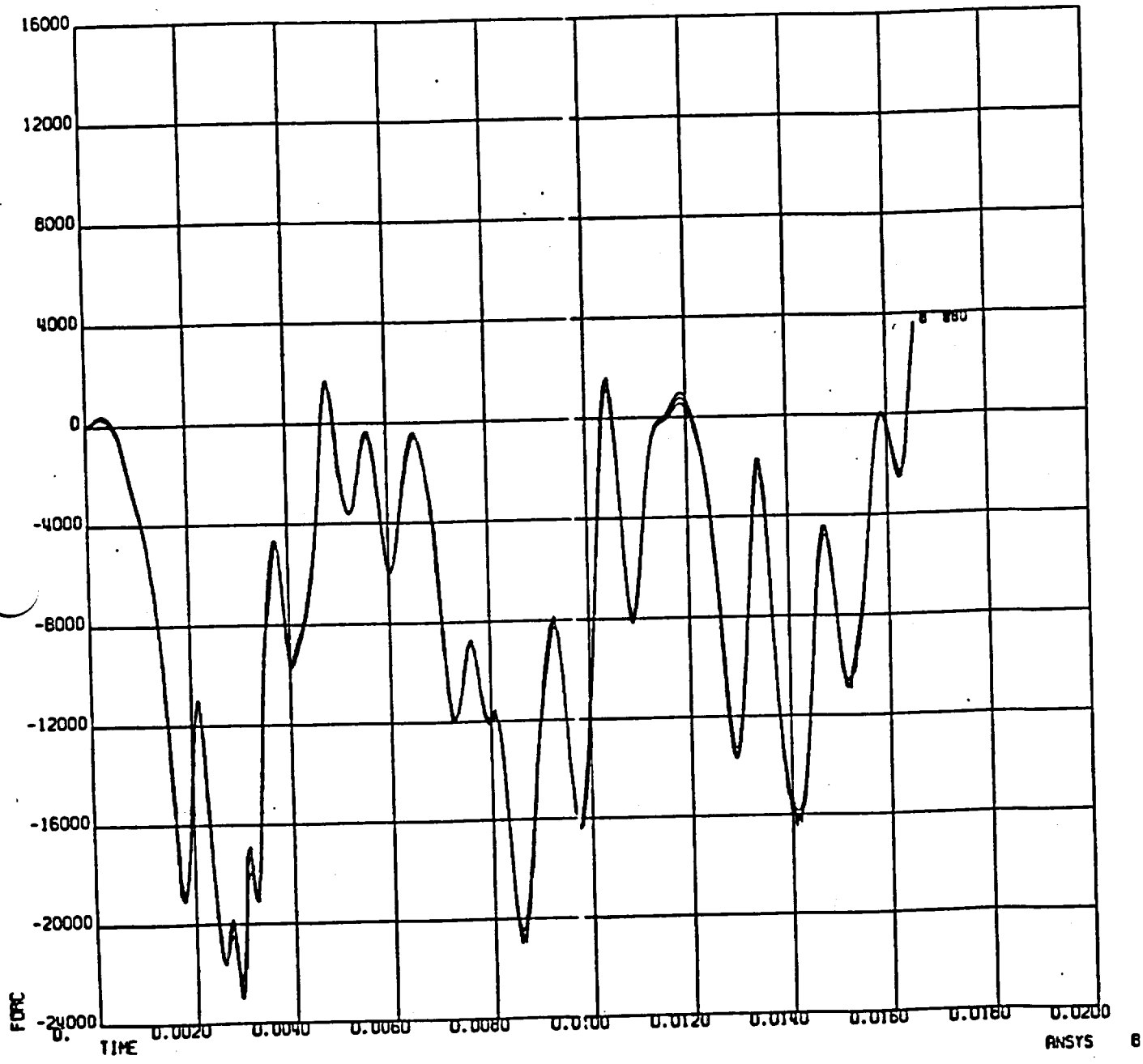

Figure 10 - Axial Stress vs. Time for Elements 98, 99, 100

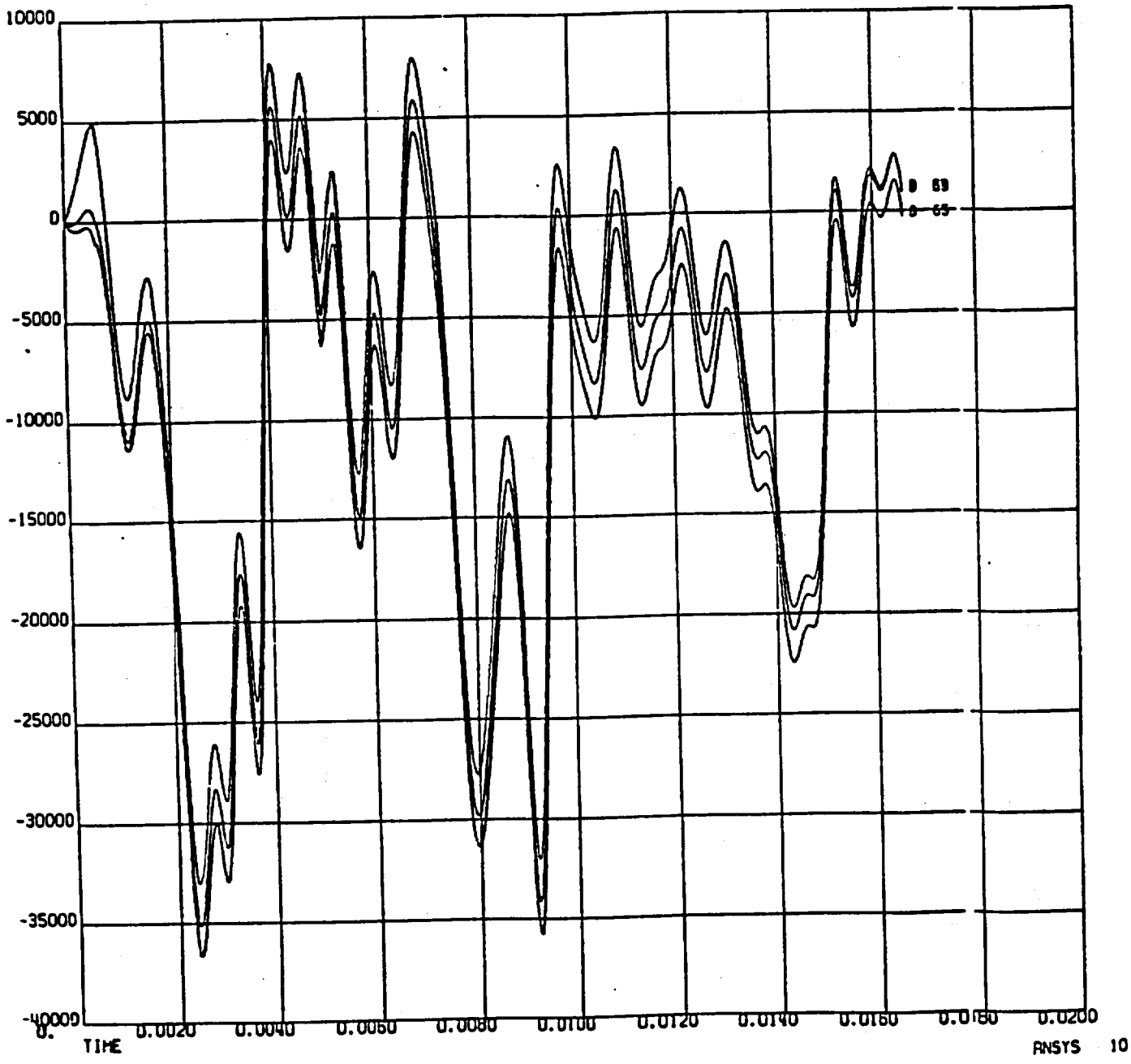

Figure 11 - Axial Stress vs. Time for Elements 63, 64, 65

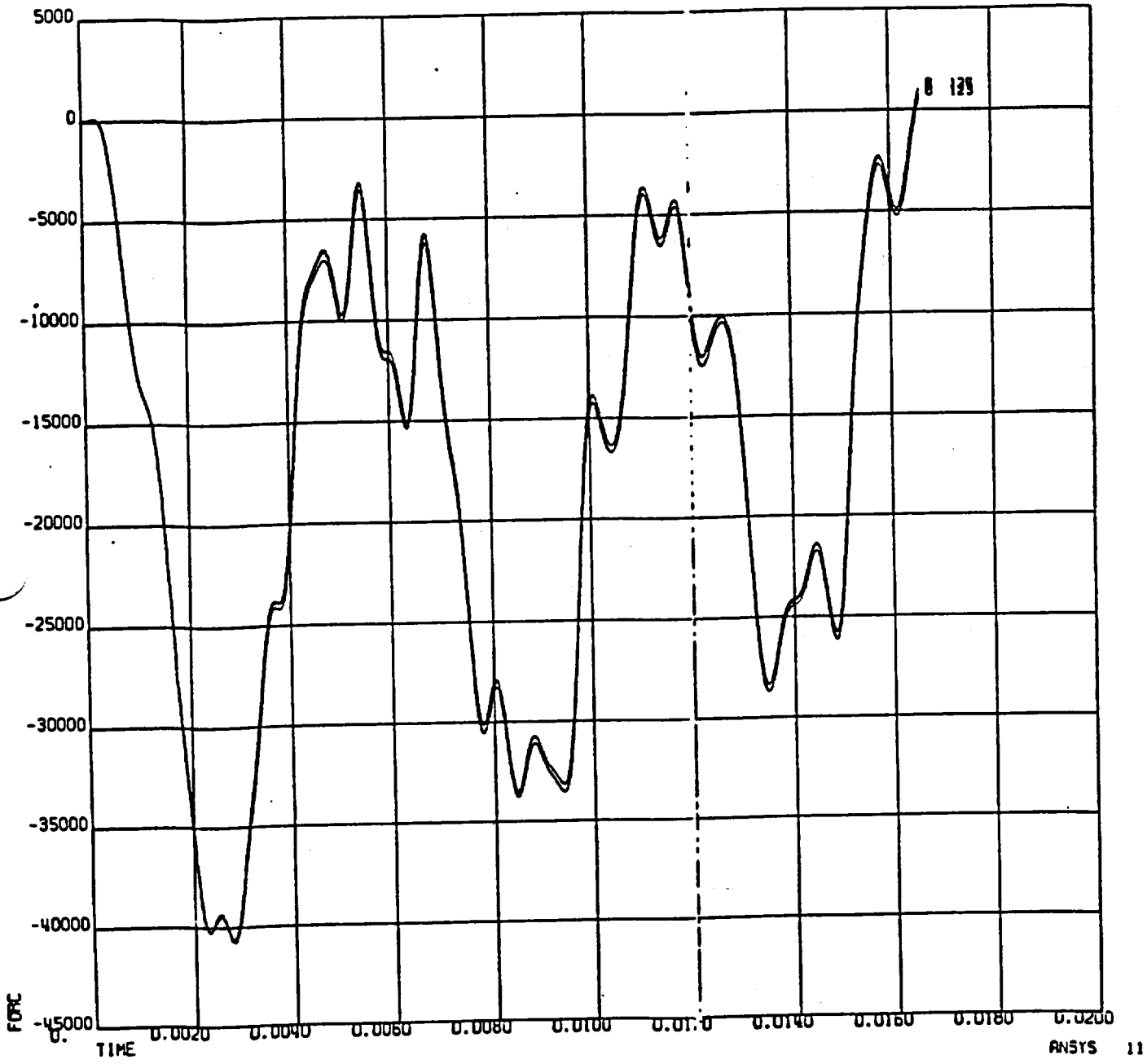

Figure 12 - Axial Stress vs. Time for Elements 123, 124, 125

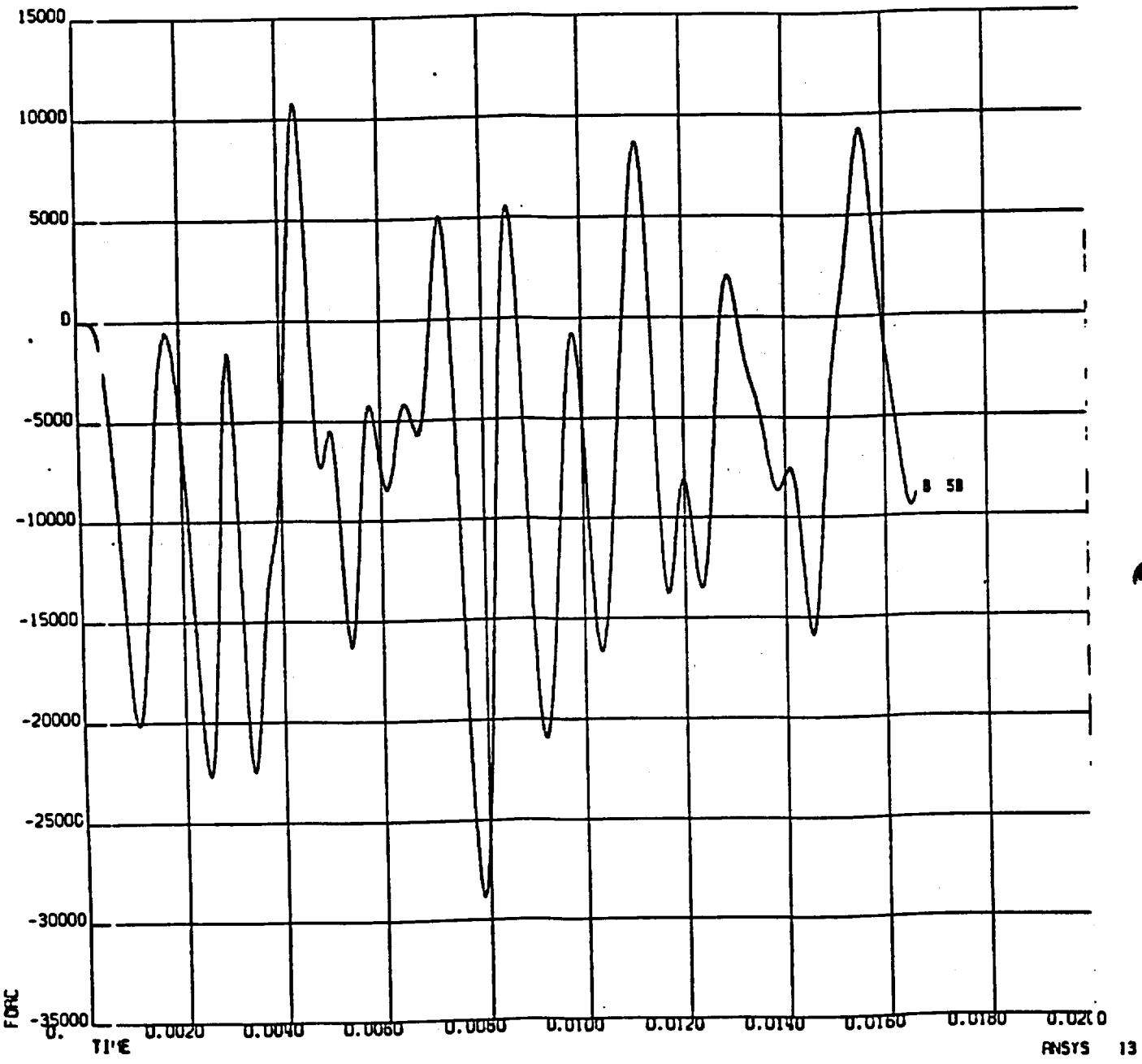

Figure 13 - Axial Stress vs. Time for Elements 56, 57, 58

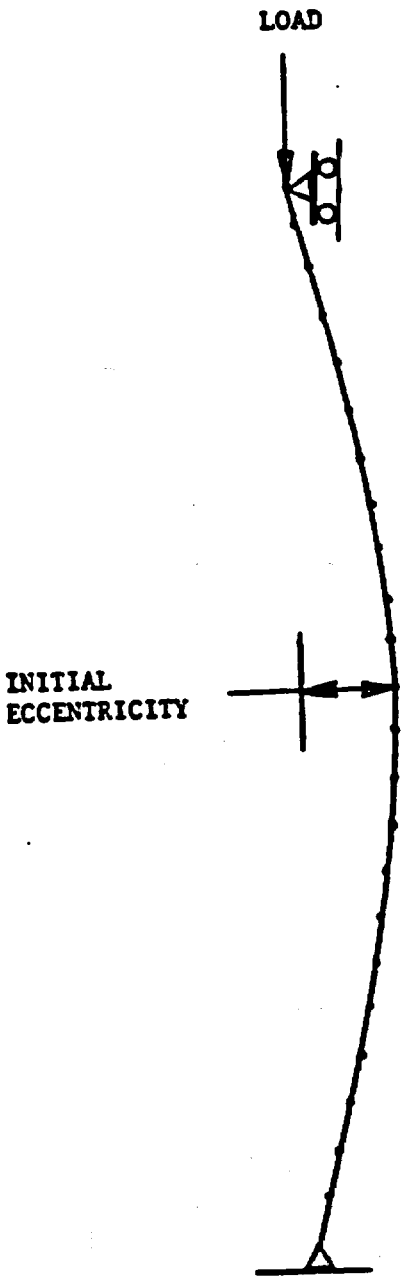

Figure A1 - ADINA Finite Element Tie Rod Model

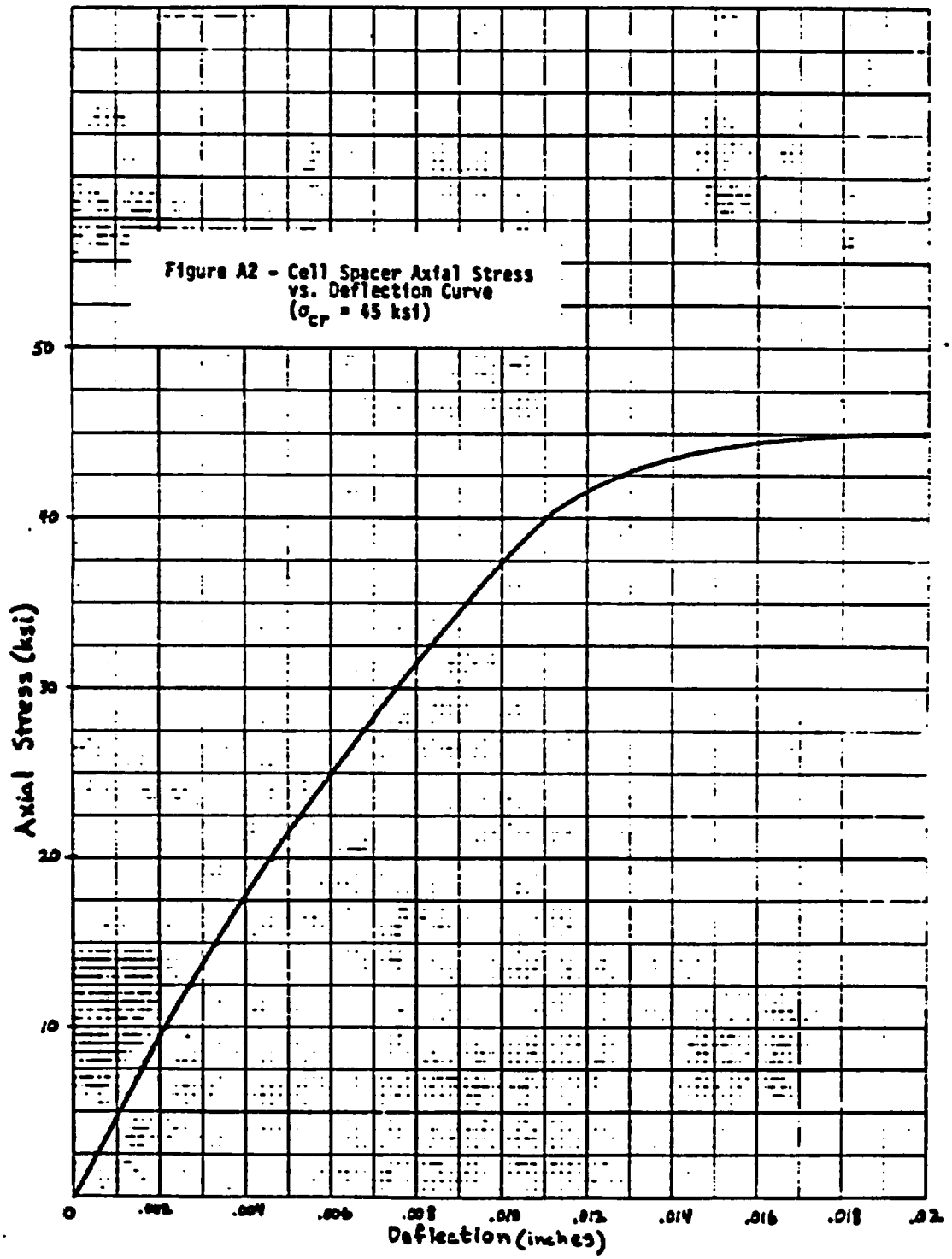

Figure A2 - Cell Spacer Axial Stress vs. Deflection Curve (σ_{cr} = 45 ksi)

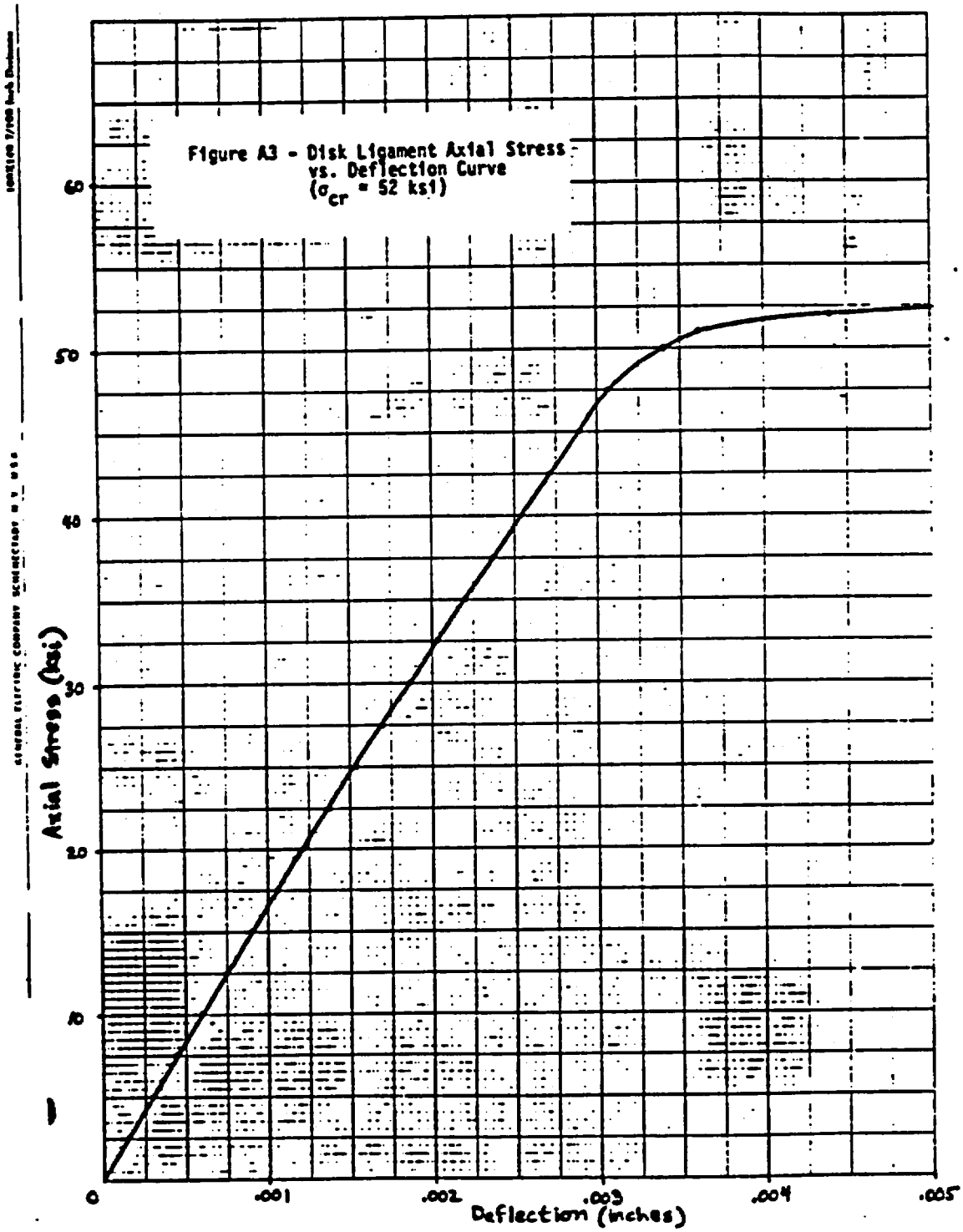

Figure A3 - Disk Ligament Axial Stress vs. Deflection Curve (σ_{cr} = 52 ksi)

APPENDIX VI-1

IF-300 SHIPPING CASK
DEMONSTRATION TESTING REPORT
CASK #301

IF-300 SHIPPING CASK
DEMONSTRATION TESTING REPORT
CASK #301

I. Introduction

As discussed in the IF-300 Cask Consolidated Safety Analysis Report (CSAR), each cask manufactured will undergo a hydrostatic test, and the first cask produced will undergo an extensive thermal demonstration test. This report discusses the testing programs conducted on cask number 301 - the first IF-300 manufactured.

A. Hydrostatic Testing.

The IF-300 cask contains three pressure retaining structures. These structures are the inner cavity, the upper neutron shielding barrel, and the lower neutron shielding barrel. The cask cavity is sealed by one of two optional heads; therefore, each head must be tested. Closure sealing is accommodated by 32 studs and nuts which compress a Grayloc metallic seal ring. Each barrel is a seal-welded structure with valve penetration via a forged manifold. No leakage is permitted from any of these structures under test pressure.

B. Thermal Testing.

The IF-300 cask is designed to dissipate 262,000 Btu/hr. To verify the design as well as gather data for operational use, the first cask produced will be given a series of thermal demonstration tests. The test sequence is described in Subsection 6.7 of the CSAR, NEDO 10084-1.

Basically, the test consisted of two parts: normal cooling, and loss-of-mechanical cooling. The latter part, LOMC, is included in the test, since it represents the most credible off-normal condition, and produces the highest non-accident temperatures. The results of these tests will form the basis for any adjustment to the cask heat load limit.

II. Hydrotesting

A. Test Set-Up.

The hydrotest was conducted in accordance with Stearns-Roger Procedure SR-PP-198 Revision 1, approved by General Electric. Each vessel to be tested was water-filled, sealed, and equipped with a recording pressure gage and a relief valve set at five percent above test pressure.

The vessels to be tested were first brought to pressure with a pump, then isolated from the pump, and finally observed for any sign of pressure decay. In addition, all penetrations and closures were observed for signs of leakage. The minimum pressures were 200 psig, and 400 psig for the neutron shielding barrels and the cavity respectively. Barrel hold time was 40 minutes; cavity hold time was 60 minutes. As mentioned earlier, both the BWR and the PWR heads were tested. The cask was tested in the vertical position.

B. Results.

The hydrostatic test was successful. No leaks or pressure decay was observed at a barrel pressure of 200 psig or at cavity pressures of 405 and 410 psig. Copies of the notarized test certifications are attached.

III. Thermal Testing

A. Test Set-up

The thermal demonstration tests were conducted in accordance with Stearns-Roger Procedure SR-PP-229 Revision 3, approved by General Electric. The PWR basket was used to hold seven immersible heaters, one per cell, each capable of producing 12 kw uniformly distributed over a 12 foot length. Heaters were centered in the cells by disk spacers. Each heater was equipped with two thermocouples, one at the mid-length, the other five feet further towards the lower end.

The basket and cask body was instrumented with thermocouples as described in Subsection 6.7 of the CSAR. A test head containing heater and TC penetrations was installed in place of the normal closure. The cask was placed in its normal transport position on the equipment skid. Power for the heaters was supplied by a diesel-generator set. TC readings were taken on three multipoint recorders. The chromel-alumel TC's had a reference junction temperature of 32°F. Ambient air temperature was measured by a mercury thermometer. Temperature data was transcribed from the recorders to log sheets on approximately one hour increments. In addition to temperatures, the cask cavity, upper barrel, and lower barrel pressures were recorded. The barrel relief valves were set to 150 psig, instead of the 50 psig indicated in the CSAR. Cavity relief pressure was 350 psig. All log sheets are contained in Appendix B.

B. Conducting the Tests

The first test in the series was normal cooling. The cooling system air flow was balanced between the four discharge ducts. Minimum airflow velocity requirements (47 fps) were met or exceeded under single fan operation. The power was initially set

at 25% or 19.2 kw, and the system allowed to come to thermal equilibrium. The power was then raised in 25% increments to 100% allowing the system to stabilize at each power level. Temperature and pressure data was recorded hourly.

The second test in the series was loss-of-mechanical cooling. It was decided to deviate from the procedure outlined in Subsection 6.7 of the CSAR. Instead of shutting down the cooling with the power at 100% (76.8 kw), the LOMC test was conducted in a manner similar to the normal test. The intial power setting with no mechanical cooling was 25% and this value was raised in 25% increments to 100%. Thermal equilibrium was achieved at each level.

As a final test, the cask and cooling were cooled to approximately 100°F and then the power was set to 100% with no mechanical cooling. The ensuing transient was recorded to about 90% of equilibrium. This test was to get an estimate of the no-cooling heat-up time for use in reactor building and reprocessing plant handling operations. It is not a part of the acceptance testing.

C. Test Results

The raw test data are contained on the log sheets in Appendix B. For evaluation purposes, four temperature points were selected, to describe the cask heat dissipation capabilities. These points are:

1. Cavity Bulk Water Temperature

The cavity bulk water temperature was estimated by averaging the basket thermocouples and the heater thermocouples (it was established during the test that the heater TC's read mostly water temperature). This average value matches quite

closely that of the cavity bottom TC. The test shows that there is less than 10°F difference in cavity water temperature from one end to the other as expected.

2. Cask Built-In Thermocouple Reading

The cask built-in thermocouple is the only temperature measurement available during cask operation. It will be calibrated against bulk water temperature for handling purposes.

3. Shield Water Thermocouple Reading

The shield water thermocouple is a single point reading, but the same mixing phenomenon which occurs in the cavity also occurs in the barrel. Thus, this value is a reasonable approximation of the barrel bulk water temperature.

4. Average Barrel Surface Temperature

The average barrel surface temperature was taken as the average of thermocouples five and eight. These are the middle units of the three co-planned TC's on the cask surface. Since there is a cooling gradient in the vertical direction (cask horizontal) due to natural convection flow, the middle TC's are reasonably the most representative temperatures.

D. Test Analyses

To form a common basis, the 25, 50, and 75 percent power setting values were normalized to the ambient air temperature of the 100 percent power readings. Normalization was accomplished by adding or subtracting the ambient air temperature differences

at each power setting. This is valid within the small range of ambient temperatures present during the tests. The normalized normal cooling and loss-of-mechanical cooling test results are shown as Figures 1 and 2. These are plotted as temperature vs. fractional power where full power is 76.8 kw (262,000 Btu/hr.) With the exception of two data points at 25% power (shown as triangles) the values increased in the expected pattern.

Since regulations stipulate that the maximum ambient temperature to be considered is 130°F, the curves in Figures 1 and 2 were normalized to this ambient temperature. The results of this are plotted as Figures 3 and 4. Normalization from the test ambient temperatures to 130°F cannot be done by simple addition of the ambient differences to the measured values. Due to increasing heat transfer rates, convective and radiative, from the cask surface with increasing temperature, plus higher thermal conductivities of materials with increasing temperature, there is not a one-to-one relationship between changes in ambient temperatures and changes in cask temperatures. Running THTD at several power levels for test ambient and 130°F ambient produces Figures 5. This figure shows that for LOMC conditions, 100% power, a change in ambient temperature of 58°F produces a change in cask temperatures of about 28°F. As the power is reduced, the correction Delta-T increases. Since the temperatures are lower and surface heat removal is far less temperature dependent, the normal cooling Delta-T correction is less significant.

The test ambient values were normalized by adding the Delta-T's corresponding to the appropriate power level. Thus, the values in Figures 3 and 4 correspond to those calculated in the CSAR.

E. Comparison - Test Vs THTD

One of the stated purposes of the test was to verify the THTD calculations performed in support of the cask design. The

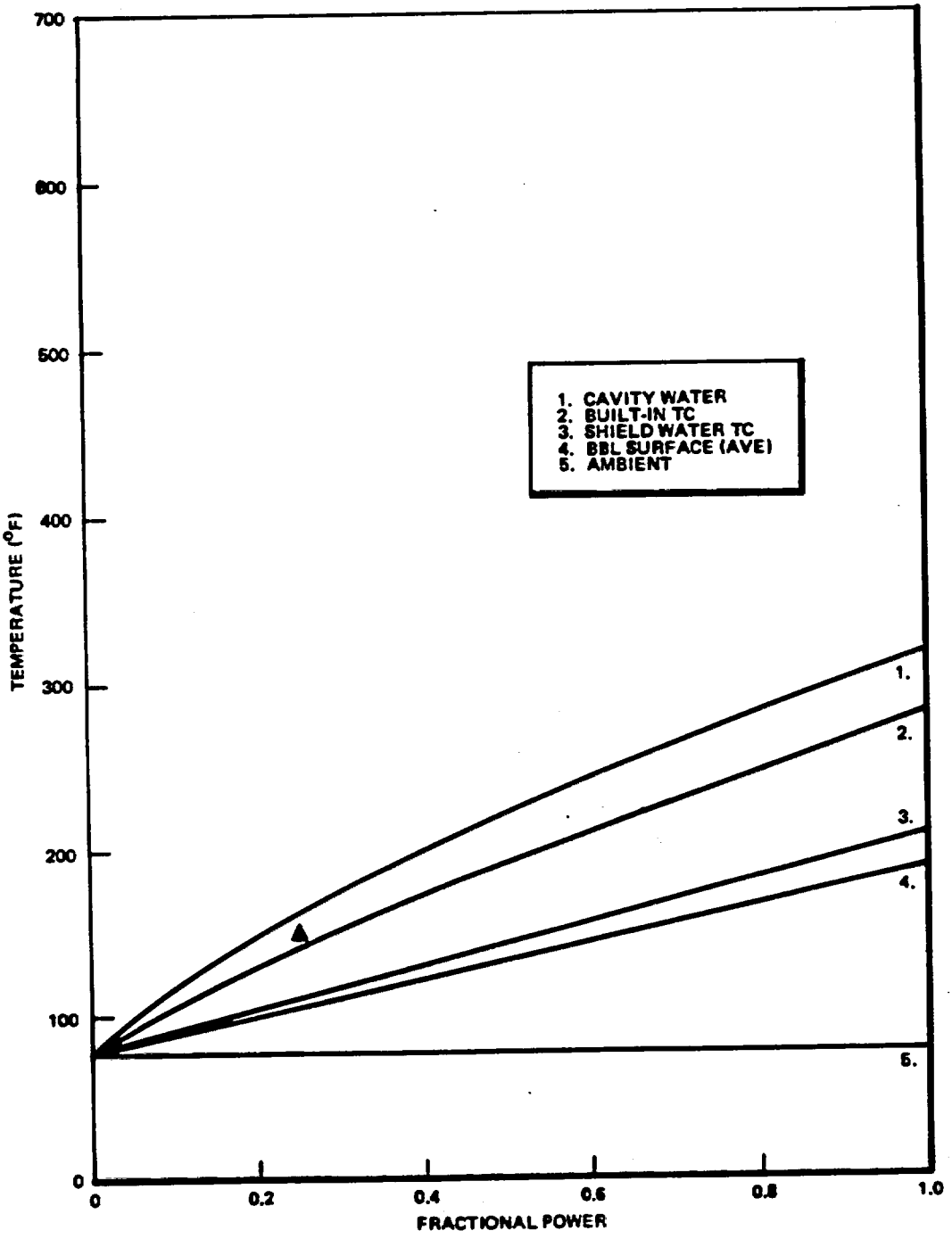

Figure 1. IF300 Cask – Normal Cooling Normalized Test Results

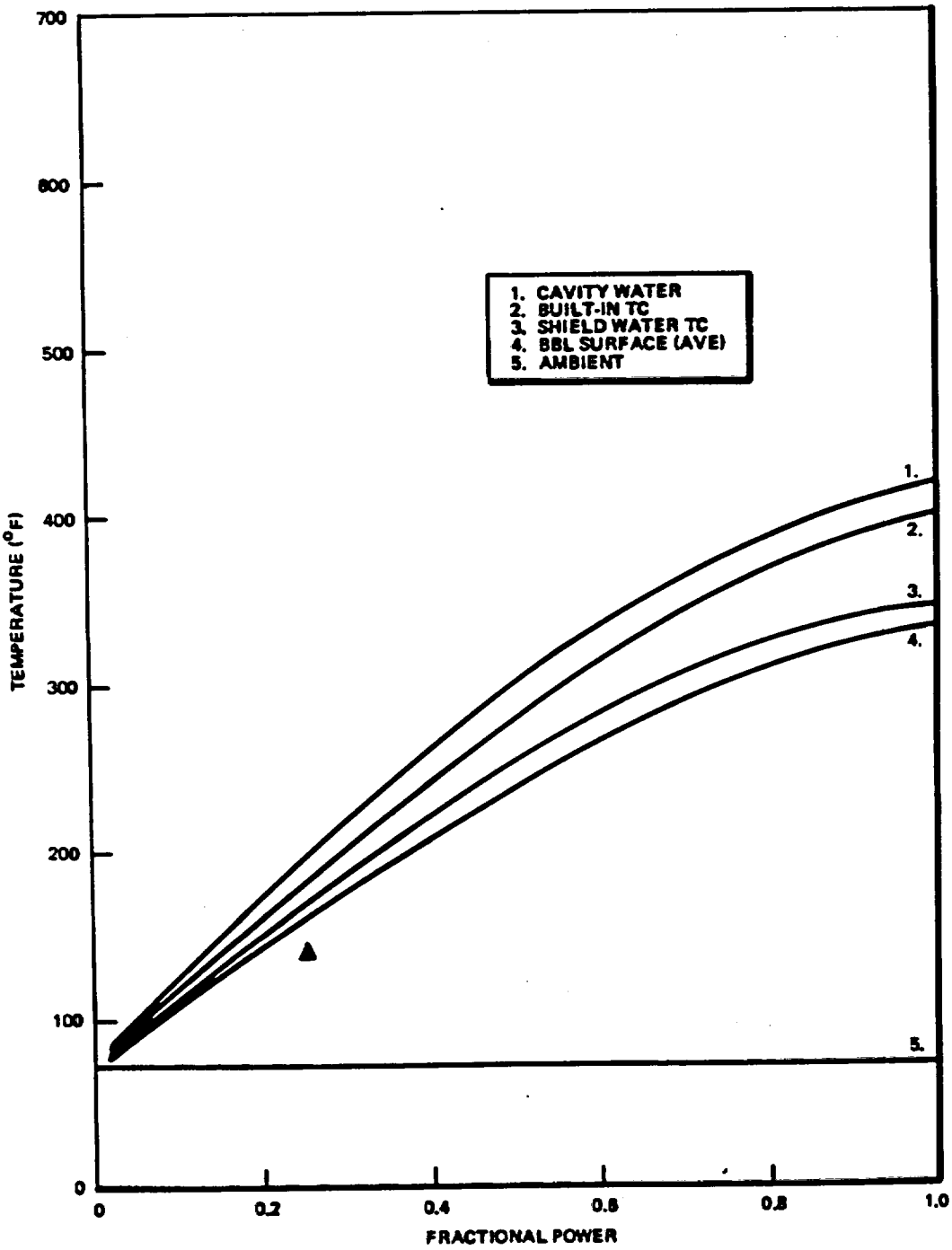

Figure 2. IF300 Cask – Loss-of-Mechanical Cooling Normalized Test Results

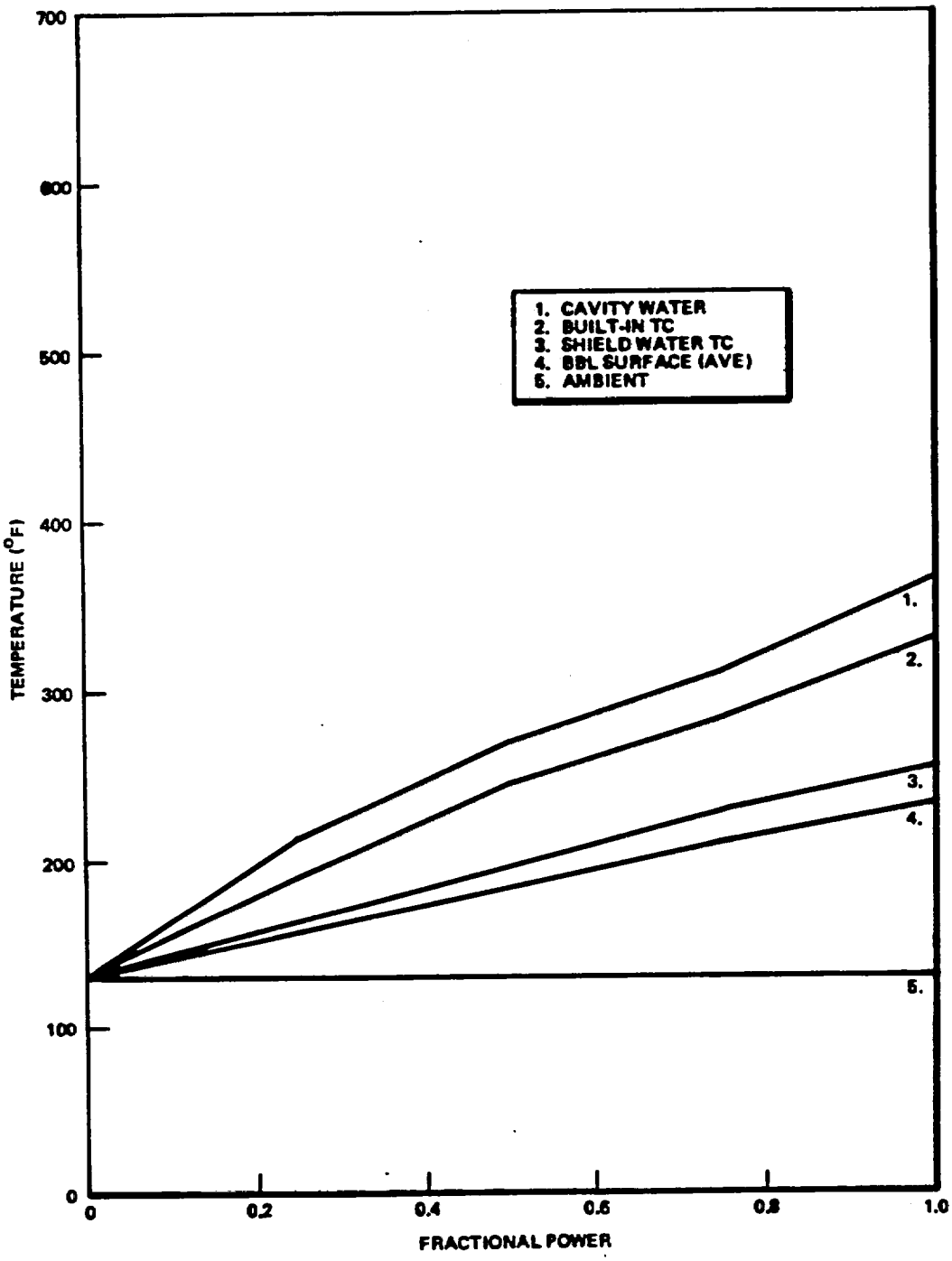

Figure 3. IF300 Cask Normal Cooling – Test Results at 130°F (Normalization)

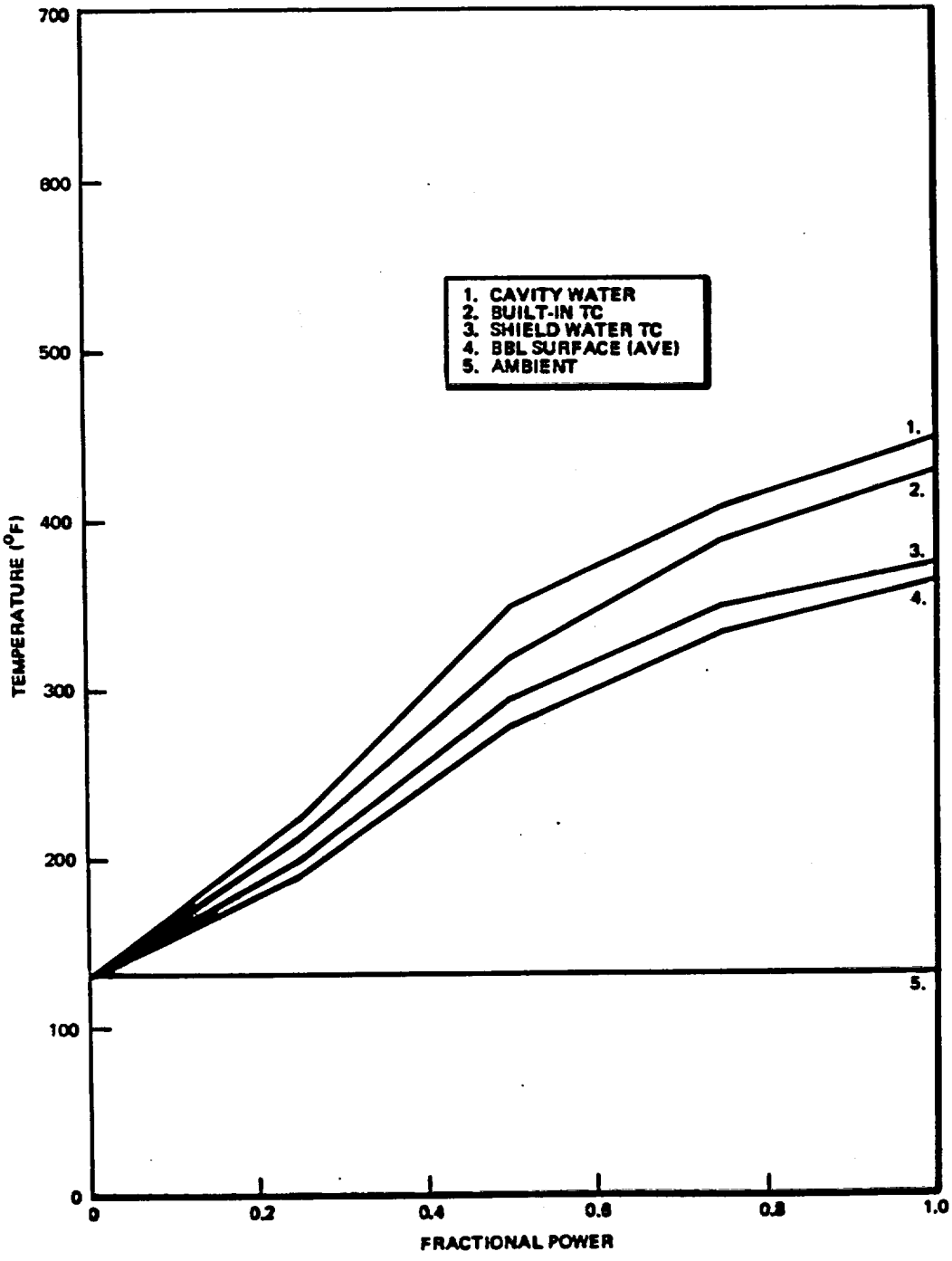

Figure 4. IF300 Cask – Loss-of-Mechanical Cooling – Test Results at 130°F (Normalization)

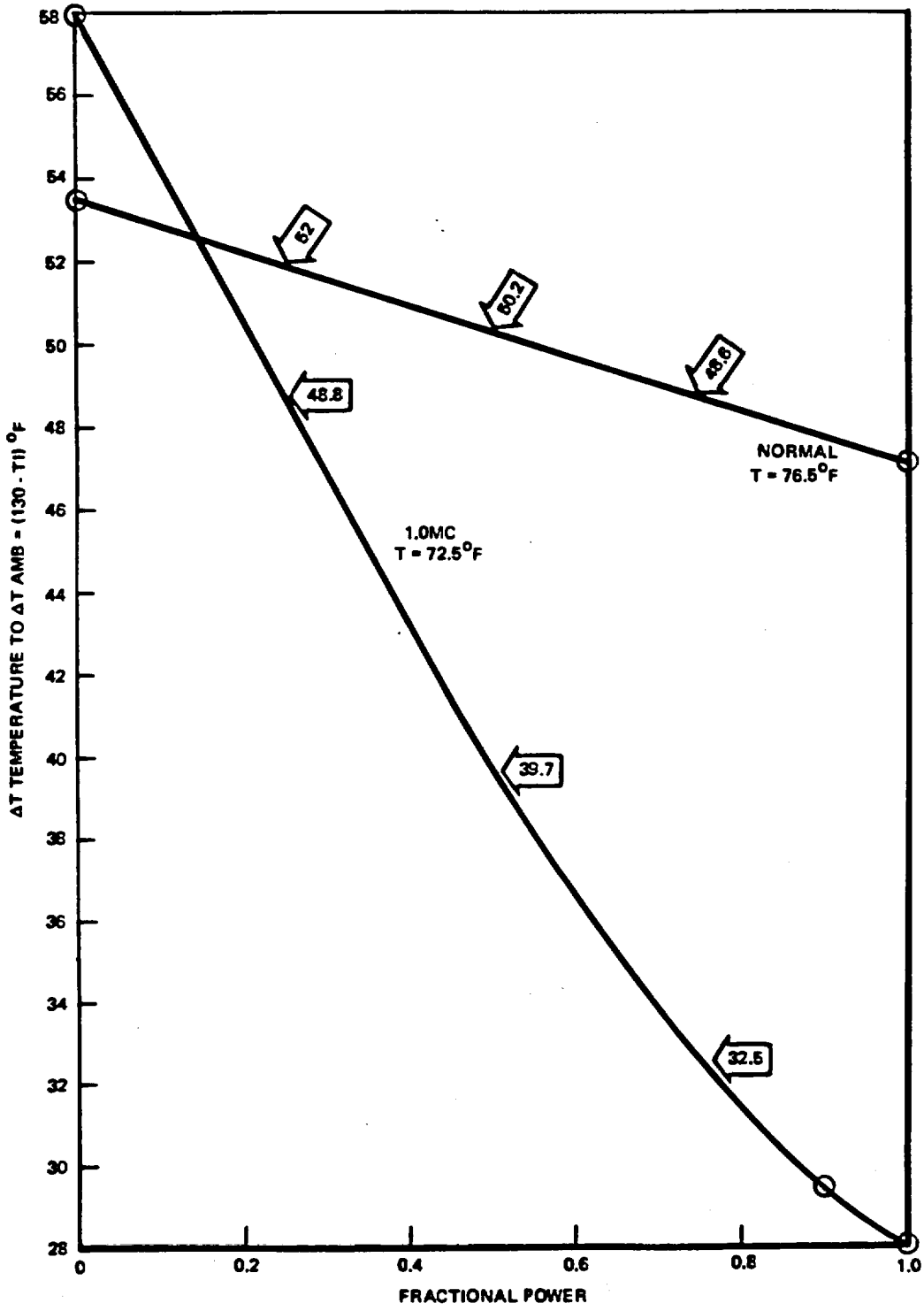

Figure 5. IF300 Cask – Test Ambient to 130°F Ambient Normalization Values

following tables compare the predicted and measured temperatures at 100% power (76.8 kw) for both the test ambient and 130°F ambient conditions.

Table 1

NORMAL COOLING - TEST AMBIENT

Item	THTD	Test	ΔT	% Var
Ambient, °F	76.5	76.5	0	0
TC #1 Built-in, °F	250	284	34	19.6
TC #3 BBL Water, °F	167	207	40	44.2
Ave. BBL Surface, °F	153	191	38	49.7
Bulk Cavity Water, °F	250	319	69	39.8

Table 2

NORMAL COOLING - 130°F AMBIENT

Item	THTD	Test	ΔT	% Var
Ambient, °F	130	130	0	0
TC #1, Built-in, °F	291	331	40	24.8
TC #3, BBL Water, °F	215	254	39	45.9
Ave. BBL Surface, °F	202	238	36	50.0
Bulk Cavity Water, °F	294	366	72	43.9

Table 3

LOMC - TEST AMBIENT

Item	THTD	Test	ΔT	% Var*
Ambient, °F	72	72.5	0.5	0.6
TC #1 Built-in, °F	414	400	14	-4.1
TC #3 BBL Water, °F	349	346	3	-1.1
Ave BBL Surface, °F	341	335	6	-2.2
Bulk Cavity Water, °F	406	421	15	4.5

*Negative sign indicates THTD prediction higher than test results.

Table 4

LOMC - 130°F AMBIENT

Item	THTD	Test	ΔT	% Var*
Ambient, °F	130	130	0	0
TC #1 Built-in, °F	442	428	14	-4.5
TC #3 BBL Water, °F	377	374	3	-1.2
Ave. BBL Surface, °F	370	363	7	-2.9
Bulk Cavity Water, °F	434	449	15	4.9

*Negative sign indicates THTD prediction higher than test results.

F. Discussion of Comparisons

Normal Cooling - There is a marked variation between the predicted and measured values with the test figures being higher in all cases. With the exception of the bulk cavity water temperature, the differences between the measured and calculated values are almost constant, approximately 38°F (Table 2). This would indicate some constant factor affecting overall heat transfer. The only reasonable conclusion to be reached is that the air impingement film coefficient is less than the calculated value of 7.0 Btu/hr-Ft^2-°F used in THTD. The variation in cavity bulk water temperature is partially due to the less efficient heat removal from the cask surface and partially due to the reduced liquid-to-wall heat transfer area within the cavity created by the expansion void volume. Nevertheless, the temperatures and pressures under these conditions are well within acceptable operating limits.

Loss-of-Mechanical Cooling - The variation between predicted and measured temperatures is quite small, amounting to less than five percent. THTD over-predicted all temperatures except the cavity bulk water. As in the normal cooling case, this elevated cavity coolant temperature is probably due to the reduced liquid-to-wall heat transfer area resulting from the expansion void volume.

It should be mentioned that a slight error in volumetric heat generation was detected in the LOMC-THTD model. As a result, the temperatures shown in the Table VI-3 of the CSAR are slightly less than the most recent computations. Table VI-3 should read as follows:

Table VI-3
CASK TEMPERATURE DISTRIBUTION-LOMC

Description	
Ambient air temperature, °F	130
Internal heat load, Btu/hr	262,000
Max. barrel surface temperature, °F	384
Max. cask body temperature, °F	404
Max. inner cavity surface temperature, °F	443
Bulk water shield temperature, °F	377
Bulk water shield pressure, psig	174
Bulk coolant temperature, °F	434
Cask cavity pressure, psig	344
Max. fuel rod cladding temperature, °F	480

G. Adjustments

As previously stated, the cask heat load limit will be adjusted in accordance with the thermal demonstration test results. The most severe off-normal case is loss-of-mechanical cooling shown in Figure 4. The normalized cavity bulk water temperature under 130°F ambient air, 100% power conditions is 449°F. This is in excess of the 436°F temperature whose saturation pressure is equal to the safety relief valve setting of 350 psig. Thus, to preclude cavity boil-off, the heat load limit must be reduced to a value which will lower the bulk temperature below 436°F. At 90 percent of power or 235,000 Btu/hr (69.12 kw), the bulk water temperature is 430°F. Saturation pressure is 329 psig, therefore, no boil-off will occur.

The significance of this heat load adjustment is minor. Considering the maximum exposure fuel elements as described in Section III of the CSAR, the BWR cooling time is extended by two days - 120 to 122. The PWR cooling time is extended by 18 days - 120 to 138.

IV. Conclusion

The hydrostatic tests demonstrated that the cavity and closure seal are able to sustain a minimum pressure of 400 psig without leakage. Furthermore, the neutron shielding barrels were shown to have the capability of retaining 200 psig internal pressure without leakage.

The thermal tests showed that under normal conditions the effectiveness of the air impingement cooling system is somewhat less than anticipated. However, the temperature distribution wtihin the cask is well within acceptable limits. The loss-of-mechanical cooling condition behaved in a very predictable manner with the maximum variation between computed and measured values being slightly less than five percent. A small adjustment in cask heat load limit was required to assure that no cavity coolant boil-off would occur under 130°F ambient air conditions.